THESE

Présentée à

L'Université des Sciences et Technologies de Lille

Pour obtenir le titre de

DOCTEUR EN CHIMIE

Spécialité: Molécules et Matière Condensée

par

Xiaofeng YI

Encapsulation d'hétéropolyacides de type Keggin et de Keplerate de type polyoxomolybdate {Mo_{132}} pour la catalyse hétérogène en phase liquide

Soutenance le 7 Décembre 2016 devant la commission d'examen :

Rapporteurs
Mme Véronique Dufaud, Directeur de recherche CNRS, Université de Lyon 1
M. Richard Villanneau, Maitre de conférences, Université Pierre et Marie Curie Paris 6
Examinateurs
Mme Catherine Roch, Maitre de conférences, Institut Lavoisier de Versailles
M. Thierry Loiseau, Directeur de recherche CNRS, Université de Lille 1
Directeur
M. Sébastien Paul, Professeur, Ecole Centrale de Lille
Co-directeur
M. Benjamin Katryniok, Maitre de conférences, Ecole Centrale de Lille

THESE

L'Université des Sciences et Technologies de Lille

For obtaining a title of

DOCTOR IN CHEMISTRY

Speciality: Molecules and Condensed Materials

by

Xiaofeng YI

Encapsulation of Keggin-type heteropolyacids and Keplerate polyoxomolybdate {Mo_{132}} for heterogeneous catalysis in liquid phase

Defensed on 7 December 2016 in front of the examination committee:

Reviewers
Mme Véronique Dufaud, Directeur de recherche CNRS, University of Lyon 1
M. Richard Villanneau, Maitre de conférences, Université Pierre et Marie Curie Paris 6
Examiners
Mme Catherine Roch, Maitre de conférences, Institut Lavoisier de Versailles
M. Thierry Loiseeau, Directeur de recherche CNRS, Lille 1 University
Director
M. Sébastien Paul, Professeur, Ecole Centrale de Lille
Co-director
M. Benjamin Katryniok, Maitre de conférences, Ecole Centrale de Lille

Acknowledgements

Time flies, my PhD study is coming to an end. At this moment, I would like to express my appreciation to all the people who have given me help and support in this period.

Firstly, I want to thank my supervisors - Prof. Sébastien Paul and Dr. Benjamin Katryniok for their kind guidance and always encouragement in the past three years, offering the enthusiastic help whatever on the research work or daily life.

I also would like to thank Dr. Catherine Roch and Prof. Emmanuel Cadot in *Institut Lavoisier de Versailles* (ILV, UMR 8180), Dr. Toru Murayama in *Catalysis Research Center, Hokkaido University*, Prof. Franck Dumeignil, Dr. Thierry Loiseau and Prof. Sébastien Royer in *Unité de Catalyse et Chimie du Solide* (UCCS, UMR 8181) for their valuable discussions and useful advices.

I am grateful to *China Scholarship Council* (CSC) for the financial support during my stay in France, as well as Mr. Xuemin Wu, Ms. Jingmei Zhao and the other staff members in *Education Service of Embassy of China* for the kind attention.

It would have been impossible to complete this work without the help of the whole team of UCCS. I wish to thank all the technicians and colleagues for their contributions, especially Gérard Cambien, Johann Jezequel, Pascale Dewalle, Joëlle Thuriot and Svetlana Heyte.

Moreover, thanks to Dr Véronique Dufaud and Dr Richard Villanneau for accepting the role of reviewers for my thesis, and Dr Catherine Roch and Dr Thierry Loiseau for accepting the role of examiners.

I would like to thank all my friends in Lille. I have received countless help, delight and support from you. Thank you for the memorable experience. Finally I want to express my special thanks to my family for their enduring support throughout the graduate school.

Contents

Résumé

Les hétéropolyacides de type Keggin (HPA) et les Keplerates sont des catalyseurs attractifs en raison, notamment, de leurs propriétés chimiques facilement ajustables (acidité, pouvoir redox, etc.). Cependant, leur mise en oeuvre en tant que catalyseurs hétérogènes pour des réactions en phase liquide est largement entravée par leur solubilité dans les solvants polaires. Ainsi, dans ce travail, le développement de catalyseurs hétérogènes basés sur des hétéropolycomposés mais résistants à la lixiviation dans les milieux polaires a été étudié.

Deux HPA de type Keggin ($H_3PW_{12}O_{40}$ et $H_3PMo_{12}O_{40}$, notés HPW et HPMo) ont été encapsulés dans deux types de MOF (MIL-101 (Cr) et MIL-100 (Fe)) en utilisant des méthodologies différentes. Les propriétés physiques et structurales de ces catalyseurs ont été caractérisées par différentes techniques, telles que: DRX, FT-IR, N_2 adsorption/désorption, etc. Par la suite les propriétés catalytiques de ces solides ont été mesurées pour l'estérification de l'acide acétique par le n-butanol et l'époxydation de cyclooctène par H_2O_2, ces deux réactions étant utilisées en tant que réactions-modèle. Pour cette dernière réaction, le catalyseur HPMo@MIL-101(Cr) a permis d'obtenir plus de 70% de conversion de cyclooctène et aucune diminution significative de l'activité après trois recyclages. Au contraire, pour HPMo@MIL-100(Fe) une lixiviation de l'HPA hors du MOF a été systématiquement observée.

Enfin, la possibilité d'encapsuler un Keplerate $\{Mo_{132}\}$ dans de la silice MCM-48 fonctionnalisée par des groupements propylamino a été réalisée. D'après les résultats des analyses infra-rouge et d'adsorption/désorption d'azote, il a pu être prouvé que l'hétérogénéisation du $\{Mo_{132}\}$ a été réalisée avec succès dans la porosité de la silice. Les propriétés catalytiques de ce catalyseur pour l'époxydation du cyclooctène ont été étudiées, mais le Keplerate $\{Mo_{132}\}$ est immédiatement décomposé en présence de peroxyde d'hydrogène.

Abstract

Heteropolycompounds such as Keggin-type heteropolyacids (HPAs) and Keplerate-type polyoxometalates (POMs) are attractive catalysts due to their easily adjustable strong acid and redox properties. However, their applications in liquid phase reactions are largely hampered by their solubility in polar solvents. Therefore, the development of heterogeneous catalysts based on heteropolycompounds, which could resist to leaching in polar media has been studied in this work. Two Keggin-type HPAs (namely $H_3PW_{12}O_{40}$ and $H_3PMo_{12}O_{40}$, denoted as HPW and HPMo) were encapsulated into two types of organic-metal-frameworks (MOFs) (MIL-101(Cr) and MIL-100(Fe)) using the "building a bottle around the ship" methodology. The physical and structural properties of these catalysts were characterized by various techniques including XRD, FT-IR and N_2-absorption/desorption. Hereby, the influence of reaction parameters in the synthesis of HPW@MIL-101(Cr) was studied and its catalytic properties were determined in the esterification of acetic acid by n-butanol. The performance was not very promising, neither in terms of activity, nor in terms of reusability. However, HPMo@MIL-101(Cr) had a good performance in the epoxidation of cyclooctene by H_2O_2 with more than 70% conversion and no significant decrease in activity after 3-run recycling. HPMo@MIL-100(Fe) was also used in the epoxidation of cyclooctene. However, the leaching of HPMo took place during the reaction. Finally, an attempt to encapsulate Keplerate-type polyoxometalate $\{Mo_{132}\}$ into porous silica MCM-48 using the "building a ship in the bottle" methodology was done. Despite various approaches, encapsulated Keplerate was not obtained, whereby several hypotheses were evoked including that the Keplerate was lost during the final washing step. In order to explore the hypothesis of the leaching of $\{Mo_{132}\}$ by washing, the functionalization of MCM-48 using propylamino groups was performed to try to immobilize $\{Mo_{132}\}$ by an ionic linkage. From the IR and N_2-adsorption/desorption results it can be evidenced that the heterogeneisation of $\{Mo_{132}\}$ was carried out successfully. The catalytic properties of $\{Mo_{132}\}$ in the epoxidation of cyclooctene were studied, but the $\{Mo_{132}\}$ Keplerate decomposed immediately in the presence of hydrogen peroxide.

Nevertheless, the decomposition products had the ability to catalyze the epoxidation of cyclooctene and the active phase was identified to be {Mo_8} clusters. It should be mentioned that this result is in conflict with those previously reported in the literature.

Key words: encapsulation, heterogeneous catalysts, heteropolyacids, metal organic framework, keplerate, porous silica.

1 Literature Review

1.1 General introduction

As a matter of fact the economy of developed and emerging countries hangs almost entirely on the use of fossil raw materials, with more than 90% of organic chemicals issued from crude oil transformations. Both the forecasted depletion of these resources and their strong contribution to the global warming effect on climate has triggered the need for new technologies capable of reducing oil dependency. As a result, chemists have been trying to develop various technologies to use new energies, including solar energies (photovoltaic catalysis and solar cells, etc.)[1-3], hydrogen energies (water decomposition)[4-5] and biomass valorization[6-8], etc. The above techniques not only utilize renewable sources but are also in-line with the principle of "Green Chemistry". However, among them, biomass valorization has been paid more and more attention due to their unique potential of "turning waste into treasure", for instance, converting organic waste generated in harvesting, processing of agricultural products to useful chemicals or clean energy.[9-11]

About 170 billion metric tons of biomass per year is produced by photosynthesis, 75% of which can be allocated to the class of carbohydrates. It is surprising that only 3-4% of these compounds are used by humans for food and other purposes.[12] Therefore, transferring the unused biomass productions into useful chemicals is of large significance. There are many chemical routes to realize transformation of biomass to chemicals, such as heterogeneous catalysis[13-14], homogeneous catalysis [15-16], enzymatic processes[17-18] and so on. Considering the ultimate purpose of industrialization, heterogeneously catalyzed processes are generally preferred to run continuous process and to avoid the problem of separation of the catalysts and products after reactions.

Among the large variety of solid catalysts, polyoxometalates (POMs) compounds are economically and environmentally attractive catalysts for the biomass valorization due to their easily adjustable strong acidity and redox properties[19]. However, the

applications of POMs in liquid phase reactions are mostly homogeneous processes due to their high solubility in polar solvents, therefore the development of innovative heterogeneous POM catalysts is of large interest and has attracted attention of researchers all over the world.[20-21] As we all know, an ideal heterogeneous catalyst should be active, selective and stable during recycling reactions, therefore avoiding leaching of active phases is particularly important, especially for POMs catalysts. Therefore, in this work, we focused on the strategies of developing heterogeneous POM catalysts which can resist the leaching of POMs in liquid phase reactions.

1.2 Polyoxometalates (POMs) / heteropolyacids (HPAs)

Polyoxometalates (POMs) are a series of ionic compounds composed of cations and various-structure polyanion clusters, in which oxometal polyhedra of MOx (x = 5, 6) are the basic units of structures. Here, M represents early transition metals (TMs) in their high oxidation state, such as W, Mo, V and so on, which can be partly substituted by other metals, including Al, Ti, Cr, Mn, Fe, Co, Ni, Cu, Zn, Zr, Ru, Pd, Ag, Hf, Ln, etc. So far, many TM-substituted POMs have been reported. The properties of polyanions can be affected by central atoms significantly. These heteroatoms are usually main-group elements, including Si, P, S, As, Se, B, Al, and Ga, but are not limited to these elements. Some late transition metals such as Co and Fe are also found as heteroatoms.[22] As is known, the parent acids of POMs are composed of protons and heteropolyanions, which are called heteropolyacids (HPAs). Here, we have concentrated our attention on two kinds of POM/HPA compounds, namely, Keggin-type HPAs and Keplerate-type POMs.

1.2.1 Keggin-type heteropolyacids (HPAs)

HPAs possess a discrete ionic structure comprised of heteropolyanions and counter cations (H^+, H_3O^+, $H_5O_2^+$, etc.), which allow itself to present an extremely high

proton mobility while heteropolyanions can stabilize cationic intermediates.[23] They can have simultaneously strong acid and redox properties, and their acidity and redox properties can be varied over a wide range by changing their chemical compositions. These properties give huge space to researchers to realize planned design and synthesis of HPAs for the desired applications.

Among various HPAs, Keggin-type HPAs are the most interesting one for catalysis. Keggin-type HPAs were first discovered by Berzelius in 1826. Since then, many researchers worked on these compounds including De Marignac, Scheibler, Sprenger, Soboleff, Kehrmann, Copauxff, etc. According to the results of dehydration experiments, most of these researchers suggested $H_3PW_{12}O_{40}$ and $H_4SiW_{12}O_{40}$ as the empirical formula of anhydrous 12-heteropolyacids. Some years later, Pauling proposed the first 3-dimensional structure for these compounds, but it is Keggin who confirmed the structure of the 12-phosphotungstic acid $H_3PW_{12}O_{40}$ by X-ray analysis in 1934.[24] In the following text of this thesis, HPAs are understood as Keggin-type heteropolyacids, unless otherwise stated.

Because of their most stable structure and the easiest availability, the Keggin structure has been most widely studied in catalysis and industry. As previously mentioned their raw formula is $XM_{12}O_{40}^{n-}$, where X is the central atom or heteroatom, M is the addenda atom and n is the charge of the heteropolyanion.

1.2.1.1 Molecular Structure

The Keggin-type HPAs possess a tetrahedral molecular structure. A central tetrahedron XO_4 (with X = P, Si, Ge or As) is surrounded by 12 edge- and corner-sharing 12 MO_6 octahedra (M = Mo, W, V, Co, Zn...). These octahedra are grouped in four M_3O_{13}, and each group is linked by the edges as shown in Figure 1-1.

In Figure 1-1, one can see that there are four different types of oxygen atoms in this configuration:

- 4 O_a atoms which link tetrahedrons and octahedral;
- 12 O_b atoms-corner-bridging oxygen atoms which link the M_3O_{13} groups by their corners;
- 12 O_c atoms-edge-bridging oxygen atoms which link the MO_6 groups of a same M_3O_{13} group by their edges;
- 12 O_d atoms-terminal oxygen atoms which are only linked to one M atom.

If this regular structure is included in a sphere, the diameter of the sphere is about 1.2 nm which is an important parameter for dispersing HPAs into porous materials (see below).

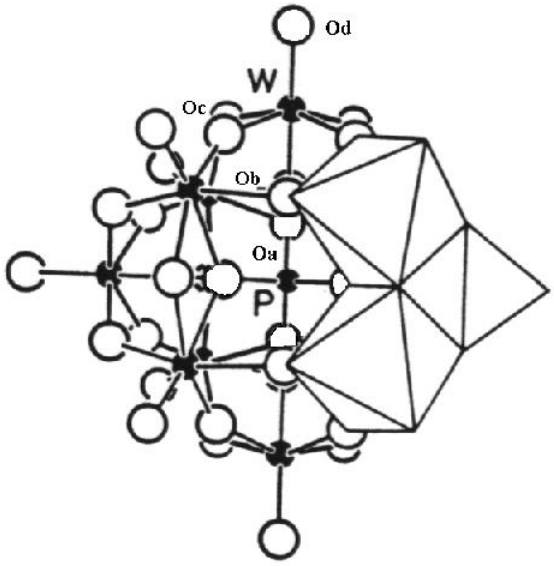

Figure 1-1 The molecular structure of Keggin-type $XM_{12}O_{40}^{n-}$ anion.

Generally, solid HPAs are composed of heteropolyanions, counter cations and hydration water. Their crystal structure depends on the amount of hydration water, which can be removed easily by heating. This reversible process can change the

volume of the crystal cell. Furthermore, unlike the rigid network structure of zeolites, HPA crystals have structural flexibility, namely, not only hydration water but also some polar organic molecules can enter and leave the HPA crystal. This is of significance when they are used as catalysts in polar media.[25]

1.2.1.2 Stability

HPA have proved their attractive acid and redox properties [23-24, 26-27], their stability is thus the main remaining critical parameter for the overall catalytic performance. The stabilities referring to HPA catalysts usually include three parts: thermal stability, hydrolytic stability and oxidative stability. Those stabilities change depending on the chemical compositions of HPAs.

Generally, HPA catalysts have fairly high thermal stabilities, so they are even applied in some gas-phase reactions run at high temperatures.[28-29] Among various Keggin-type HPAs, the thermal stability follows $H_3PW_{12}O_{40}$ (HPW)> $H_4SiW_{12}O_{40}$ (HSiW) > $H_3PMo_{12}O_{40}$ (HPMo) > $H_4SiMo_{12}O_{40}$ (HSiMo).[30] Apparently, HPW is the most thermally stable in this family. However, the high thermal stabilities of HPAs are relative. Take HPW as an example, it loses 1.5 H_2O at 723−743 K to form $PW_{12}O_{38.5}$, and the structure is destroyed completely at about 873 K.[30] Therefore, appropriate reaction temperatures are crucial for HPA catalysts.

HPAs usually have excellent hydrolytic stabilities and oxidative stabilities since they are inorganic compounds and do not contain organic ligands. Although in presence of water, the subunits of heteropolyanions may detach from the skeletons, they are quite stable in a certain pH range. Some reactions with HPA catalysts can even be run in pure water.[31-33] Furthermore, POM anions have strong persistence against oxidants. Therefore, HPA catalysts can be used in water- and oxygen-rich environments without the protection of noble gases which is essential for many organometallic catalysts.

In summary, the three stabilities (thermal, hydrolytic, and oxidative stability) of HPA catalysts are good enough to meet the demands of many reactions, and which kind of stabilities is more important depends on the type of catalysis.

1.2.1.3 Chemical properties

i. Acidity

Solid HPAs. HPAs are very strong Brønsted acids, stronger than conventional solid acids (SiO_2-Al_2O_3, H_3PO_4/SiO_2 ...). The strong delocalization of the charge in the Keggin structure is responsible for this property. In the solid state, these structures present two types of protons: (1) delocalized protons, which are rapidly exchanged with those of the water of crystallization; (2) more localized protons, which are located near the O_d atoms.[34-35]

The acidity of solid HPAs strongly depends on the nature of the addenda atoms. The acid strength of crystalline HPAs decreases following the series HPW > HSiW > HPMo > HSiMo.[25] The Brønsted acidity strongly decreases with the loss of constitutional water because all the residual protons are then localized. The exchange of the protons of the heteropolyacid by cations results in a decreased number of Brønsted acid sites. But, according to Misono and his coworkers, the electronegativity of the counter cation is also an important factor that influences the acidic properties of the HPAs, as some cations can provide their own Lewis acidity (e.g. Al^{3+}).[36] In supported heteropolyacids, the acidity is also influenced by the support due to the electrostatic interactions between the support and the heteropolyacids.

HPAs in solutions. HPAs possess very high solubility in polar solvents such as water, alcohols, ethers, esters, etc. On the other hand, they are insoluble in nonpolar solvents such as benzene, CCl_4 and so on. The acid properties of HPAs in solutions can be described by dissociation constants and Hammett acidity function. The

dissociation constants of HPAs were measured in different solvents like H_2O, Me_2CO, EtOH and AcOH, etc.[25, 37] and some results are displayed in Table 1-1. In aqueous solution, HPAs such as HPW, HSiW and HPMo are strong acids which fully dissociated. In organic solvents, the acidities of HPAs are stronger than those of usual mineral acids (H_2SO_4, HCl, HNO_3, etc.). The strength of HPAs depends on their compositions. For instance, the tungsten-based acids are much stronger than the molybdenum-based ones. The strongest acid in the Keggin series is HPW. The titration in presence of Hammett indicators can classify HPAs according to their decreasing acidity in acetonitrile[38]:

$$H_3PW_{12}O_{40} > H_4SiW_{12}O_{40} > H_4GeW_{12}O_{40} > H_5BW_{12}O_{40} > H_6CoW_{12}O_{40}$$

It is obvious that, for Keggin-type HPAs, the acidity decreases with the increase of the number of protons. The acidities of HPA concentrated solutions in terms of the Hammett acidity function also weakly depends on their compositions and is stronger than that of equimolar solutions of H_2SO_4.[35]

Table 1-1 Dissociation constants of various polyoxometalates and mineral acids measured in acetone, ethanol and acetic acid.

Acid	Acetone			Ethanol			Acetic acid
	pK_1	pK_2	pK_3	pK_1	pK_2	pK_3	pK_1
$H_3PW_{12}O_{40}$	1.6	3.0	4.0	1.6	3.0	4.1	4.8
$H_4PW_{11}VO_{40}$	1.8	3.2	4.4	-	-	-	4.7
$H_4SiW_{12}O_{40}$	2.0	3.6	5.3	2.0	4.0	6.3	5.0
$H_3PMo_{12}O_{40}$	2.0	3.6	5.3	1.8	3.4	5.1	4.7
$H_4PMo_{11}VO_{40}$	2.1	3.7	5.6	1.9	3.7	5.8	4.7

$H_4SiMo_{12}O_{40}$	2.1	3.9	5.9	-	-	-	4.8
H_2SO_4	6.6	-	-	-	-	-	7.0
HCl	4.3	-	-	-	-	-	8.4
HNO_3	9.4	-	-	-	-	-	10.1

ii. Redox properties

HPAs can also be used as strong oxidants.[39-40] Their redox properties can be influenced by the composition of the Keggin heteropolyanion and the nature of the counter cations.[41-42] The sequence of the oxidation power of HPAs consisting of purely tungstic or molybdic acids is $H_3PMo_{12}O_{40}$ > $H_4SiMo_{12}O_{40}$ >> $H_3PW_{12}O_{40}$ > $H_4SiW_{12}O_{40}$. By replacement of one or more Mo=O groups in the $PMo_{12}O_{40}^{3-}$ Keggin structure by V=O one obtains $H_{3+x}PV_xMo_{12-x}O_{40}$ which has highest redox potential than the initial HPA. Molybdenum heteropolyacids are easily reduced, which gives them a blue coloration, the so-called Molybdenum Blues. The electron in excess is localized on a precise metallic site. For instance, in the case of $H_{3+x}PV_xMo_{12-x}O_{40}$, the electron is on V.

A 2-stepped mechanism for the reduction of $H_3PMo_{12}O_{40}$ with H_2 was suggested by Misono *et al*.[43]:

$$H_2 + O\text{-}Mo^{VI}\text{-}O\text{-}Mo^{VI}\text{-}O \longrightarrow H_2O + Mo^{V}\text{-}O\text{-}Mo^{V}\text{-}O$$

As one can see HPAs present an unique combination of acid and redox properties. Moreover, these properties are easily tuned by appropriate changes of their structures such as the replacement of the central atom, the addenda atom, the counter cations and so on, which provides the feasibility of planned synthesis of desired catalysts.

Due to their excellent acidity or redox properties of HPAs, different HPAs have been employed in acid-catalyzed reactions and oxidation reactions. $H_3PW_{12}O_{40}$ and

$H_4SiW_{12}O_{40}$ haven been applied in the esterification of hexanoic acid and methanol[44], the hydrolysis of cellulose and lignocellulose[45] and the condensation of isophytol with 2,3,5-trimethylhydroquinone to vitamin E[46]. And those HPAs which have oxidation power such as $H_3PMo_{12}O_{40}$ and $H_4SiMo_{12}O_{40}$ etc. exhibits good activities in oxidation of alkanes [47], oxidation of alkenes[48-49] and oxidative dehydrogenation of alkanes[50].

1.2.2 Keplerate-type polyoxometalates (POMs)

The Keplerate-type POMs is a family of the spherical polyoxomolybdates of icosahedral symmetry. Müller and his coworkers reported the first member, $\{Mo_{132}\}$, in 1998.[51] Afterwards, many Keplerate-type POMs were observed via the change of the ligands, the replacement of Mo_2^{VI} units by $M^{III}(H_2O)$ (M=Fe, V and Cr) and the introduction of tungsten-oxide based on the structure of $\{Mo_{132}\}$. This flexibility in their structure and the possibility to take-up (or exchange) certain species in their cavities from the structure itself let Keplerate-type POMs be considered as a new type of nanomaterials comparable to Keggin-type POMs. The researchers have paid much attention on their potential applications in catalytic materials, sensors and delivery system of biologically active substances.[52-54]

In the following, we will briefly describe $\{Mo_{132}\}$ which has been studied a lot among various Keplerate-type POMs.

1.2.2.1 $\{Mo_{132}\}$

$\{Mo_{132}\}$ is the representative of Keplerate-type POMs synthesized by partial reduction of Mo^{VI} atoms present in $(NH_4)_6Mo_7O_{24}$, which formula is $(NH_4)_{42}[Mo^{VI}_{72}Mo^{V}_{60}O_{372}\text{-}(L)_{30}(H_2O)_{72}]$ where L presents the ligands such as acetate[51], oxalate[55], butyrate[56], propionate[57], isobutyrate and pivalate[58]. The cluster of $\{Mo_{132}\}$ is formed by self-assembly of a reduced and acidified aqueous solution of molybdate.[59] Here, we take the $\{Mo_{132}\}$ with the ligands of acetate to

introduce the structures and the properties of this type of POMs. In the following, $\{Mo_{132}\}$ are understood as the Keplerate-type $\{Mo_{132}\}$ with acetate ligands, unless otherwise stated.

The $\{Mo_{132}\}$ cluster is composed of 12 $\{(Mo)\text{-}Mo_5O_{21}(H_2O)_6\}$ (denoted as $\{(Mo^{VI})Mo^{VI}_5\}$) pentagons and 30 $\{[Mo_2{}^{V}O_4(CH_3CO_2)]\}$ (denoted as $\{Mo^{V}_2\}$) dumbbells. The pentagonal $\{(Mo^{VI})Mo^{VI}_5\}$ unit is constructed by linking 5 $\{MoO_6\}$ octahedra to a central pentagonal bipyramidal $\{MoO_7\}$ unit by bridging O atoms. Each $\{Mo^{V}_2\}$ unit links two $\{MoO_6\}$ octahedra from different $\{(Mo^{VI})Mo^{VI}_5\}$ units to form a spherical structure in which the 12 Mo_6O_{21} pentagons occupy the vertices of an icosahedron, while the 30 $\{Mo^{V}_2\}$ dumbbells span a truncated icosahedron with 12 regular pentagons and 20 hexagons of trigonal symmetry.[51, 60] The structure is illustrated in Figure 1-2. The $\{Mo_{132}\}$ molecule is 2.9 nm in diameter and 1.5 nm^3 in volume and the pore size is 0.6~0.8 nm.

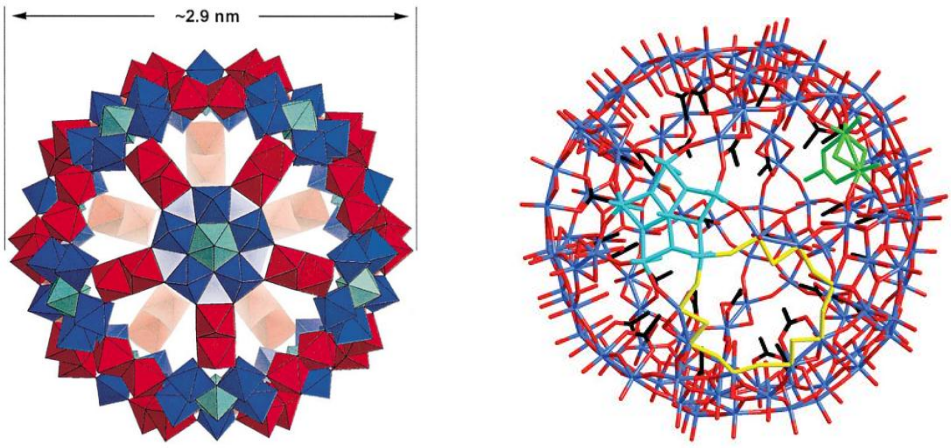

Figure 1-2 (Left) Structure of the $\{Mo_{132}\}$-type clusters in polyhedral representation. 12 $\{(Mo^{VI})Mo^{VI}_5\}$ groups (blue, with the pentagonal MoO_7 bipyramids in bright blue), 30 $\{Mo^{V}_2\}$ groups (red);[54] (Right) Structure of $\{Mo_{132}\}$ in stick representation (Mo: blue; O: red; C: black). One of the 12$\{(Mo^{VI})Mo^{VI}_5\}$ building blocks is high-lighted in light blue, one of the 30 $\{Mo^{V}_2\}$ groups in green, and the Mo–O bond atoms defining

the rim of one of the 20 pores in yellow. H atoms are omitted for clarity.[52]

The structure of {Mo_{132}} cluster is heat-resistant up to 190 ˚C according to the investigation of its thermal behavior in air and nitrogen.[61] At 200 ˚C, amorphization occurs and at 250 ˚C, molybdenum oxide MoO_3, acetamide and acetonitrile appear which indicate the destruction of {Mo_{132}} cluster.

{Mo_{132}} is water-soluble because of its charge and hydrophilic surface (a layer of water ligands). The structure of {Mo_{132}} is pH dependent in solutions. When the pH value of the solution is less than or equal to 8, it is not stable and the structure destroys to form smaller species according to a UV-vis study.[53] Actually, in practical applications, in order to keep the stability of the structure, it is better to control the pH of the solution between 3 and 6 and the temperature below 363 K.

The existence of 70 Mo^{VI}, the highest-valence of Mo, in the cluster gives a strong oxidation power to {Mo_{132}} in theory, and the sizes of their cages and pores limited the size of the molecules in and out of the cluster, which is favorable to the selectivity of the reactions. Therefore, the {Mo_{132}} cluster should be a good oxidant in selective oxidation. Some reports have proved this and {Mo_{132}} performs as a good nanoreactor in a regioselective Huisgen reaction between a surface-attached azide function and propiolic acid[52], oxidation of sulfides and olefins[53, 62-63], epoxidation of alkenes[64].

1.3 Porous materials

Dispersing homogeneous catalysts into/onto insoluble porous materials is an effective strategy to realize the heterogenization of catalysts to simplify their recovery and even increase the specific surface areas of active phases due to the numerous pores of the host. In the following, we will introduce two main types of porous materials which have been used widely as supports for HPAs/POMs, namely, metal−organic frameworks (MOFs) and mesostructured silica.

1.3.1 Metal−organic frameworks (MOFs)

Metal-organic frameworks (MOFs), also known as porous coordination polymers (PCPs), are a new class of crystalline porous materials whose structure is composed of metal ions or clusters of metals (secondary building units, SBUs) and organic linkers connecting the SBUs by strong bonds (reticular synthesis).[65-68] The systematic design of the coordination polymers introducing organic molecular by Hoskins and Robson in 1990 is generally accepted as the beginning of a new chapter about the study of MOFs.[69] The discovery of MOF-5[70] and HKUST-1[71] in 1999 further promoted the devolvement of MOFs. Afterwards, MIL-100 and MIL-101 series materials were synthesized by Férey's group.[72-73] MIL series materials exhibit a high stability and several potential applications, which led to the fast increase of publications in this area[67, 74], as clearly shown in Figure 1-3. More than 10000 MOF structures have been discovered according to the Cambridge Structure Database (CSD).

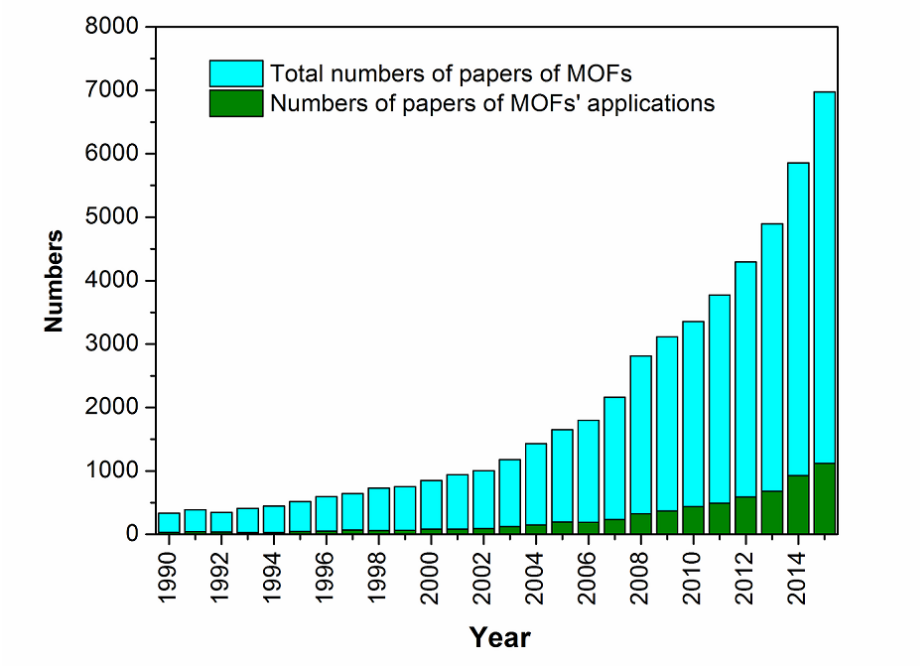

Figure 1-3 The variation tendency of academic papers about MOFs between 1990 and 2015.

MOFs have been mainly applied in gas storage, separations, catalysis and sensors due to their structural and functional flexibility and exceptional porosity.[21, 65, 75-79] However, compared with the studies about the development of new MOFs and the tuning of MOFs' structures, their applications were much less investigated (Figure 1-3). The applications of MOFs in catalysis can be roughly classified into two categories: catalysis using MOFs themselves as catalysts and MOFs as support. In the latter, three main types of MOFs have been studied as the supports, HKUST-1, MIL-101(Cr) and MIL-100(Fe), which are introduced here.

1.3.1.1 HKUST-1

HKUST-1 is one of the first discovered MOFs, whose raw formula is $[Cu_3(TMA)_2(H_2O)_3]_n$ (where TMA is benzene-1,3,5-tricarboxylate). As mentioned above, it was first synthesized by Chui *et al.* via a hydrothermal treatment in 1999.[71] HKUST-1 presents a three-dimensional (3D) structure with large square-shaped pores, whose size is about 1 nm. The octahedral units with Cu_2 dimers at its six vertices and four trimesate ions tetrahedrally disposed as "panels" for four of the eight triangular faces of the octahedron is the SBU of HKUST-1 which forms the framework through the corner sharing of each other, as shown in Figure 1-4.

The aqua ligands and Cu in the framework of HKUST-1 can be respectively replaced by pyridines and oxophilic metals (Os_2 and others), which reveals the appealing flexibility of this solid. Furthermore, HKUST-1 also possesses a good accessible porosity (~40.7% in the solid) and stability (stable up to 513 K according to the results of TGA analysis). It is these properties that attract researchers' attention on its potential applications. This framework has been applied in the separation and purification of mixed gases such as carbon dioxide–carbon monoxide, carbon dioxide–methane and ethylene–ethane mixtures[80], hydrogen and nitric oxide storage[81-82], the removal of Hg^{2+} from water[83] and supporting HPAs in heterogeneous catalysis[84].

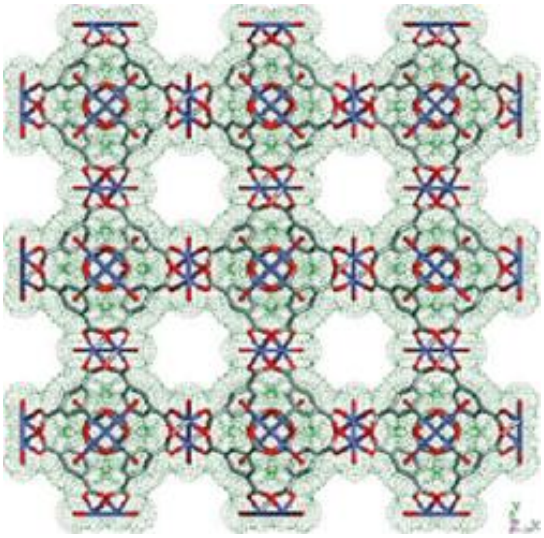

Figure 1-4 $[Cu_3(TMA)_2(H_2O)_3]_n$ polymer framework viewed down the [100] direction, showing nanochannels with fourfold symmetry.[71]

1.3.1.2 MIL-101(Cr)

MIL-101(Cr) was discovered by Ferey's group in 2005.[73] The raw formula of MIL-101(Cr) is $Cr_3F(H_2O)_2O(BDC)_3 \bullet nH_2O$ (where BDC is 1,4-benzene dicarboxylate). In 2012, Bromberg *et al.*[85] obtained the framework of MIL-101(Cr) without HF via a similar hydrothermal treatment. MIL-101(Cr) has zeotype cubic structure with very large pore sizes and surface area (BET area ~4100 cm^2/g). MIL-101(Cr) owns two types of quasi-spherical mesoporous cages limited by 12 pentagonal faces for the smaller and by 16 faces for the larger. The smaller cavities with the size of 29 Å are accessible through the pentagonal windows of 12 Å, while the large cavities with the size of 34 Å are communicated through the same pentagonal windows and the hexagonal windows of 15 Å (Figure 1-5).

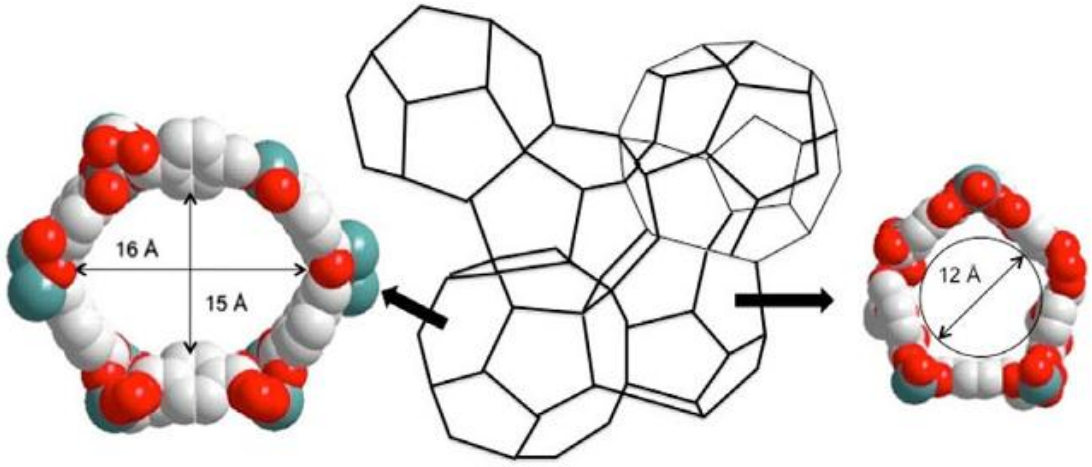

Figure 1-5 MIL-101(Cr) structure. (Left) Hexagonal windows; (center) zeotype structure; and (right) pentagonal windows. Red: oxygen; green: chromium; and white: carbon.[86]

Compared with HKUST-1, MIL-101(Cr) has larger surface areas and higher stability. The structure of MIL-101 can be intact over months under air atmosphere, various organic solvents at room temperature and under solvent thermal conditions. These properties make the framework an attractive material in gas storage and separation[87-89], heterogeneous catalysis[85-86, 90-93] and separation of substituted aromatics in liquid chromatography[94]. In particular, MIL-101(Cr) is a promising candidate as a support of soluble active phases like HPAs because their cages have enough space to load great amount of active phases whereas the windows with a smaller size than that of cages allow the diffusion of small molecules and prevent the leaching of supported active phases.

1.3.1.3 MIL-100(Fe)

MIL-100(Fe) was developed based on the structure of MIL-100(Cr) for the sake of less toxicity.[95] Its formula is $Fe^{III}_3O(H_2O)_2F\cdot\{C_6H_3(CO_2)_3\}_2\cdot nH_2O$ (n ~ 14.5). The framework also has a zeotype structure and the mesoporous cages with ca. 25 and 29

Å free diameters are accessible through pentagonal and hexagonal windows of free diameter close to 5.5 and 8.6 Å, respectively, as shown in Figure 1-6.

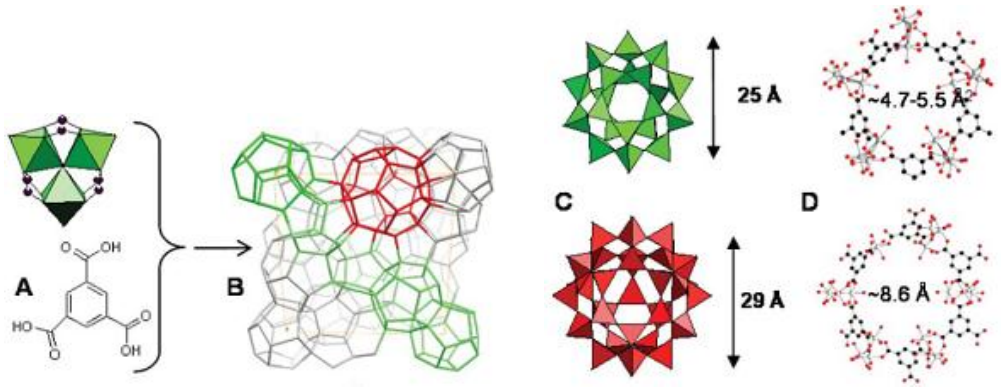

Figure 1-6 Structure of MIL-100(Fe). (A) A trimer of iron octahedra and trimesic acid. (B) Schematic view of one unit cell of MIL-100(Fe). (C) The two types of cages in polyhedral mode. (D) Pentagonal and hexagonal windows in balls and sticks (Fe: grey; O: red; C: black).[95]

As a member of MIL family, MIL-100(Fe) has a considerable porosity (Langmuir surface area ~ 2800 cm^2/g). Furthermore, the solid can be stable up to 543 K according to the results of X-ray thermodiffractometry. Due to these properties, MIL-100(Fe) has applications in gas storage and separation [87, 89], removal of organic dyes from water[96] and heterogeneous catalysis like Friedel–Crafts type reactions[95]. Because of its smaller windows compared to those of MIL-101(Cr), MIL-100(Fe) has a better capacity in preventing the leaching of some small supported active phase, together with the oxidation power and the less toxicity of Fe^{III}, which makes the application of MIL-100(Fe) in heterogeneous catalysis promising.

1.3.2 Mesoporous silica materials

Since mesoporous silica materials possess controllable and high-ordered porous

structures, high surface areas, thermal stabilities and excellent mechanical properties, they have been widely used in controlled release drug delivery [97-99], biosensing [98], catalysis[100-102], adsorption and separation[103] etc.

Since the discovery of the first mesoporous silica by Kresge and Beck in 1992[104-105], various silica materials with mesostructures have been developed. Among them, the most widely used are MCM-41[104], MCM-48[105] and SBA-15[106]. These three materials have a well-defined porous network with a very narrow distribution of the pore sizes. Their general synthesis is based on a self-assembled molecular array of surfactants as the structure-directing agent. The surfactants used consist of a hydrophilic head and a hydrophobic tail within the same molecule. When dissolved in an aqueous reaction media, they will self-organize in such a way that the contact surface between the hydrophobic tail and water is minimized (therefore, the energy of the system is minimal). Depending on the concentration and the temperature, different types of agglomerations can be obtained, like micelles, rods, or lamellar liquid crystals (Figure 1-7).[34]

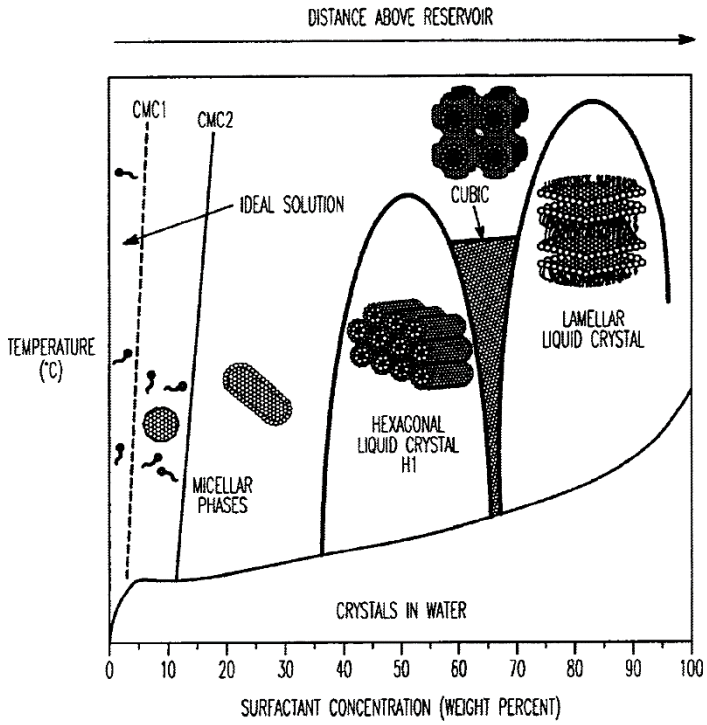

Figure 1-7 A schematic phase diagram for surfactants in water.[107]

In a general mesoporous silica synthesis, a silica source like tetraethyl orthosilicate (TEOS) is added into the aqueous surfactant solution. Hydrolysis and condensation leads to the formation of structured silica materials by self-assembly around the surfactant like cetyltrimethylammonium bromide (CTAB). This self-organization can take place by two different mechanisms. The first mechanistic model is that the liquid-crystal phase is already formed before the addition of the silicate species (liquid-crystal initiated pathway); the second is that the addition of the silica species induces ordering of silicate-encased surfactant micelles simultaneously, meaning that the micelle formation requires silicate (silicate initiated pathway). A schematic illustration of the two mechanisms is shown in Figure 1-8. The final silica is formed by condensation of the silica species in basic conditions as follows:

$Si(EtO)_4 + 4\ H_2O \rightarrow Si(OH)_4 + 4\ EtOH$

$n\ Si(OH)_4 \rightarrow OH–(Si(OH)_2)_n–Si(OH)_3 + (n-1)\ H_2O$

After the completion of the polymerization, the mesostructured silica is obtained by a calcination process to remove the surfactant, whereby the silica structure is the negative pattern of the surfactants' one. Therefore, the silica can have a hexagonal structure like MCM-41 and SBA-15 or cubic structure like MCM-48. The structural and physical properties, such as the geometry of the porous-network, the porosity, the pore-size and the wall thickness, can be controlled via the choice of the structure-directing template and/or the change of experimental conditions including the surfactants' concentration and the reaction temperature.

In the following, we will give a brief description of three common mesoporous silica in turn, MCM-41, MCM-48 and SBA-15, which have been used as catalyst supports.

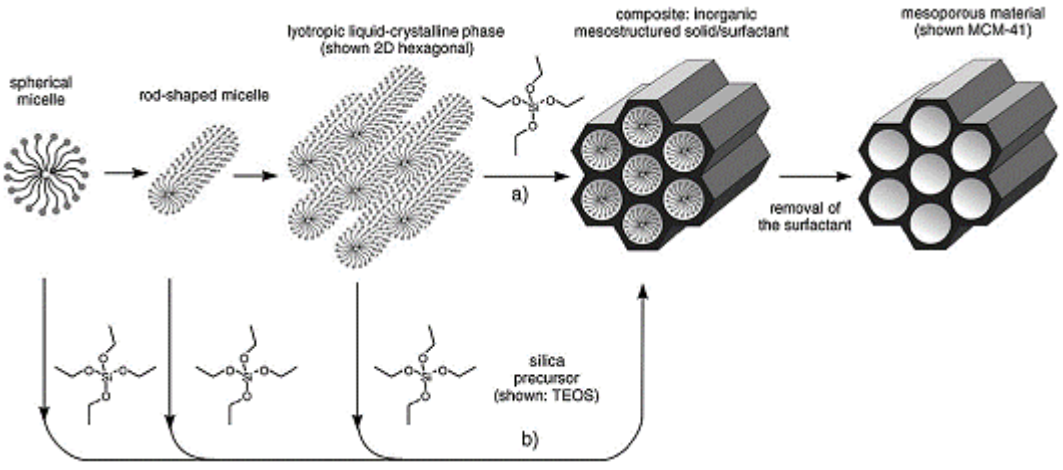

Figure 1-8 Liquid-crystal templating (LCT) mechanism of MCM-41: (a) the liquid-crystal-initiated and (b) the silicate-initiated pathways.[108]

1.3.2.1 MCM-41

MCM-41 was discovered by the Mobil Research and Development Corporation in 1992 as the first member of M41S materials,[105] which started the research of mesostructural materials. It has a 2-dimensional hexagonal structure with the unidirectional pores and the structure is often compared to a honeycomb, as is shown in Figure 1-9. As aforementioned, the preparation of MCM-41 is based on the LCT method, and the commonly used surfactant is CTAB. Generally, the specific surface area of MCM-41 is more than 1000 m^2/g, but decreases with increasing pore size which can vary in the range of 2-10 nm. The high-ordered structure with high surface areas and adjustable pore size bring many applications to MCM-41 in drug delivery system[109], absorption and separation[110], and heterogeneous catalysts[111]. As the support of heterogeneous catalysts, the 2-dimensional hexagonal structure facilitates the loading of active phase, on the other hand, the leaching of active phase easily take places as well.

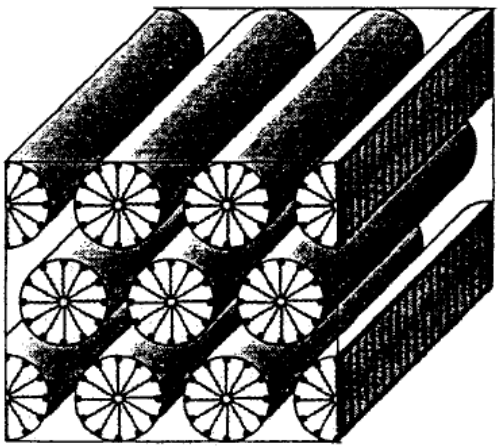

Figure 1-9 The structure of MCM-41.[112]

1.3.2.2 MCM-48

MCM-48 is another typical representative of M41S family. But the structure of MCM-48 is different from that of MCM-41 and is classified as a body-centered cubic structure, as shown in Figure 1-10. From the figure, one can see that this structure is three-dimensional, which gives MCM-48 opposite nature as a support of heterogeneous catalysts, compared with MCM-41, namely, a relatively difficult dispersion of active phase and a better resistance to the leaching. The synthesis of MCM-48 is same as that of MCM-41 except the different ratio of surfactants and water. The typical specific area of MCM-48 is also more than 1000 cm^2/g and varies with the pore sizes. The pore size of MCM-48 can be tuned to less than 2 nm,[113] which is favorable to the heterogenization of the catalysts with a small diameter of molecules.

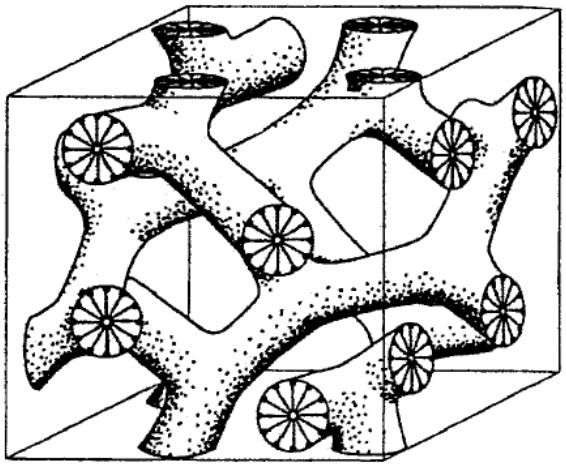

Figure 1-10 The structure of MCM-48.[112]

1.3.2.3 SBA-15

SBA-15 was first developed by Zhao *et al.* in 1998,[106] which is another milestone in the preparation of mesoporous materials. Similarly to MCM-41, SBA-15

is also of hexagonal type, but can the cylindrical pores are connected between each other by some small channels. Therefore the structure of SBA-15 is 3-dimensional and the interconnections bring micropores to SBA-15, as is shown in Figure 1-11. The synthesis of SBA-15 use another surfactant, $EO_{20}PO_{70}EO_{20}$ (Pluronic P123), which is a poly-triblock copolymer. The specific-surface of SBA-15 is generally less than 1000 m²/g and decreases when increasing the pore diameter. The pore sizes of SBA-15 can be tuned in the range of 5~30 nm via the reaction conditions, and/or the addition of a variety of poly-triblock copolymers or co-solvent organic molecules, 1,3,5-trimethylbenzene (TMB).[114]

SBA-15 silica is more widely used as a catalyst support for reactions in vapor-rich atmosphere due to its better hydrothermal stability than M41S materials, but their pore size is too large to prevent f HPAs leaching. Therefore, some modifications like the surface modification of SBA-15 by ammonia groups are utilized to create some chemical bonds to avoid the leaching of HPAs.[29, 115-117]

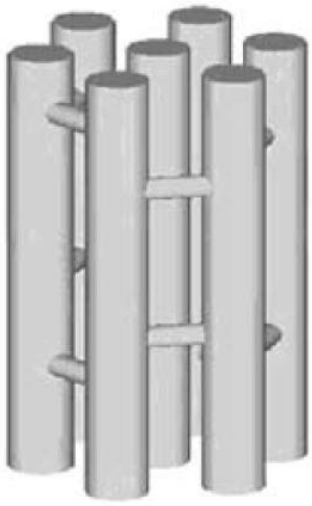

Figure 1-11 The structure of SBA-15.[118]

1.4 Strategies of heterogenizing HPAs/POMs into insoluble porous materials

As is well-known, heterogeneous catalysis is favorable in view of the principles of green chemistry: facilitating easy separation and recovery of the catalysts. Although Keggin-type HPAs and Keplerate-type POMs have been applied in heterogeneous catalysis in non-polar solvents, their high solubility in polar solvents (notably water) renders them into their homogeneous phase. In this case, the heterogenization of HPAs/POMs is of significance. Furthermore, in the case of HPAs, increasing the accessible surface active sites could be also considered in the heterogenization process because of the low surface area of bulk HPAs (5–10 m^2/g).[25] Therefore, insoluble porous materials have been chosen as supports for heterogenizing HPAs/POMs. There are three main strategies to carry out the heterogenization: impregnation, chemical immobilization and encapsulation. In the following, we will illustrate these three strategies successively.

1.4.1 Impregnation

Impregnation is heterogenizing of HPAs/POMs on supports through the free diffusion of molecules without any specific anchoring. It is a traditional method to prepare the heterogeneous catalysts. Acidic or neutral porous materials such as porous silica and active carbon are suitable as supports and related catalysts have been reported.[119-121]

Kozhevnikova *et al.* prepared silica-supported HPA catalysts by impregnating Aerosil 300 silica (S_{BET}~300 m^2/g) with $H_3PW_{12}O_{40}$ aqueous solutions with different concentrations of HPW and investigated their catalytic activities in the liquid-phase Fries rearrangement of aryl esters.[120] The HPW/SiO_2 catalyst with 40% of the HPW loading exhibited the best activity (conversion of aryl esters was 71% for 2 h), however, during the recycling reactions, the activity decreased gradually and the leaching of HPW occurred even in non-polar solvents such as dodecane, according to

the ICP results.

HPW was also dispersed in MIL-101(Cr) via the impregnation method by Juan-Alcañiz *et al.*[86] to compare with the HPW/MIL-101(Cr) catalysts obtained by the encapsulation method. The surface area of impregnated sample decreased more than for encapsulated samples, which indicates that HPW was correctly incorporated in the impregnated sample. However, the impregnated sample had a much worse performance than the encapsulated samples in the Knoevenage condensation of benzaldehyde and ethyl cyanoacetate, which may be a direct consequence of the lower specific surface area.

From the above, one can easily observe that heterogeneous catalysts obtained by the impregnation method cannot avoid the leaching of the HPA active phases due to the lack of interactions between active phases and supports, which is a serious drawback in liquid phase reactions. However, it should be noticed that this method is very simple and convenient and notably applicable in gas-solid reactions where the leaching of HPAs hardly happened.[28, 122]

From the above, one can easily observe that heterogeneous catalysts obtained by the impregnation method cannot avoid the leaching of the HPA active phases due to the lack of interactions between active phases and supports, which is a serious drawback in liquid phase reactions. However, it should be noticed that this method is very simple and convenient and notably applicable in gas-solid reactions where the leaching of HPAs hardly happened.[28, 122] For instance, Dufaud's group[122] dispersed $H_3PW_{12}O_{40}$ or $H_4SiW_{12}O_{40}$ on SBA-15 by incipient wetness impregnation. The resulting catalysts were active for the gas-phase isomerization of n-hexane, and $H_4SiW_{12}O_{40}$/SBA-15 catalyst exhibited a better selectivity for the isomerization than $H_3PW_{12}O_{40}$/ SBA-15 (89.7% vs 84.5% for 12 h).

1.4.2 Chemical immobilization

Chemical immobilization is an alternative heterogenization of HPAs/POMs through chemical bonds. In order to form the chemical bonds, functionalizing the support or the HPAs/POMs is essential.

The surface of supports can be modified by organic groups such as aminosilane groups.[123] Kaleta and his coworkers synthesized MCM-41 supported $H_6PMo_9V_3O_{40}$ catalysts (denoted as HPMoV/MCM-41) via this method.[124] An aminosilylation procedure for MCM-41 was made to introduce the amine groups inside the channels of the mesoporous material which would be able to react with heteropolyacid to form the ammonia salt $\equiv Si(CH_2)_3NH_3$ HPA, resulting in the strong anchoring of heteropolyanions. The catalytic properties of HPMoV/MCM-41 were studied in cyclohexane oxidation. The catalyst had an activity similar with that of free HPAs in the same amount and only 2% HPAs leaching occurred in a 2-run recycling experiment according to the ICP results, which shows that this method can effectively prevent the leaching of HPAs. However, it should be noticed that these strong interactions might lead to a minor distortion in the structure of the HPAs and a decreased acidity.[125]

Yang *et al.* [126] employed the opposite strategy to carry out the heterogenization of HPAs, using modified HPAs. A HPA-functionalized mesoporous hybrid silica was synthesized with TEOS and Keggin-type $SiW_{11}O_{39}^{8-}$ (SiW_{11}) as precursors in the presence of $EO_{20}PO_{70}EO_{20}$ (P123) as a block copolymer. The formation of this SiW_{11}/SBA-15 hybrid material was proposed to comprise two steps. In the first step, SiW_{11} reacted with TEOS first to form free $SiW_{11}Si_2$ molecules and then, in the second step, the $SiW_{11}Si_2$ penetrates into the pre-organized silica framework and reacts with the framework by condensation between Si-OH groups. Finally, SiW_{11} can be grafted on the surface of SBA-15, as is shown in Figure 1-12. This SiW_{11}/SBA-15 hybrid material has a better ability to resist to leaching of SiW_{11} than an impregnated sample

at room temperature. However, when the temperature was raised to 80 ˚C, 80% SiW_{11} leached into water after 5 h. Furthermore, only a small amount of free $SiW_{11}Si_2$ can penetrate into the framework of SBA-15. Therefore, this kind of grafting of HPAs is still problematic in actual liquid phase reactions.

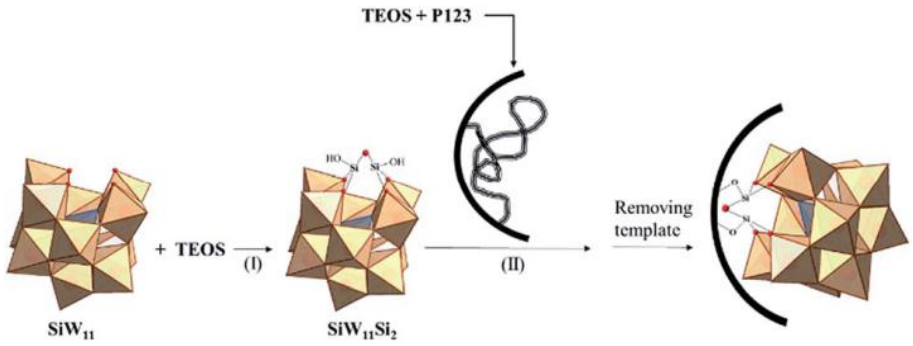

Figure 1-12 The illustration of incorporation of SiW_{11} and bonding with the framework.[20]

Villanneau's group combined the two strategies described above to heterogenize POMs, namely pre-functionalizing both the POMs and the supports.[127] They synthesized three different catalysts through changing the functionalized groups for the same support (amine vs. carboxylic acid for SBA-15) or changing the support itself (SBA-15 vs. mesocellular foams (MCF). The corresponding solids were denoted as POM-CO_2H@SBA-NH_2, POM-NH_2@SBA-CO_2H and POM-CO_2H@MCF-NH_2. Let's take POM-CO_2H@SBA-NH_2 as an example to illustrate this strategy. As shown in Figure 1-13, a vacant POM was derived to an organophosphonate comprising carboxylic acid groups, which can covalently link onto the NH_2-SBA-15 support by CO-NH bonds. Their catalytic properties were investigated for the epoxidation of cyclooctene with H_2O_2 and these three catalysts all showed activities, with the highest conversion of 97% after 24 h. The recyclability experiments and a filtration test performed in the case of the POM-CO_2H@SBA-NH_2 indicated that no significant

leaching of POMs took place during the reaction.

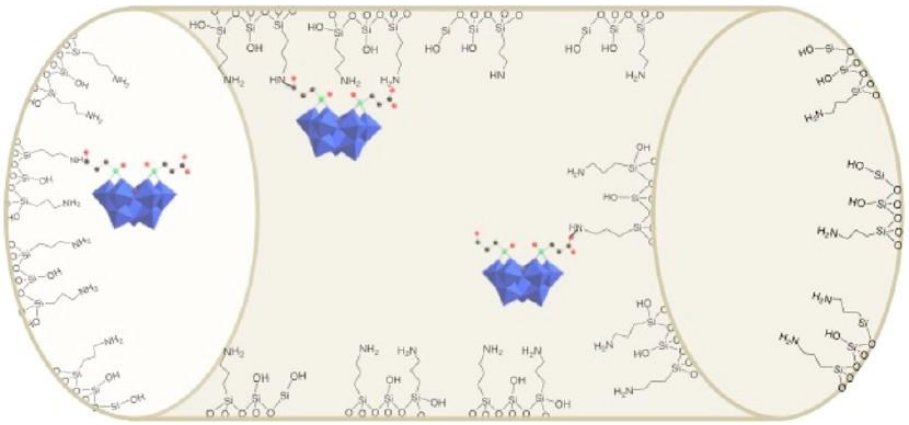

Figure 1-13 Covalent grafting of phosphonate derivatives of vacant POMs onto the walls of NH_2-functionalized SBA-15 silica. Counterions associated with the POMs are not represented for sake of clarity.[127]

1.4.3 Encapsulation

The encapsulation of HPAs/POMs into porous materials with a high surface area and suitable pore sizes is a promising method of heterogenization for improving their catalytic performance and recyclability because the leaching of HPAs/POMs is avoided through space confinement, not strong chemical bonds, whereby the characteristics of the HPA remain close to the free HPA. Many types of porous materials have been applied for the encapsulation of HPAs, including metal organic frameworks (MOFs), zeolites, mesoporous metal oxides and so on. Although the used materials are numerous, the encapsulation process can be classified into two major categories: the synthesis according to the concept of “building a bottle around the ship” and the synthesis according to the concept of “building a ship in the bottle”.

1.4.3.1 Concept of building of a bottle around the ship

The concept of building a bottle around the ship is illustrated in Figure 1-14. Here, HPAs/POMs molecules are the ships and the reactants for synthesizing the porous materials are the materials for building the bottle. During the synthesis, the pores of supports are formed around the HPAs/POMs molecules. Since the accessible windows of the pores are smaller than the diameter of the encapsulated HPAs/POMs molecules, the HPAs molecules can maintain inside the pores of supports. Most of the encapsulation of HPAs/POMs into MOFs follows this concept.

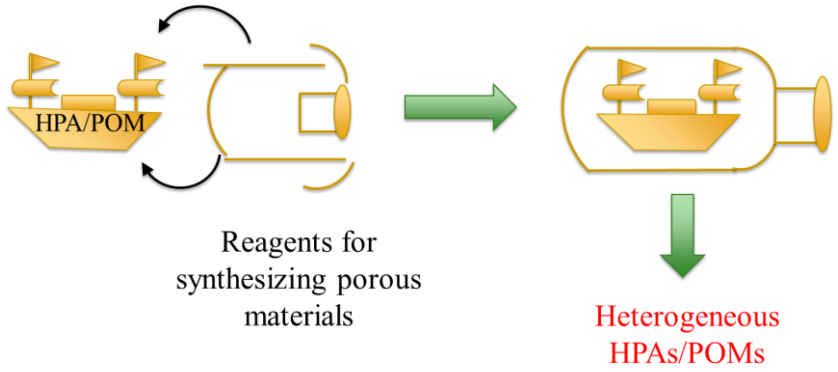

Figure 1-14 Schematic illustration of "building a bottle around the ship" synthesis.

Sun *et al.*[84] synthesized a series of remarkable crystalline compounds $[Cu_2(BTC)_{4/3}(H_2O)_2]_6[H_nXM_{12}O_{40}]\cdot(C_4H_{12}N)_2$ (where X=Si, Ge, P, As; M=W, Mo, BTC is benzenetricarboxylate) denoted as NENU-n (n = 1-6) using simple one-step hydrothermal reaction of copper nitrate, BTC and different Keggin HPAs. The loaded amount of HPAs was in the range from 35.4% to 47.1%. This framework is isostructural with HKUST-1, and there are two kinds of pores (A and B) in the structure, with free diameters of ca. 13 and 10 Å, accessible through the windows of ca. 11 and 9.3 Å, respectively (Figure 1-15). The authors claimed that the larger type

of pore, Pore A, accommodates the HPAs whereas the smaller type of pore, Pore B, cannot incorporate the HPAs and thus provides the access for the reactants. Their catalytic properties were investigated in the hydrolysis of esters in excess of water, which showed a high catalytic activity and reusability in at least 15-cycle without activity loss.

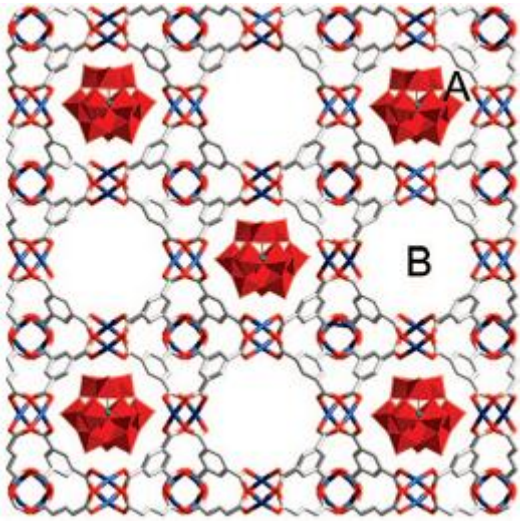

Figure 1-15 View of a (001) plan with two kinds of pores, A and B, in NENU-n (n=1-6). The Cu-BTC framework and Keggin polyanions are represented by wireframe and polyhedral models.[84]

Férey and coworkers demonstrated the feasibility of encapsulating HPAs into MIL-101(Cr) when they reported the discovery of this type of MOF.[73] Afterwards, Juan-Alcañiz *et al.* applied HPAs@MIL-101(Cr) in several liquid phase reactions including the Knoevenagel condensation of benzaldehyde with ethyl cyanoacetate and the esterification of n-butanol with acetic acid, and one gas phase condensation of methanol to dimethyl ether. In all these reactions, HPAs@MIL-101(Cr) catalysts exhibit a remarkable activity. No activity loss was observed during consecutive tests, and some samples were reused up to eight times. Bromberg *et al.* [85] also synthesized HPW@MIL-101(Cr) catalysts without HF via microwave-assisted heating, and

investigated their catalytic properties in the acetaldehyde-phenol condensation and dimethylacetal formation from benzaldehyde and methanol. Xiaofu Hu and coworkers [128] obtained the host-guest composite materials HPW@MIL-101(Cr) with different loading of HPW from 17~50 wt% and demonstrated their catalytic performance in the oxidative desulfurization process of the refractory sulfur-containing compounds.

Canioni *et al.* [129] successfully obtained HPMo@MIL-100(Fe). It is worth mentioning that the materials possesses a high porosity (Langmuir surface area ~ 1600 cm^2/g) and a remarkable stability (no POM leaching after 2 months in aqueous solution and no exchange by tetrabutylammonium perchlorate in organic media), which proofs its potential applications in the future.

1.4.3.2 Concept of building of a ship in the bottle

The concept of "building a ship in the bottle" is illustrated in Figure 1-16. Porous materials are prepared first to play the role of the bottle. During the synthesis, the HPA/POM molecules are formed inside the pores of supports. Due to the well-matched sizes of molecules and the pores of supports, HPA/POM molecules can be encapsulated inside the pores.

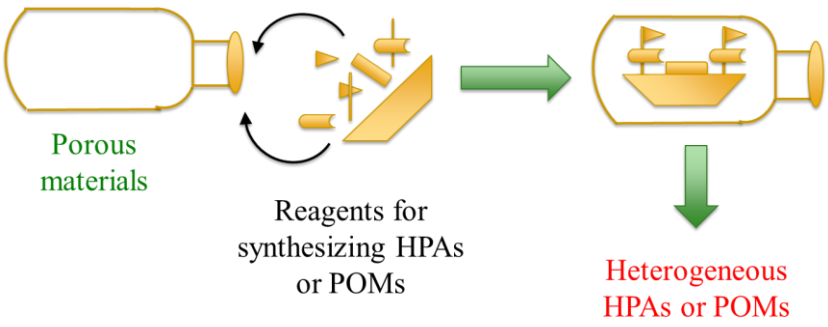

Figure 1-16 Schematic illustration of "building a bottle around the ship" synthesis.

Up to now, only the encapsulation of HPA/POM into Y-type zeolite follows the concept of "building a ship in the bottle". Sulikowski *et al.* firstly reported that HPW could be encapsulated in the supercages of Y-type zeolite in 1996.[130] Soon afterwards, Mukai *et al.* [131] encapsulated HPMo in dealuminated Y-type zeolite and investigated the influences of the Si/Al ratio and the type and amount of counter cations of the zeolite on the amount of encapsulation of HPMo. More HPAs/POMs@Y-type zeolite catalysts were synthesized based on the research of Mukai's group.[132-134]

These catalysts have been applied in the isomerization and disproportionation of m-xylene[130], the esterification of acetic acid with ethanol[131], the esterification of glycerol with acetic acid[134] and the photodegradation of the probe compound 1,2-dichlorobenzene (DCB) in water[132]. However, its activity is found lower than that of dissolved HPMo with the same amount. The authors claimed that only the PMo_{12} molecules in the supercages, which face the surface layer of HY contribute to the reaction. In fact, the size of a supercage (~1.3 nm) and a HPA anion (~1.2 nm) is so close so that the diffusion of reactant molecules is limited through the space between them. Therefore, if a HPA anion encapsulated in a supercage is surrounded by supercages which also encapsulate HPAs, it is not accessible for the reactants and thus the activity of catalysts is decreased.

Besides the above strategies of encapsulation of HPAs/POMs, some other methods have been developed recently. Dufaud's group synthesized $H_3PMo_{12}O_{40}$ encapsulated SBA-15, HPMo@SBA-15, by a one-pot encapsulation of HPMo into the walls of SBA-15 silica.[135] Tetraethoxysilane and HPMo were directly incorporated by using a sol–gel technique in the presence of a mixed structure-directing agents consisting of nonionic (Pluronic P123) and ionic (cetyltrimethylammonium bromide). The removal of the templates by calcination at 490 ˚C led to the partial destruction of HPMo in the hybrid material that was reconstructed by refluxing with methanol (Figure 1-17). HPMo@SBA-15 exhibited a nearly twice activity than the impregnated catalysts in the hydrogenation of toluene. The enhanced activity was believed to be

produced by a stronger stabilization of HPMo in the walls of SBA-15 and more acidic sites generated by the interactions between HPMo and SBA-15.

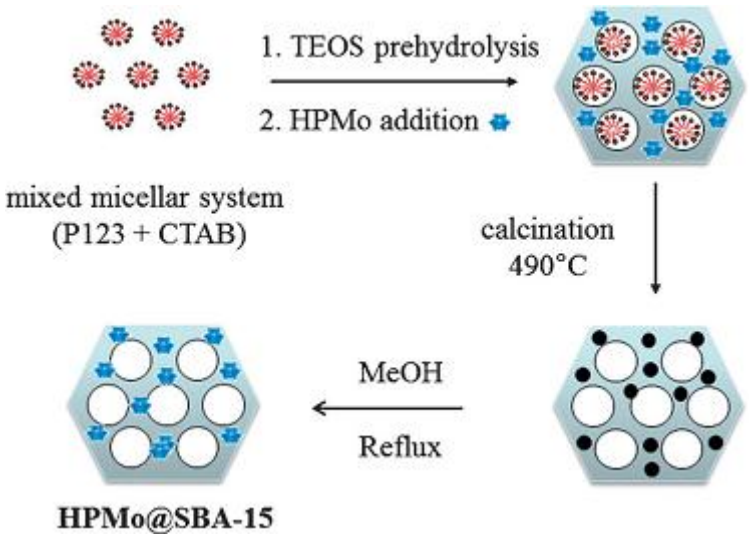

Figure 1-17 Synthetic strategy for the encapsulation and stabilization of HPMo within the silica framework. CTAB=cetyltrimethylammonium bromide; TEOS=tetraethoxysilane.[135]

1.5 The objectives of this thesis

Based on the literature survey, one can see that Keggin-type HPAs and Keplerate-type POMs both possess excellent catalytic properties, which makes them potential catalysts for biomass valorization in liquid phase reactions if their heterogenization can be solved successfully. Among various strategies of heterogenization of HPAs/POMs, the encapsulation is clearly the most promising method considering the restrain of the leaching of HPAs/POMs. Through the comparison of the advantages and disadvantages of the above porous materials in liquid phase reactions, MOFs and MCM-48 are suitable to encapsulate HPAs/POMs. Therefore, in this work, we will focus on the development of two heterogeneous

catalyst systems in the following:

The system of "building a bottle around the ship"

We will first encapsulate Keggin-type HPAs into MIL-101(Cr) and MIL-100(Fe) via a hydrothermal synthesis and optimize the synthetic conditions to obtain the catalysts with the best catalytic properties. After the completion of their preparation, the catalytic performance of the as-synthesized catalysts will be studied including the activity and the stability in recycling experiments.

The system of "building a ship in the bottle"

We will explore the method of encapsulating Keplerate-type $\{Mo_{132}\}$ into MCM-48. According to the previous paragraphs, the comparable size of the pores of MCM-48 and the diameter of $\{Mo_{132}\}$ and the unique three-dimensional structure of MCM-48 provide the feasibility of this encapsulation methodology. The obtained catalysts will also be applied in liquid phase reactions to evaluate their catalytic performance. .

1.6 Reference

[1] Y. Shi, C. Zhao, H. Wei, J. Guo, S. Liang, A. Wang, T. Zhang, J. Liu, T. Ma, Single-Atom Catalysis in Mesoporous Photovoltaics: The Principle of Utility Maximization. *Adv. Mater.* **2014,** *26* (48), 8147-8153.

[2] J. Burschka, N. Pellet, S.-J. Moon, R. Humphry-Baker, P. Gao, M. K. Nazeeruddin, M. Gratzel, Sequential deposition as a route to high-performance perovskite-sensitized solar cells. *Nature* **2013,** *499* (7458), 316-319.

[3] A. Kojima, K. Teshima, Y. Shirai, T. Miyasaka, Organometal Halide Perovskites as Visible-Light Sensitizers for Photovoltaic Cells. *J. Am. Chem. Soc.* **2009,** *131* (17), 6050-6051.

[4] X. Wang, K. Maeda, X. Chen, K. Takanabe, K. Domen, Y. Hou, X. Fu, M. Antonietti, Polymer Semiconductors for Artificial Photosynthesis: Hydrogen Evolution by Mesoporous Graphitic Carbon Nitride with Visible Light. *J. Am. Chem. Soc.* **2009,** *131* (5), 1680-1681.

[5] P. V. Tuza, R. L. Manfro, N. F. P. Ribeiro, M. M. V. M. Souza, Production of renewable hydrogen by aqueous-phase reforming of glycerol over Ni–Cu catalysts derived from hydrotalcite precursors. *Renewable Energy* **2013,** *50*, 408-414.

[6] R. Cortright, R. Davda, J. A. Dumesic, Hydrogen from catalytic reforming of biomass-derived hydrocarbons in liquid water. *Nature* **2002,** *418* (6901), 964-967.

[7] M. J. Climent, A. Corma, S. Iborra, Conversion of biomass platform molecules into fuel additives and liquid hydrocarbon fuels. *Green Chem.* **2014,** *16* (2), 516-547.

[8] P. Azadi, O. R. Inderwildi, R. Farnood, D. A. King, Liquid fuels, hydrogen and chemicals from lignin: A critical review. *Renewable and Sustainable Energy Reviews* **2013,** *21*, 506-523.

[9] R. A. Sheldon, Green and sustainable manufacture of chemicals from biomass: state of the art. *Green Chem.* **2014,** *16* (3), 950-963.

[10] A. Sivasamy, K. Y. Cheah, P. Fornasiero, F. Kemausuor, S. Zinoviev, S. Miertus, Catalytic applications in the production of biodiesel from vegetable oils. *ChemSusChem* **2009,** *2* (4), 278-300.

[11] K. Wu, Y. Wu, Y. Chen, H. Chen, J. Wang, M. Yang, Heterogeneous Catalytic Conversion of Biobased Chemicals into Liquid Fuels in the Aqueous Phase. *ChemSusChem* **2016,** *9* (12), 1355-1385.

[12] A. Corma, S. Iborra, A. Velty, Chemical Routes for the Transformation of Biomass into Chemicals. *Chem. Rev.* **2007,** *107* (6), 2411-2502.

[13] R. Karinen, K. Vilonen, M. Niemelä, Biorefining: heterogeneously catalyzed reactions of carbohydrates for the production of furfural and hydroxymethylfurfural. *ChemSusChem* **2011,** *4* (8), 1002-1016.

[14] W. R. H. Wright, R. Palkovits, Development of heterogeneous catalysts for the conversion of levulinic acid to γ-valerolactone. *ChemSusChem* **2012,** *5* (9), 1657-1667.

[15] J. Tian, J. Wang, S. Zhao, C. Jiang, X. Zhang, X. Wang, Hydrolysis of cellulose by the heteropoly acid H3PW12O40. *Cellulose* **2010,** *17* (3), 587-594.

[16] C. Sievers, I. Musin, T. Marzialetti, M. B. V. Olarte, P. K. Agrawal, C. W. Jones, Acid-catalyzed conversion of sugars and furfurals in an ionic-liquid phase. *ChemSusChem*

2009, *2* (7), 665-671.
[17] M. E. Himmel, S. Y. Ding, D. K. Johnson, W. S. Adney, M. R. Nimlos, J. W. Brady, T. D. Foust, Biomass recalcitrance: Engineering plants and enzymes for biofuels production. *Science* **2007,** *315* (5813), 804-807.
[18] Z. Zhang, M. D. Harrison, D. W. Rackemann, W. O. S. Doherty, I. M. O'Hara, Organosolv pretreatment of plant biomass for enhanced enzymatic saccharification. *Green Chem.* **2016,** *18* (2), 360-381.
[19] B. Katryniok, S. Paul, F. Dumeignil, Recent Developments in the Field of Catalytic Dehydration of Glycerol to Acrolein. *ACS Catal.* **2013,** *3* (8), 1819-1834.
[20] E. Rafiee, S. Eavani, Heterogenization of heteropoly compounds: a review of their structure and synthesis. *RSC Advances* **2016,** *6* (52), 46433-46466.
[21] J. Liu, L. Chen, H. Cui, J. Zhang, L. Zhang, C.-Y. Su, Applications of metal-organic frameworks in heterogeneous supramolecular catalysis. *Chem. Soc. Rev.* **2014**.
[22]S.-S. Wang, G.-Y. Yang, Recent Advances in Polyoxometalate-Catalyzed Reactions. *Chem. Rev.* **2015,** *115* (11), 4893-4962.
[23] Y. Izumi, R. Hasebe, K. Urabe, Catalysis by heterogeneous supported heteropoly acid. *J. Catal.* **1983,** *84* (2), 402-409.
[24] J. Keggin In *The structure and formula of 12-phosphotungstic acid*, Proceedings of the Royal Society of London A: Mathematical, Physical and Engineering Sciences, The Royal Society: 1934; pp 75-100.
[25] I. V. Kozhevnikov, Catalysis by heteropoly acids and multicomponent polyoxometalates in liquid-phase reactions. *Chem. Rev.* **1998,** *98* (1), 171-198.
[26] I. V. Kozhevnikov, K. I. Matveev, Homogeneous catalysts based on heteropoly acids (review). *Applied Catalysis* **1983,** *5* (2), 135-150.
[27] M. M. Heravi, S. Sadjadi, Recent developments in use of heteropolyacids, their salts and polyoxometalates in organic synthesis. *Journal of the Iranian Chemical Society* **2009,** *6* (1), 1-54.
[28] F. Jing, B. Katryniok, F. Dumeignil, E. Bordes-Richard, S. Paul, Catalytic selective oxidation of isobutane to methacrylic acid on supported (NH4)3HPMo11VO40 catalysts. *J. Catal.* **2014,** *309* (0), 121-135.
[29] B. Katryniok, S. Paul, M. Capron, C. Lancelot, V. Belli ère-Baca, P. Rey, F. Dumeignil, A long-life catalyst for glycerol dehydration to acrolein. *Green Chem.* **2010,** *12* (11), 1922-1925.
[30] I. V. Kozhevnikov, Sustainable heterogeneous acid catalysis by heteropoly acids. *J. Mol. Catal. A: Chem.* **2007,** *262* (1–2), 86-92.
[31]H. Lv, Y. V. Geletii, C. Zhao, J. W. Vickers, G. Zhu, Z. Luo, J. Song, T. Lian, D. G. Musaev, C. L. Hill, Polyoxometalate water oxidation catalysts and the production of green fuel. *Chem. Soc. Rev.* **2012,** *41* (22), 7572-7589.
[32] Y. Ding, W. Zhao, W. Song, Z. Zhang, B. Ma, Mild and recyclable catalytic oxidation of pyridines to N-oxides with H2O2 in water mediated by a vanadium-substituted polyoxometalate. *Green Chem.* **2011,** *13* (6), 1486-1489.
[33] S. S. Mal, N. H. Nsouli, M. Carraro, A. Sartorel, G. Scorrano, H. Oelrich, L. Walder, M. Bonchio, U. Kortz, Peroxo-Zr/Hf-Containing Undecatungstosilicates and -Germanates. *Inorg.*

Chem. **2010,** *49* (1), 7-9.
[34] B. Katryniok. Nouvelle voie de synthèse d'acroléine à partir de biomasse. Lille 1, 2010.
[35] I. V. Kozhevnikov, Advances in Catalysis by Heteropolyacids. *Russ. Chem. Rev.* **1987,** *56* (9), 811.
[36] N. Mizuno, T. Watanabe, M. Misono, Catalysis by heteropoly compounds. VIII. Reduction-oxidation and catalytic properties of 12-molybdophosphoric acid and its alkali salts. The role of redox carriers in the bulk. *The Journal of Physical Chemistry* **1985,** *89* (1), 80-85.
[37] S. M. Kulikov, I. V. Kozhevnikov, An investigation of the acid properties of heteropoly acids in acetone and acetic acid by the electrical conductivity method. *Bulletin of the Academy of Sciences of the USSR, Division of chemical science* **1981,** *30* (3), 348-353.
[38] R. S. Drago, J. A. Dias, T. O. Maier, An Acidity Scale for Brönsted Acids Including H3PW12O40. *J. Am. Chem. Soc.* **1997,** *119* (33), 7702-7710.
[39] J. Lan, J. Lin, Z. Chen, G. Yin, Transformation of 5-hydroxymethylfurfural (HMF) to maleic anhydride by aerobic oxidation with heteropolyacid catalysts. *ACS Catal.* **2015,** *5* (4), 2035-2041.
[40] J. H. Choi, T. H. Kang, J. H. Song, Y. Bang, I. K. Song, Redox behavior and oxidation catalysis of HnXW 12O40 (X = Co2 +, B3 +, Si 4 +, and P5 +) Keggin heteropolyacid catalysts. *Catal. Commun.* **2014,** *43*, 155-158.
[41] N. Mizuno, M. Misono, Catalytic oxidation and isotopic exchange of hydrogen over 12-tungstophosphoric acid. *The Journal of Physical Chemistry* **1989,** *93* (8), 3334-3339.
[42] M. Akimoto, K. Shima, H. Ikeda, E. Echigoya, 12-Heteropolymolybdates as catalysts for vapor-phase oxidative dehydrogenation of isobutyric acid. *J. Catal.* **1984,** *86* (1), 173-186.
[43] M. Misono, Heterogeneous Catalysis by Heteropoly Compounds of Molybdenum and Tungsten. *Catalysis Reviews* **1987,** *29* (2-3), 269-321.
[44] A. Alsalme, E. F. Kozhevnikova, I. V. Kozhevnikov, Heteropoly acids as catalysts for liquid-phase esterification and transesterification. *Appl. Catal. A* **2008,** *349* (1–2), 170-176.
[45] K.-i. Shimizu, H. Furukawa, N. Kobayashi, Y. Itaya, A. Satsuma, Effects of Brønsted and Lewis acidities on activity and selectivity of heteropolyacid-based catalysts for hydrolysis of cellobiose and cellulose. *Green Chem.* **2009,** *11* (10), 1627-1632.
[46] I. Kozhevnikov, S. Kulikov, N. Chukaeva, A. Kirsanov, A. Letunova, V. Blinova, Syntheses of vitamins E and K1 catalyzed by heteropoly acids. *React. Kinet. Catal. Lett.* **1992,** *47* (1), 59-64.
[47] J. E. Lyons, P. E. Ellis Jr, H. K. Myers Jr, G. Suld, W. A. Langdale, Oxidation of alkanes. Google Patents: 1989.
[48] E. G. Zhizhina, M. V. Simonova, V. F. Odyakov, K. I. Matveev, Homogeneous catalytic oxidation of propene to acetone and butene-1 to butanone in the presence of palladium and molybdovanadophosphoric heteropoly acid. *Appl. Catal. A* **2007,** *319*, 91-97.
[49] N. K. Raj, S. Deshpande, R. H. Ingle, T. Raja, P. Manikandan, Heterogenized molybdovanadophosphoric acid on amine-functionalized SBA-15 for selective oxidation of alkenes. *Catal. Lett.* **2004,** *98* (4), 217-224.
[50] S. Hong, J. Moffat, The oxidative dehydrogenation of ethane on silica-supported

metal-oxygen cluster compounds. *Appl. Catal. A* **1994,** *109* (1), 117-134.
[51] A. Müller, E. Krickemeyer, H. Bögge, M. Schmidtmann, F. Peters, Organizational Forms of Matter: An Inorganic Super Fullerene and Keplerate Based on Molybdenum Oxide. *Angew. Chem. Int. Ed.* **1998,** *37* (24), 3359-3363.
[52] C. Besson, S. Schmitz, K. M. Capella, S. Kopilevich, I. A. Weinstock, P. Kögerler, A regioselective Huisgen reaction inside a Keplerate polyoxomolybdate nanoreactor. *Dalton Trans.* **2012,** *41* (33), 9852-9854.
[53] A. Rezaeifard, R. Haddad, M. Jafarpour, M. Hakimi, Catalytic epoxidation activity of keplerate polyoxomolybdate nanoball toward aqueous suspension of olefins under mild aerobic conditions. *J. Am. Chem. Soc.* **2013,** *135* (27), 10036-10039.
[54] A. Muller, P. Gouzerh, From linking of metal-oxide building blocks in a dynamic library to giant clusters with unique properties and towards adaptive chemistry. *Chem. Soc. Rev.* **2012,** *41* (22), 7431-7463.
[55] A. Muller, L. Toma, H. Bogge, M. Henry, E. T. K. Haupt, A. Mix, F. L. Sousa, Reactions inside a porous nanocapsule/artificial cell: encapsulates' structuring directed by internal surface deprotonations. *Chem. Commun.* **2006,** (32), 3396-3398.
[56] C. Schäffer, H. Bögge, A. Merca, I. A. Weinstock, D. Rehder, E. T. K. Haupt, A. Müller, A Spherical 24 Butyrate Aggregate with a Hydrophobic Cavity in a Capsule with Flexible Pores: Confinement Effects and Uptake–Release Equilibria at Elevated Temperatures. *Angew. Chem. Int. Ed.* **2009,** *48* (43), 8051-8056.
[57] C. Schäffer, A. M. Todea, H. Bögge, O. A. Petina, D. Rehder, E. T. K. Haupt, A. Müller, Hydrophobic Interactions and Clustering in a Porous Capsule: Option to Remove Hydrophobic Materials from Water. *Chemistry – A European Journal* **2011,** *17* (35), 9634-9639.
[58] A. Ziv, A. Grego, S. Kopilevich, L. Zeiri, P. Miro, C. Bo, A. Müller, I. A. Weinstock, Flexible Pores of a Metal Oxide-Based Capsule Permit Entry of Comparatively Larger Organic Guests. *J. Am. Chem. Soc.* **2009,** *131* (18), 6380-6382.
[59] S. Biswas, D. Melgar, A. Srimany, A. Rodríguez-Fortea, T. Pradeep, C. Bo, J. M. Poblet, S. Roy, Direct Observation of the Formation Pathway of [Mo132] Keplerates. *Inorg. Chem.* **2016,** *55* (17), 8285-8291.
[60] X.-J. Kong, L.-S. Long, Z. Zheng, R.-B. Huang, L.-S. Zheng, Keeping the Ball Rolling: Fullerene-like Molecular Clusters. *Acc. Chem. Res.* **2010,** *43* (2), 201-209.
[61] A. A. Ostroushko, M. O. Tonkushina, A. P. Safronov, S. Y. Men'shikov, V. Y. Korotaev, Thermal behavior of polyoxometalate Mo132. *Russ. J. Inorg. Chem.* **2009,** *54* (2), 172-179.
[62] A. Rezaeifard, R. Haddad, M. Jafarpour, M. Hakimi, $\{Mo_{132}\}$ Nanoball as an Efficient and Cost-Effective Catalyst for Sustainable Oxidation of Sulfides and Olefins with Hydrogen Peroxide. *ACS Sustainable Chemistry & Engineering* **2014,** *2* (4), 942-950.
[63] F. Jalilian, B. Yadollahi, M. R. Farsani, S. Tangestaninejad, H. A. Rudbari, R. Habibi, New perspective to Keplerate polyoxomolybdates: Green oxidation of sulfides with hydrogen peroxide in water. *Catal. Commun.* **2015,** *66*, 107-110.
[64] F. Jalilian, B. Yadollahi, M. Riahi Farsani, S. Tangestaninejad, H. Amiri Rudbari, R. Habibi, Catalytic performance of Keplerate polyoxomolybdates in green epoxidation of alkenes with hydrogen peroxide. *RSC Advances* **2015,** *5* (86), 70424-70428.

[65] H. Furukawa, K. E. Cordova, M. O'Keeffe, O. M. Yaghi, The chemistry and applications of metal-organic frameworks. *Science* **2013,** *341* (6149), 1230444.
[66] J. R. Long, O. M. Yaghi, The pervasive chemistry of metal-organic frameworks. *Chem. Soc. Rev.* **2009,** *38* (5), 1213-1214.
[67] W. Lu, Z. Wei, Z.-Y. Gu, T.-F. Liu, J. Park, J. Park, J. Tian, M. Zhang, Q. Zhang, T. Gentle Iii, M. Bosch, H.-C. Zhou, Tuning the structure and function of metal-organic frameworks via linker design. *Chem. Soc. Rev.* **2014,** *43* (16), 5561-5593.
[68] H.-C. Zhou, J. R. Long, O. M. Yaghi, Introduction to Metal–Organic Frameworks. *Chem. Rev.* **2012,** *112* (2), 673-674.
[69] B. Hoskins, R. Robson, Design and construction of a new class of scaffolding-like materials comprising infinite polymeric frameworks of 3D-linked molecular rods. A reappraisal of the zinc cyanide and cadmium cyanide structures and the synthesis and structure of the diamond-related frameworks [N (CH3) 4][CuIZnII (CN) 4] and CuI [4, 4', 4", 4"'-tetracyanotetraphenylmethane] BF4. xC6H5NO2. *J. Am. Chem. Soc.* **1990,** *112* (4), 1546-1554.
[70] H. Li, M. Eddaoudi, M. O'Keeffe, O. M. Yaghi, Design and synthesis of an exceptionally stable and highly porous metal-organic framework. *Nature* **1999,** *402* (6759), 276-279.
[71] S. S.-Y. Chui, S. M.-F. Lo, J. P. Charmant, A. G. Orpen, I. D. Williams, A chemically functionalizable nanoporous material [Cu_3 (TMA) $_2$ (H_2O) $_3$] n. *Science* **1999,** *283* (5405), 1148-1150.
[72] G. Férey, C. Serre, C. Mellot‐Draznieks, F. Millange, S. Surblé, J. Dutour, I. Margiolaki, A hybrid solid with giant pores prepared by a combination of targeted chemistry, simulation, and powder diffraction. *Angew. Chem.* **2004,** *116* (46), 6456-6461.
[73] G. Férey, C. Mellot-Draznieks, C. Serre, F. Millange, J. Dutour, S. Surblé, I. Margiolaki, A chromium terephthalate-based solid with unusually large pore volumes and surface area. *Science* **2005,** *309* (5743), 2040-2042.
[74] S. Kitagawa, Metal–organic frameworks (MOFs). *Chem. Soc. Rev.* **2014,** *43* (16), 5415-5418.
[75] Z. Hu, B. J. Deibert, J. Li, Luminescent metal–organic frameworks for chemical sensing and explosive detection. *Chem. Soc. Rev.* **2014,** *43* (16), 5815-5840.
[76] J. Gascon, A. Corma, F. Kapteijn, F. X. Llabrés i Xamena, Metal Organic Framework Catalysis: Quo vadis? *ACS Catal.* **2014,** *4* (2), 361-378.
[77] J. Canivet, A. Fateeva, Y. Guo, B. Coasne, D. Farrusseng, Water adsorption in MOFs: fundamentals and applications. *Chem. Soc. Rev.* **2014**.
[78] M. Alhamami, H. Doan, C.-H. Cheng, A Review on Breathing Behaviors of Metal-Organic-Frameworks (MOFs) for Gas Adsorption. *Materials* **2014,** *7* (4), 3198.
[79] A. Dhakshinamoorthy, M. Alvaro, H. Garcia, Metal–organic frameworks as heterogeneous catalysts for oxidation reactions. *Catalysis Science & Technology* **2011,** *1* (6), 856-867.
[80] Q. M. Wang, D. Shen, M. Bülow, M. L. Lau, S. Deng, F. R. Fitch, N. O. Lemcoff, J. Semanscin, Metallo-organic molecular sieve for gas separation and purification. *Micropor.*

Mesopor. Mater. **2002,** *55* (2), 217-230.

[81] K. S. Lin, A. K. Adhikari, C. N. Ku, C. L. Chiang, H. Kuo, Synthesis and characterization of porous HKUST-1 metal organic frameworks for hydrogen storage. *Int. J. Hydrogen Energy* **2012,** *37* (18), 13865-13871.

[82] B. Xiao, P. S. Wheatley, X. Zhao, A. J. Fletcher, S. Fox, A. G. Rossi, I. L. Megson, S. Bordiga, L. Regli, K. M. Thomas, R. E. Morris, High-capacity hydrogen and nitric oxide adsorption and storage in a metal-organic framework. *J. Am. Chem. Soc.* **2007,** *129* (5), 1203-1209.

[83] F. Ke, L. G. Qiu, Y. P. Yuan, F. M. Peng, X. Jiang, A. J. Xie, Y. H. Shen, J. F. Zhu, Thiol-functionalization of metal-organic framework by a facile coordination-based postsynthetic strategy and enhanced removal of Hg 2+ from water. *J. Hazard. Mater.* **2011,** *196*, 36-43.

[84] C. Sun, S. Liu, D. Liang, K. Shao, Y. Ren, Z. Su, Highly stable crystalline catalysts based on a microporous metal− organic framework and polyoxometalates. *J. Am. Chem. Soc.* **2009,** *131* (5), 1883-1888.

[85] L. Bromberg, Y. Diao, H. Wu, S. A. Speakman, T. A. Hatton, Chromium (III) Terephthalate Metal Organic Framework (MIL-101): HF-Free Synthesis, Structure, Polyoxometalate Composites, and Catalytic Properties. *Chem. Mater.* **2012,** *24* (9), 1664-1675.

[86] J. Juan-Alcañiz, E. V. Ramos-Fernandez, U. Lafont, J. Gascon, F. Kapteijn, Building MOF bottles around phosphotungstic acid ships: One-pot synthesis of bi-functional polyoxometalate-MIL-101 catalysts. *J. Catal.* **2010,** *269* (1), 229-241.

[87] P. L. Llewellyn, S. Bourrelly, C. Serre, A. Vimont, M. Daturi, L. Hamon, G. De Weireld, J.-S. Chang, D.-Y. Hong, Y. Kyu Hwang, High Uptakes of CO2 and CH4 in Mesoporous Metal Organic Frameworks MIL-100 and MIL-101. *Langmuir* **2008,** *24* (14), 7245-7250.

[88] Y. Lin, C. Kong, L. Chen, Direct synthesis of amine-functionalized MIL-101 (Cr) nanoparticles and application for CO 2 capture. *RSC Advances* **2012,** *2* (16), 6417-6419.

[89] M. Latroche, S. Surblé, C. Serre, C. Mellot‐Draznieks, P. L. Llewellyn, J. H. Lee, J. S. Chang, S. H. Jhung, G. Férey, Hydrogen Storage in the Giant‐Pore Metal–Organic Frameworks MIL‐100 and MIL‐101. *Angew. Chem. Int. Ed.* **2006,** *45* (48), 8227-8231.

[90] A. E. R. S. Khder, H. M. A. Hassan, M. S. El-Shall, Metal-organic frameworks with high tungstophosphoric acid loading as heterogeneous acid catalysts. *Appl. Catal. A* **2014,** *487*, 110-118.

[91] E. Rafiee, N. Nobakht, Keggin type heteropoly acid, encapsulated in metal-organic framework: A heterogeneous and recyclable nanocatalyst for selective oxidation of sulfides and deep desulfurization of model fuels. *J. Mol. Catal. A: Chem.* **2015,** *398*, 17-25.

[92] Y. Zhang, V. Degirmenci, C. Li, E. J. Hensen, Phosphotungstic Acid Encapsulated in Metal–Organic Framework as Catalysts for Carbohydrate Dehydration to 5‐Hydroxymethylfurfural. *ChemSusChem* **2011,** *4* (1), 59-64.

[93] N. V. Maksimchuk, K. A. Kovalenko, S. S. Arzumanov, Y. A. Chesalov, M. S. Melgunov, A. G. Stepanov, V. P. Fedin, O. A. Kholdeeva, Hybrid Polyoxotungstate/MIL-101 Materials: Synthesis, Characterization, and Catalysis of H2O2-Based Alkene Epoxidation. *Inorg. Chem.* **2010,** *49* (6), 2920-2930.

[94] C.-X. Yang, X.-P. Yan, Metal–organic framework MIL-101 (Cr) for high-performance liquid chromatographic separation of substituted aromatics. *Anal. Chem.* **2011,** *83* (18), 7144-7150.

[95] P. Horcajada, S. Surble, C. Serre, D.-Y. Hong, Y.-K. Seo, J.-S. Chang, J.-M. Greneche, I. Margiolaki, G. Ferey, Synthesis and catalytic properties of MIL-100(Fe), an iron(iii) carboxylate with large pores. *Chem. Commun.* **2007,** (27), 2820-2822.

[96] S.-H. Huo, X.-P. Yan, Metal–organic framework MIL-100 (Fe) for the adsorption of malachite green from aqueous solution. *J. Mater. Chem.* **2012,** *22* (15), 7449-7455.

[97] J. L. Vivero-Escoto, I. I. Slowing, C.-W. Wu, V. S.-Y. Lin, Photoinduced intracellular controlled release drug delivery in human cells by gold-capped mesoporous silica nanosphere. *J. Am. Chem. Soc.* **2009,** *131* (10), 3462-3463.

[98] I. I. Slowing, B. G. Trewyn, S. Giri, V. Y. Lin, Mesoporous silica nanoparticles for drug delivery and biosensing applications. *Adv. Funct. Mater.* **2007,** *17* (8), 1225-1236.

[99] B. G. Trewyn, I. I. Slowing, S. Giri, H.-T. Chen, V. S.-Y. Lin, Synthesis and functionalization of a mesoporous silica nanoparticle based on the sol–gel process and applications in controlled release. *Acc. Chem. Res.* **2007,** *40* (9), 846-853.

[100] L. F. Gutiérrez, S. Hamoudi, K. Belkacemi, Synthesis of gold catalysts supported on mesoporous silica materials: Recent developments. *Catalysts* **2011,** *1* (1), 97-154.

[101] A. Corma, From microporous to mesoporous molecular sieve materials and their use in catalysis. *Chem. Rev.* **1997,** *97* (6), 2373-2420.

[102] H.-Y. Wu, X.-L. Zhang, X. Chen, Y. Chen, X.-C. Zheng, Preparation, characterization and catalytic properties of MCM-48 supported tungstophosphoric acid mesoporous materials for green synthesis of benzoic acid. *J. Solid State Chem.* **2014,** *211* (0), 51-57.

[103] H. Y. Huang, R. T. Yang, D. Chinn, C. L. Munson, Amine-grafted MCM-48 and silica xerogel as superior sorbents for acidic gas removal from natural gas. *Ind. Eng. Chem. Res.* **2003,** *42* (12), 2427-2433.

[104] J. S. Beck, J. C. Vartuli, W. J. Roth, M. E. Leonowicz, C. T. Kresge, K. D. Schmitt, C. T. W. Chu, D. H. Olson, E. W. Sheppard, A new family of mesoporous molecular sieves prepared with liquid crystal templates. *J. Am. Chem. Soc.* **1992,** *114* (27), 10834-10843.

[105] C. Kresge, M. Leonowicz, W. Roth, J. Vartuli, J. Beck, Ordered mesoporous molecular sieves synthesized by a liquid-crystal template mechanism. *Nature* **1992,** *359* (6397), 710-712.

[106] D. Zhao, J. Feng, Q. Huo, N. Melosh, G. H. Fredrickson, B. F. Chmelka, G. D. Stucky, Triblock copolymer syntheses of mesoporous silica with periodic 50 to 300 angstrom pores. *Science* **1998,** *279* (5350), 548-552.

[107] H. Fan, G. P. Lopez, C. J. Brinker, Y. Lu, Prototyping of patterned functional nanostructures. Google Patents: 2005.

[108] F. Hoffmann, M. Cornelius, J. Morell, M. Fröba, Silica - Based Mesoporous Organic–Inorganic Hybrid Materials. *Angew. Chem. Int. Ed.* **2006,** *45* (20), 3216-3251.

[109] M. Vallet-Regi, A. Ramila, R. Del Real, J. Pérez-Pariente, A new property of MCM-41: drug delivery system. *Chem. Mater.* **2001,** *13* (2), 308-311.

[110] Y. Belmabkhout, R. Serna-Guerrero, A. Sayari, Adsorption of CO2-containing gas mixtures over amine-bearing pore-expanded MCM-41 silica: application for gas purification. *Ind. Eng. Chem. Res.* **2009,** *49* (1), 359-365.

[111] K. Mukhopadhyay, B. R. Sarkar, R. V. Chaudhari, Anchored Pd complex in MCM-41 and MCM-48: novel heterogeneous catalysts for hydrocarboxylation of aryl olefins and alcohols. *J. Am. Chem. Soc.* **2002,** *124* (33), 9692-9693.

[112] K. Schumacher, P. I. Ravikovitch, A. Du Chesne, A. V. Neimark, K. K. Unger, Characterization of MCM-48 Materials. *Langmuir* **2000,** *16* (10), 4648-4654.

[113] M. Widenmeyer, R. Anwander, Pore Size Control of Highly Ordered Mesoporous Silica MCM-48. *Chem. Mater.* **2002,** *14* (4), 1827-1831.

[114] J. Zhu, Z. Kónya, V. F. Puntes, I. Kiricsi, C. Miao, J. W. Ager, A. P. Alivisatos, G. A. Somorjai, Encapsulation of metal (Au, Ag, Pt) nanoparticles into the mesoporous SBA-15 structure. *Langmuir* **2003,** *19* (10), 4396-4401.

[115] N. K. K. Raj, S. S. Deshpande, R. H. Ingle, T. Raja, P. Manikandan, Heterogenized molybdovanadophosphoric acid on amine-functionalized SBA-15 for selective oxidation of alkenes. *Catal. Lett.* **2004,** *98* (4), 217-223.

[116] S. Wu, J. Wang, W. Zhang, X. Ren, Preparation of Keggin and Preyssler heteropolyacid catalysts on amine-modified SBA-15 and their catalytic performances in esterification of n-butanol with acetic acid. *Catal. Lett.* **2008,** *125* (3-4), 308-314.

[117] A. Popa, V. Sasca, O. Verdes, C. Ianasi, R. Banica, Heteropolyacids anchored on amino-functionalized MCM-41 and SBA-15 and its application to the ethanol conversion reaction. *J. Therm. Anal. Calorim.* **2016**, 1-16.

[118] W. Yue, W. Zhou, Crystalline mesoporous metal oxide. *Progress in Natural Science* **2008,** *18* (11), 1329-1338.

[119] G. S. Kumar, M. Vishnuvarthan, M. Palanichamy, V. Murugesan, SBA-15 supported HPW: Effective catalytic performance in the alkylation of phenol. *J. Mol. Catal. A: Chem.* **2006,** *260* (1), 49-55.

[120] E. F. Kozhevnikova, E. Rafiee, I. V. Kozhevnikov, Fries rearrangement of aryl esters catalysed by heteropoly acid: catalyst regeneration and reuse. *Appl. Catal. A* **2004,** *260* (1), 25-34.

[121] J. Kaur, K. Griffin, B. Harrison, I. Kozhevnikov, Friedel–Crafts acylation catalysed by heteropoly acids. *J. Catal.* **2002,** *208* (2), 448-455.

[122] T. Pinto, V. Dufaud, F. Lefebvre, Isomerization of n-hexane on heteropolyacids supported on SBA-15. 1. Monofunctional impregnated catalysts. *Appl. Catal. A* **2014,** *483*, 103-109.

[123] P. Van Der Voort, E. Vansant, Modification of the silica surface with aminosilanes. *Pol. J. Chem.* **1997,** *71* (5), 550-567.

[124] W. Kaleta, K. Nowinska, Immobilisation of heteropoly anions in Si-MCM-41 channels by means of chemical bonding to aminosilane groups. *Chem. Commun.* **2001,** (6), 535-536.

[125] M. H. Haider, N. F. Dummer, D. Zhang, P. Miedziak, T. E. Davies, S. H. Taylor, D. J. Willock, D. W. Knight, D. Chadwick, G. J. Hutchings, Rubidium-and caesium-doped

silicotungstic acid catalysts supported on alumina for the catalytic dehydration of glycerol to acrolein. *J. Catal.* **2012,** *286*, 206-213.

[126] R. Zhang, C. Yang, A novel polyoxometalate-functionalized mesoporous hybrid silica: synthesis and characterization. *J. Mater. Chem.* **2008,** *18* (23), 2691-2703.

[127] F. Bentaleb, O. Makrygenni, D. Brouri, C. Coelho Diogo, A. Mehdi, A. Proust, F. Launay, R. Villanneau, Efficiency of Polyoxometalate-Based Mesoporous Hybrids as Covalently Anchored Catalysts. *Inorg. Chem.* **2015,** *54* (15), 7607-7616.

[128] X. Hu, Y. Lu, F. Dai, C. Liu, Y. Liu, Host–guest synthesis and encapsulation of phosphotungstic acid in MIL-101 via " bottle around ship": an effective catalyst for oxidative desulfurization. *Micropor. Mesopor. Mater.* **2013,** *170*, 36-44.

[129] R. Canioni, C. Roch-Marchal, F. Sécheresse, P. Horcajada, C. Serre, M. Hardi-Dan, G. Férey, J.-M. Grenèche, F. Lefebvre, J.-S. Chang, Stable polyoxometalate insertion within the mesoporous metal organic framework MIL-100 (Fe). *J. Mater. Chem.* **2011,** *21* (4), 1226-1233.

[130] B. Sulikowski, J. Haber, A. Kubacka, K. Pamin, Z. Olejniczak, J. Ptaszyński, Novel "ship-in-the-bottle" type catalyst: evidence for encapsulation of 12-tungstophosphoric acid in the supercage of synthetic faujasite. *Catal. Lett.* **1996,** *39* (1-2), 27-31.

[131] S. R. Mukai, T. Masuda, I. Ogino, K. Hashimoto, Preparation of encaged heteropoly acid catalyst by synthesizing 12-molybdophosphoric acid in the supercages of Y-type zeolite. *Appl. Catal. A* **1997,** *165* (1–2), 219-226.

[132] R. R. Ozer, J. L. Ferry, Photocatalytic Oxidation of Aqueous 1,2-Dichlorobenzene by Polyoxometalates Supported on the NaY Zeolite. *J Phys. Chem. B.* **2002,** *106* (16), 4336-4342.

[133] S. R. Mukai, M. Shimoda, L. Lin, H. Tamon, T. Masuda, Improvement of the preparation method of "ship-in-the-bottle" type 12-molybdophosphoric acid encaged Y-type zeolite catalysts. *Appl. Catal. A* **2003,** *256* (1), 107-113.

[134] P. Ferreira, I. M. Fonseca, A. M. Ramos, J. Vital, J. E. Castanheiro, Esterification of glycerol with acetic acid over dodecamolybdophosphoric acid encaged in USY zeolite. *Catal. Commun.* **2009,** *10* (5), 481-484.

[135] S. Silva, A. Chaumonnot, A. Bonduelle-Skrzypczak, F. Lefebvre, S. Loridant, V. Dufaud, Towards the improvement of hydrotreatment catalysts through the encapsulation of heteropolyoxometalates inside the framework of SBA-15 silica. *ChemCatChem* **2014,** *6* (2), 464-467.

2 Study of the encapsulation of Keggin-type Heteropolyacids (HPAs) in Metal-Organic Frameworks (MOFs)

2.1 Introduction

Keggin-type heteropolyacids (HPAs) are economically and environmentally attractive catalysts for biomass valorization due to their easy syntheses and adjustable acid and redox properties. Many studies of HPA catalysts in non-polar solvents have been reported in the recent years.[1-4] However, their application as heterogeneous catalysts in liquid phase reactions is largely hampered by their solubility in polar solvents. Nevertheless, with respect to the valorization of biomass, the use of these polar solvents (notably water), is of large interest and in-line with the principles of Green Chemistry. Hence, the development of innovative solid heterogeneous HPA-based catalysts resistant to the leaching phenomenon is of high significance.

As mentioned in the first chapter, among the various strategies followed to heterogenize HPAs efficiently, the encapsulation of HPAs into porous materials such as Metal−Organic Frameworks (MOFs) is one of the most promising options. In this work, we focused on the preparation of heterogeneous HPAs@MOFs according to the concept of "building of a bottle around the ship" (Figure 1-14), which has been described in Chapter 1. In Férey *et al.*'s work, the feasibility of encapsulating HPAs into MIL-101(Cr) has been reported.[5] Afterward, several groups have modified the synthetic method of HPAs@MIL-101(Cr). Among these modifications, the influence of adding of HF or not, adjusting pH value of initial reaction mixture or not and of the amount of HPA did not have a definite conclusion. Therefore, a systematic study about the influences of these three factors on the physicochemical properties and catalytic performance of HPAs@MIL-101(Cr) successively is still missing. It will be completed in this thesis.

Besides the studies about the synthesis of HPAs@MIL-101(Cr), their catalytic properties in liquid phase reactions have also been explored.[6-12] At the same time, another MOF material, MIL-100(Fe), also attracted more and more attention as an alternative to encapsulate HPAs in reason of its lower toxicity (absence of Cr) and of the lower window size of its cages. Canioni and co-workers have successfully carried

out the encapsulation of HPAs in MIL-100(Fe) and also demonstrated that $H_3PMo_{12}O_{40}$@MIL-100(Fe) has potential applications in catalysis due to its stability in aqueous solution and maintained porosity after encapsulation.[13] We therefore chose the epoxidation of cyclooctene to investigate its catalytic properties. To the best of our knowledge, no report is available about the catalytic performance of $H_3PMo_{12}O_{40}$@MIL-100(Fe) in this reaction.

In the present work, we chose two typical Keggin-type HPAs, $H_3PW_{12}O_{40}$ (HPW) and $H_3PMo_{12}O_{40}$ (HPMo) as the active phases, which have been proved to have good performances in acid-catalyzed and oxidation reactions, respectively. All samples were synthesized via a hydrothermal treatment based on the concept of "building a bottle around the ship". In the synthesis of HPW@MIL-101(Cr), the influence of the addition of HF, of the pH and of the amount of HPAs was studied to establish the most suitable method of preparation. Esterification of n-butanol and acetic acid and epoxidation of cyclooctene were chosen as model reactions to determine the catalytic properties of the as-prepared acid (respectively redox) catalysts. Recycling experiments were also performed for these catalysts in order to evaluate their stabilities in the liquid phase reactions.

2.2 Experimental

2.2.1 Chemicals Chemicals

Chromium (III) nitrate nonahydrate ($Cr(NO_3)_3 \cdot 9H_2O$; 99%), terephthalic acid [1,4-benzenedicarboxylic acid] (C_6H_4-$(COOH)_2$; 98%), phosphomolybdic acid ($H_3PMo_{12}O_{40} \cdot xH_2O$, 99%) phosphotungstic acid ($H_3PW_{12}O_{40} \cdot xH_2O$; 99%) hydrofluoric acid (HF; 48%), iron(III) chloride hexahydrate ($FeCl_3 \cdot 6H_2O$, ACS reagent, 97%), trimethyl 1,3,5-benzenetricarboxylate ($C_6H_3(CO_2CH_3)_3$, 98%), n-butanol ($CH_3(CH_2)_3OH$, 99.5%), acetic acid (CH_3COOH, ACS reagent, ⩾99.7%), cis-cyclooctene (C_8H_{14}, contains 100-200 ppm Irganox 1076 FD as antioxidant, 95%) and hydrogen peroxide solution (H_2O_2, ⩾30%, for trace analysis), were purchased

from Sigma Aldrich and used as received without further purification.

2.2.2 Catalysts preparations

2.2.2.1 MIL-101(Cr)

MIL-101(Cr) was synthesized hydrothermally either adding HF or not. The method with HF is based on the procedure described by Férey *et al.*[5]:

0.44 mL of hydrofluoric acid was added into a solution of 4 g of chromium (III) nitrate nonahydrate ($Cr(NO_3)_3 \cdot 9H_2O$) in 48 mL of water. 1.66 g of terephthalic acid (denoted as H_2BDC) was further added into the solution after 10 min stirring. When the mixture became a well-distributed suspension, it was introduced in a Teflon-lined autoclave, which was heated at 473 K for 8 h.

The synthesis without HF followed the same procedure, the only difference being the absence of HF.

In both syntheses, after natural cooling, the solid obtained was washed with water, DMF and ethanol, separated from the liquid by centrifugation and then dried at 353 K overnight. The resulting solids were extracted by a Soxhlet extractor in methanol overnight, then dispersed in 96% ethanol and heated at 373 K for 20 h in a Teflon-lined autoclave. Green solids were obtained finally after drying at 353 K overnight. The samples were denoted as MIL-101(Cr)-no HF and MIL-101(Cr)-HF, respectively to distinguish the method of synthesis.

2.2.2.2 HPAs@MIL-101(Cr)

The typical synthesis of HPAs@MIL-101(Cr) is based on the procedure described by Zhang[9] :

4 g of chromium (III) nitrate nonahydrate ($Cr(NO_3)_3 \cdot 9H_2O$) are dissolved into a solution of 3 g of phosphotungstic acid ($H_3PW_{12}O_{40} \cdot xH_2O$) or phosphomolybdic acid ($H_3PMo_{12}O_{40} \cdot xH_2O$) in 48 mL of water. After a clear solution is obtained, further

addition of 0.44 mL of hydrofluoric acid solution was stirred for 10 min and then terephthalic acid H_2BDC (1.66 g, 10 mmol) was added to the mixture. After sufficient stirring, the solution pH was 1.16. This mixture was placed in a Teflon-lined autoclave and heated to 493 K for 8 h. After cooling, the reaction mixture was separated by centrifugation and the solid was washed by water, DMF and ethanol, and finally dried at 353 K overnight. The obtained solids were extracted in methanol overnight using a Soxhlet, and then dispersed in 96% ethanol and heated at 373 K for 20 h in a Teflon-lined autoclave. The resulting solid was dried at 353 K in an oven, and denoted as HPW@MIL-101(Cr) (encapsulated $H_3PW_{12}O_{40} \cdot xH_2O$) or HPMo@MIL-101(Cr) (encapsulated $H_3PMo_{12}O_{40} \cdot xH_2O$).

In order to optimize the synthetic conditions, samples with different pH value and different amounts of HPAs were synthesized. The sample prepared without HF was synthesized in the same conditions as for the typical synthesis except that HF is not added. The corresponding samples were denoted respectively as HPW@MIL-101(Cr)-HF and HPW@MIL-101(Cr)-no HF.

The adjustment of pH was made after all reactants were added including $Cr(NO_3)_3 \cdot 9H_2O$, $H_3PW_{12}O_{40} \cdot x\ H_2O$, HF and H_2BDC. NaOH was used to adjust the pH to 2.6, because 2.6 is the pH value of the initial reaction mixture of MIL-101(Cr) without HPAs. Other experimental conditions were the same as for HPW@MIL-101(Cr). The sample was denoted as HPW@MIL-101(Cr)-pH 2.6.

The amounts of $H_3PW_{12}O_{40} \cdot xH_2O$ added were 0.5 g, 1 g, 2 g and 3 g respectively to obtain samples with different loadings of HPAs. Other experimental conditions were the same as for HPW@MIL-101(Cr). The samples with different loadings are designed hereafter as HPW(0.5)@MIL-101(Cr), HPW(1)@ MIL-101(Cr), HPW(2)@ MIL-101(Cr) and HPW(3)@ MIL-101(Cr).

2.2.2.3 MIL-100(Fe)

MIL-100(Fe) synthesis is based on the procedure described by Canioni *et al.*[13]:

A mixture of 1.62 g of $FeCl_3\ 6H_2O$ and 1.39 g of trimethyl 1,3,5-benzenetricarboxylate (denoted as 1,3,5-BTC) was dispersed in 50 mL of water and then heated for three days at 403 K in a Teflon-lined autoclave. The resulting orange solid was recovered by centrifugation, washed with acetone and ether, and dried under air. The sample was denoted as MIL-100(Fe).

2.2.2.4 HPAs@MIL-100(Fe)

1.89 g of $FeCl_3\ 6H_2O$ was dissolved into a solution of 3 g of $H_3PW_{12}O_{40}\ xH_2O$ or $H_3PMo_{12}O_{40}\ xH_2O$ in 50 mL of water. 1.36 g 1,3,5-BTC was further added into the solution after 10 minutes of stirring. The mixture was heated for three days at 403 K in a Teflon-lined autoclave. Finally, the orange solid was recovered by centrifugation and washed with ethanol, acetone and ether. The samples were denoted as HPW@MIL-100(Fe) or HPMo@MIL-100(Fe).

2.2.3 Catalysts characterization

The as-prepared MOFs and catalysts were characterized using X-Ray Diffraction, nitrogen adsorption/desorption, Scanning and Transmission Electron Microscopies, Fourier Transformed Infrared Spectroscopy and Solid-state Nuclear Magnetic Resonance. The atomic composition of the catalysts was determined by elementary analysis. Details about these techniques are given in the following paragraphs.

2.2.3.1 X-Ray Diffraction

The crystal structure of the supports and catalysts were revealed by X-Ray Diffraction (XRD) on a Bruker D8 diffractometer using a CuKα radiation (λ=0.15406 nm) as an X-ray source. A range of $3° < 2\theta < 12°$ was scanned with a step of 0.01 °/s and an integration time of 2 s.

2.2.3.2 Nitrogen adsorption/desorption

A Micromeritics ASAP 2010 analyzer was used to measure the textural properties of materials including the specific surface area, pore size distribution and pore volume using N_2 adsorption/desorption experiments at liquid nitrogen temperature. Prior to analysis, the samples were degassed at 423 K for 3 h. The specific surface area (S_{BET}) was calculated using the linear part of the B.E.T plot. The mesoporous size distributions were obtained by applying the Barrett-Joyner-Halenda (BJH) equation to the desorption branch of isotherms. The total pore volume (V_p) was made using the value at relative pressure P/P_0 value of 0.995.

2.2.3.3 Transmission Electron Microscopy

The Transmission Electron Microscopy (TEM) observations of the samples were carried out on a FEI Tecnai F30 electron microscope, operating at 300 kV. The samples were dispersed by ultrasound in ethanol and a drop of suspension was deposited onto a 400 microscope copper grid covered with carbon film.

2.2.3.4 Scanning Electron Microscopy and Energy-dispersive X-ray Spectroscopy

Scanning electron microscopy (SEM) images of some samples were recorded on Hitachi S-4800 instrument, operating at 15.0 kV. The samples were dispersed in ethanol and a drop of suspension was deposited onto a silicon wafer as a holder. Some samples' images were taken using a scanning electron microscope (Hitachi S3600N SEM) equipped with an EDX detector (Thermo Ultra Dry) under an acceleration voltage of 15 kV. The EDX data was obtained from four different areas of one sample.

2.2.3.5 Fourier Transformed Infrared Spectroscopy

Fourier Transformed Infrared (FT-IR) Spectra were recorded with a Nicolet

Protégé 460 FT-IR spectrometer equipped with a MCT detector at 4 cm^{-1} optical resolution from 400 to 4000 cm^{-1}. Prior to the measurements, the samples were pressed with KBr.

2.2.3.6 Solid-state Nuclear Magnetic Resonance

^{31}P MAS NMR spectra were conducted on a Bruker Avance 400 spectrometer with a 4 mm probe operated with at 9.4 T (Larmor frequency 161.9 MHz). The spinning speed was 10 kHz and the pulse length was 4 microseconds (radio frequency field 62.5 KHz). The chemical shifts of ^{31}P nuclei are given relative to H_3PO_4 at 0 ppm.

2.2.3.7 Inductively Coupled Plasma Optical Emission Spectroscopy

The samples were analysed by Inductively Coupled Plasma Optical Emission Spectroscopy (ICP-OES) using an Agilent 700 Series ICP-OES to determine the contents of chromium, iron, phosphorus, tungsten and molybdenum.

2.2.4 Catalytic reactions

2.2.4.1 Esterification of n-butanol and acetic acid

Every sample was heated at 423 K under vacuum overnight prior to the reaction in order to activate them. The esterification of n-butanol and acetic acid was performed without solvent using an equimolar ratio of the reactants, i.e. loading 3.71 g of n-butanol with 3 g of acetic acid [14] in a Radley carousel reaction station (Figure 2-1), while being stirred at 383 K for 4 h. 0.15 g catalyst was used in each reaction. After completion of the reaction, the solid catalyst was removed by centrifugation and washed with ethanol and dried at 313 K overnight for the next run. The filtrate was diluted using methanol to 10-fold and the 0.5 μL of the diluted solution was analysed by gas chromatography equipped with FID detector and an Alltech® EC-1000 capillary column (30 m × 0.53 mm × 1.2 μm). The conversion of n-butanol and acetic

acid, the yield of butyl acetate and the selectivity of butyl acetate were calculated as follows:

Conversion (%)

$$X = \frac{n_0 - n}{n_0} \times 100\%$$

Where n_0 is the number of mole of acetic acid (or n-butanol) initially introduced in the reactor and n is the final number of mole of acetic acid or n-butanol remaining in the reactor after reaction.

Yield of butyl acetate (mole%)

$$Y = \frac{n_a}{n_0} \times 100\%$$

Where n_a is the number of mole of butyl acetate obtained after reaction and n_0 the number of mole of acetic acid (or n-butanol) initially introduced in the reactor.

Selectivity (%)

$$S = \frac{n_i}{n_0 - n} \times 100\%$$

Where n_i is the number of mole of butyl acetate obtained after reaction, n_0 the initial number of moles of acetic acid or n-butanol and n the final number of mole of acetic acid or n-butanol after reaction.

Figure 2-1 Photograph of the Radley carousel reaction station.

2.2.4.2 Epoxidation of cyclooctene

The reaction was performed according to a procedure described by Rezaeifard *et al.*[15]: 0.15 g of HPMo@MIL-101(Cr) or HPMo@MIL-100(Fe) was added into a mixture of cyclooctene (2 mmol, 0.26 mL) and hydrogen peroxide (≥30%, 4 mmol, 0.4 mL) in 4.0 mL ethanol, then the mixture was stirred in the Radley carousel reaction at 348 K for 1 h. After completion of the reaction, the solid catalyst was removed by centrifugation and washed with ethanol and dried at 313 K overnight for the next run. The filtrate was analysed by gas chromatography equipped with FID detector and an Alltech® EC-1000 capillary column (30 m × 0.53 mm × 1.2 μm). The injected volume of the filtrate was 0.5 μL each time. The conversion of cyclooctene, the yield of cyclooctene oxide and the selectivity of cyclooctene oxide were calculated as follows:

Conversion (mole%)

$$X = \frac{n_0 - n}{n_0} \times 100\%$$

Where n_0 is the initial molar amount of cyclooctene and n is the final number of mole of cyclooctene remaining in the reactor after reaction.

Yield of cyclooctene oxide (mole%)

$$Y = \frac{n_a}{n_0} \times 100\%$$

Where n_a is the number of mole of cyclooctene oxide obtained after reaction and n_0 is the number of mole of cyclooctene loaded initially in the reactor.

Selectivity (%)

$$S = \frac{n_i}{n_0 - n} \times 100\%$$

Where n_i is the number of mole of cyclooctene oxide obtained after reaction,

n_0 the number of mole of cyclooctene loaded initially in the reactor and n the final number of mole of cyclooctene remaining in the reactor after reaction.

2.3 Results and Discussion

2.3.1 HPW@MIL-101(Cr)

2.3.1.1 Influence of HF addition on HPW@MIL-101(Cr)

Bromberg and coworkers claimed that MIL-101(Cr) samples prepared in absence of HF had similar chemical properties as the MIL-101(Cr) samples obtained using HF although there were differences in the crystal structures.[8] Obviously, it is environmentally friendly to avoid using HF due to its harmful nature. However, the majority of reports about using MIL-101(Cr) as supports of heterogeneous catalysts described the utilization of HF.[7, 12, 14] Therefore, in this study, we utilized hydrothermal treatment to prepare MIL-101(Cr) and HPW@MIL-101(Cr) samples adding HF or not and we compared their textural and catalytic properties by different characterization techniques including XRD, N_2 physisorption, elemental analysis and model reactions in order to find out the influence of HF addition. Here, we chose the esterification of n-butanol and acetic acid as a model reaction to test the stability of MIL-101(Cr)-HF and MIL-101(Cr)-no HF in liquid phase reactions.

The structures of as-prepared samples were studied by XRD. As shown in Figure 2-2, in all patterns, the diffraction peak positions and relative intensities match those reported in literature and thus confirm the formation of the MIL-101(Cr) structure.[5, 9, 16] However, the patterns of the sample prepared in absence of HF exhibited significantly broader peaks and lower intensities compared to that of the sample synthesized in presence of HF, which indicates that crystallinity of the samples without HF is lower, which might lead to a lower thermal stability in liquid media. In the patterns of HPW-encapsulated samples, some extra peaks appeared between 6 and 8 ˚ and some redistribution of intensities took place, especially in the range of 8-10 ˚,

which should be caused by HPA's incorporation.

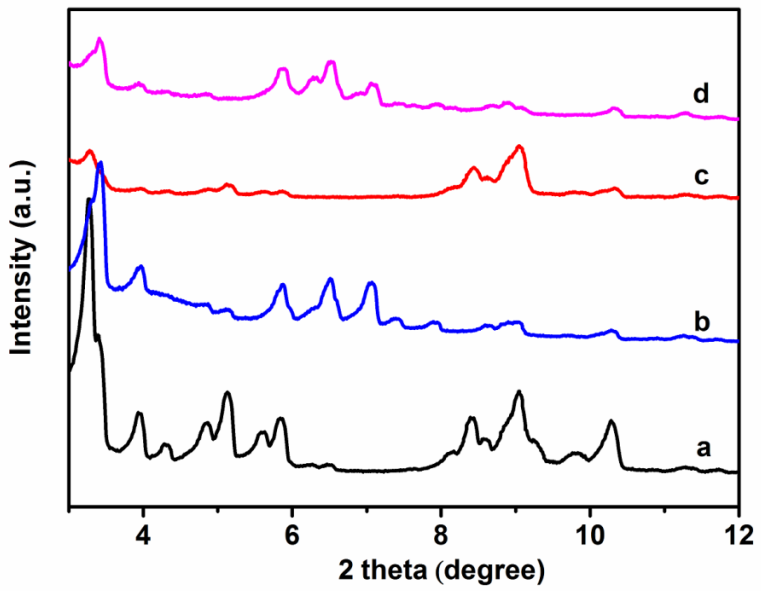

Figure 2-2 XRD patterns of (a) MIL-101(Cr)-HF, (b) HPW@MIL-101(Cr)-HF, (c) MIL-101(Cr)-no HF and (d) HPW@MIL-101(Cr)-no HF.

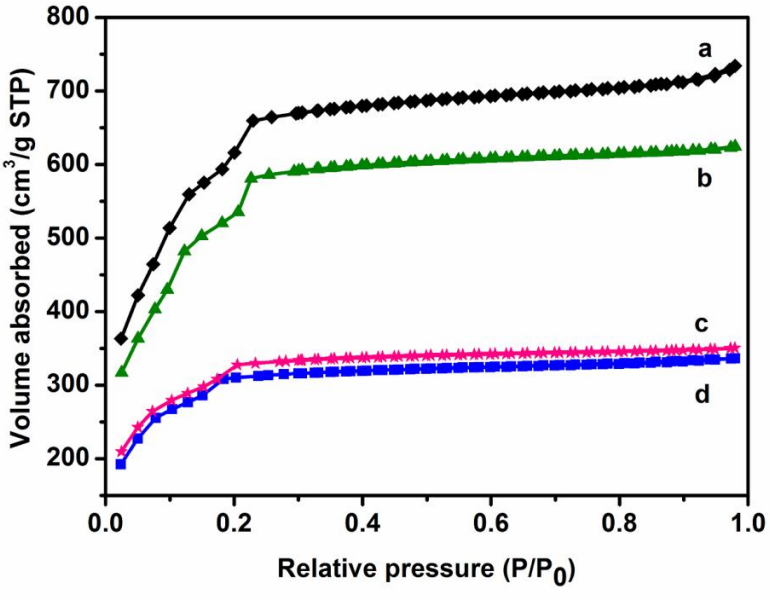

Figure 2-3 N_2 adsorption-desorption isotherms of (a) MIL-101(Cr)-no HF, (b) MIL-101(Cr)-HF, (c) HPW@MIL-101(Cr)-no HF and (d) HPW@MIL-101(Cr)-HF.

Table 2-1 Textural properties of MIL-101(Cr) samples

Samples	BET surface area (m^2/g)	Langmuir surface area (m^2/g)	Pore volume (cm^3/g)	Average pore diameter (nm)
MIL-101(Cr)-no HF	2216	3320	1.14	2.2
MIL-101(Cr)-HF	1949	2800	0.96	2.4
HPW@MIL-101(Cr)-no HF	1130	1546	0.54	2.2
HPW@MIL-101(Cr)-HF	1023	1484	0.52	2.4

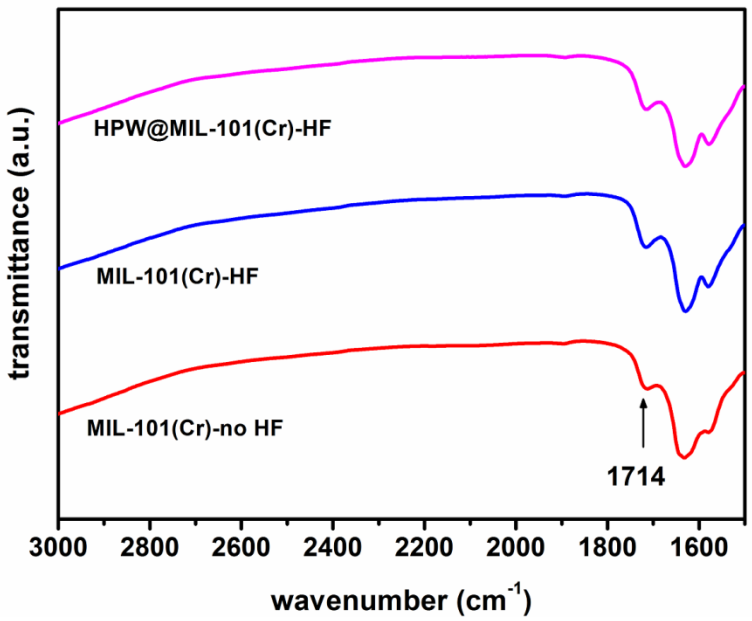

Figure 2-4 FT-IR spectra of MIL-101(Cr)-no HF, MIL-101(Cr)-HF and HPW@MIL-101(Cr)-HF.

The porosities of these four samples were verified by N_2 physisorption analysis. The N_2 adsorption-desorption isotherms show strong uptake at a low relative pressure (Type I behavior), which is typical of microporous materials (Figure 2-3). MIL-101(Cr)-no HF sample has a bit larger BET surface area (2183 m^2/g) compared to MIL-101(Cr)-HF sample (1949 m^2/g), in accordance with the presence of larger pores (Table 2-1). The BET surface area we obtained for MIL-101(Cr) is lower than the value reported in the literature (5900 m^2/g). As Wee *et al.* [16] explained in their work MIL-101(Cr) with a BET surface area larger than 4500 m^2/g is very difficult to obtain due to the presence of trapped recrystallized terephthalic acid residues within the pores. In the IR spectra of our samples, a band at 1714 cm^{-1} attributed to the carbonyl group of carboxylic acid is clearly observed. This evidenced the presence of free dicarboxylic acid impurities in our MIL-101(Cr) samples (Figure 2-4). Although many attempts have been made to purify the MIL-101(Cr) samples through various purification steps, the BET surface area of our MIL-101(Cr) samples was still lower than those reported in literature.

The BET surface areas and pore volumes of the HPW@MIL-101(Cr)-HF and HPW@MIL-101(Cr)-no HF samples were always lower compared to their corresponding pure MIL-101(Cr) materials, which is expected since HPW occupied partially the pores.

The performance in the model catalytic reactions is the ultimate criterion to decide whether or not HF is necessary for HPW@MIL-101(Cr) synthesis. Therefore, esterification of n-butanol and acetic acid was used to assess the catalytic properties of these four samples. The reactions were run at 353 K for 2 h and the results are reported in Table 2-2. The HPW@MIL-101(Cr)-HF catalyst gave the best activity and yield (35%) of butyl acetate, much higher than HPW@MIL-101(Cr)-no HF (24%), MIL-101(Cr)-HF (25%) and MIL-101(Cr)-no HF (22%). It is interesting to note that the reaction run without catalyst in the same experimental conditions gave 20% yield. Therefore the only significant catalytic activity was observed for HPW@MIL-101(Cr)-HF. All the other tests are similar to a blank test without catalyst.

This means that HPW@MIL-101(Cr)-no HF is totally inactive. However, the ICP results showed that the HPW@MIL-101(Cr)-no HF samples had 50.5 wt% loading of HPW and very little leaching of HPW occurred during the reactions (Table 2-3). In this case, the loss of HPW's acidity after encapsulation could be considered as the probable reason for its inactivity. Since the classical techniques NH_3-TPD are not suitable to MOFs supporting catalysts due to the high temperature using in the determination, their acidity still need further study. Nevertheless, the adding of HF during the synthesis of catalysts was clearly found favourable.

Table 2-2 Catalytic properties of different catalysts for esterification of n-butanol and acetic acid.

Samples	Acetic acid conversion (%)	N-butanol conversion (%)	Butyl acetate yield (%)	Butyl acetate selectivity (%)
Blank	26	28	20	78
MIL-101(Cr)-HF	31	32	25	82
MIL-101(Cr)- no HF	29	30	22	77
HPW@MIL-101(Cr)-HF	43	44	35	82
HPW@MIL-101(Cr)-no HF	30	33	24	81

Reaction conditions: Catalyst (0.15 g), n-butanol (0.05 mol), acetic acid (0.05 mol), T=353 K, t=2 h.

Table 2-3 ICP analysis of HPW@MIL-101(Cr) materials

Samples	Cr (wt%)		W (wt%)		HPW (wt%)	
	before	after	before	after	before	after
HPW@MIL-101(Cr)-HF	7.7	7.6	36.8	33.3	48.0	43.4
HPW@MIL-101(Cr)-no HF	7.5	7.2	38.7	33.1	50.5	43.3

Before means before catalytic reactions. After means after catalytic reactions.

2.3.1.2 Influence of pH on HPW@MIL-101(Cr) properties

As one knows, HPAs have strong acidic properties, their addition in the synthesis medium therefore leads to a lower pH of the reaction mixture of MIL-101(Cr). The pH value is an important factor to influence the syntheses of nanomaterials and it has been reported that the pH of the reaction mixture influences the surface area of MIL-101(Cr) nanoparticles.[8] In the present work, the initial pH of the chromium nitrate and terephthalic acid suspension is around 2.60 and the pH will be 1.15 after adding a certain amount of HPW, therefore one HPW@MIL-101(Cr) sample with an initial pH of 2.6 (adjusted using solid NaOH) was prepared to study the influence of the pH value on HPW@ MIL-101(Cr) properties. The corresponding sample is denoted as HPW@ MIL-101(Cr)-pH 2.6.

Various techniques were employed to characterize the obtained samples. The XRD patterns of all samples (Figure 2-5), show the main characteristic peaks of MIL-101(Cr) structure which indicates that the adding of HPW in the initial reactant mixture did not affect the formation of the MOF structure. Some extra peaks appeared between 6 ˚ and 8 ˚ in the patterns of the two HPW-encapsulated samples, which should be an evidence of the incorporation of HPW, and the positions of peaks in these two patterns were actually almost the same so that it can be concluded that no matter the pH

value was adjusted or not, the HPW molecules can be encapsulated in MIL-101(Cr) structure. However, the pattern of MIL-101(Cr)-pH 2.6 sample exhibited significantly lower intensities compared to that of HPW@MIL-101(Cr)-HF sample, which indicates that the crystallinity of the samples synthesized at pH 2.6 is lower. Generally, lower crystallinity might lead to a lower thermal stability in liquid media.

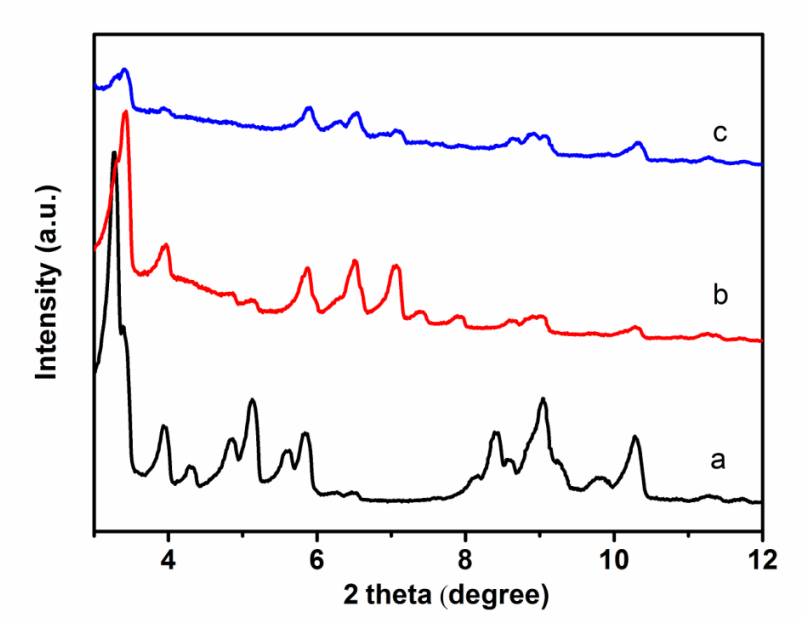

Figure 2-5 XRD patterns of (a) MIL-101(Cr)-HF, (b) HPW@MIL-101(Cr)-HF and (c) HPW@MIL-101(Cr)-pH 2.6.

The textural properties of these three samples were determined by N_2 physisorption analysis. The N_2 adsorption-desorption isotherms show Type I behaviour, which is typical for microporous materials (Figure 2-6). One can see from Table 2-4, the BET surface areas and pore volumes of the HPW-encapsulated samples. HPW@MIL-101(Cr)-HF and HPW@MIL-101(Cr)-pH 2.6 surfaces were both lower compared to their corresponding pure MIL-101(Cr) materials due to the incorporation of HPW. However, it is obvious that HPW@MIL-101(Cr)-pH 2.6 had higher surface area (1276 m^2/g) and pore volume (0.65 cm^3/g) than the HPW@MIL-101(Cr)-HF sample (1023 m^2/g and 0.52 cm^3/g, respectively) which indicates that the loading of

HPW in HPW@MIL-101(Cr)-pH 2.6 sample is lower than that of HPW@MIL-101(Cr)-HF sample. The ICP results of these two samples confirmed this conclusion. The loading of HPW in HPW@MIL-101(Cr)-pH 2.6 sample was 36.3 wt% whereas the HPW@MIL-101(Cr)-HF sample had a 48.0 wt% loading (Table 2-6).

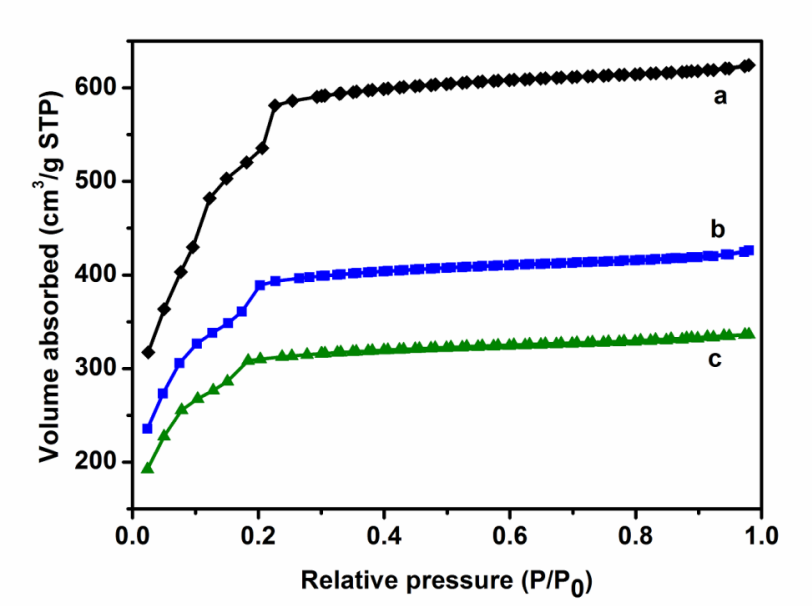

Figure 2-6 N_2 adsorption-desorption isotherms of (a) MIL-101(Cr)-HF, (b) HPW@MIL-101(Cr)-pH 2.6 and (c) HPW@MIL-101(Cr)-HF.

Table 2-4 Textural properties of MIL-101(Cr) samples

Samples	BET surface area (m^2/g)	Langmuir surface area (m^2/g)	Pore volume (cm^3/g)
MIL-101(Cr)-HF	1949	2800	0.96
HPW@MIL-101(Cr)-HF	1023	1484	0.52
HPW@MIL-101(Cr)-pH 2.6	1276	1883	0.65

Esterification of acetic acid was employed to compare the catalytic performance of HPW@MIL-101(Cr)-HF and HPW@MIL-101(Cr)-pH 2.6 samples. As shown in

Table 2-5, the activity of pure support MIL-101(Cr)-HF was almost the same as that of the blank test. The performances obtained on HPW@MIL-101(Cr)-pH 2.6 were also very close to those of the blank test, which means that this catalyst is not active at all. Only HPW@MIL-101(Cr)-HF sample proved to be more active than MIL-101(Cr)-HF with 43-44% of conversion of the reactants vs. 31-32%. According to the ICP analysis, the loading of HPW in HPW@MIL-101(Cr)-pH 2.6 sample was 36.3% and still remained 33.6 wt% after the catalytic reaction (Table 2-6).Therefore, the reason for the inactivity of HPW@MIL-101(Cr)-pH 2.6 was not that no HPW was encapsulated in MIL-101(Cr) and still needs further study.

Based on the above results, one can conclude that the change of pH value from 2.6 to 1.15 caused by the addition of HPW did not influence the formation of MIL-101(Cr) and encapsulation of HPW. On the contrary, the deliberate maintain of pH led to the low catalytic activity although the reason have not been figured out.

Table 2-5 Catalytic performances in esterification of n-butanol and acetic acid.

Samples	Acetic acid conversion (%)	N-butanol conversion (%)	Butyl acetate yield (%)	Butyl acetate selectivity (%)
Blank	26	28	20	78
MIL-101(Cr)-HF	31	32	25	82
HPW@MIL-101(Cr)-HF	43	44	35	82
HPW@MIL-101(Cr)-pH 2.6	30	31	22	72

Reaction conditions: Catalyst (0.15 g), n-butanol (0.05 mol), acetic acid (0.05 mol), T=353 K, t=2 h.

Table 2-6 ICP analysis of HPW@MIL-101(Cr) materials

Samples	Cr (wt%)		W (wt%)		HPW (wt%)	
	before	after	before	after	before	after
HPW@MIL-101(Cr)-HF	7.7	7.6	36.8	33.3	48.0	43.4
HPW@MIL-101(Cr)-pH 2.6	9.1	9.0	27.8	25.7	36.3	33.6

Before means before catalytic reactions. After means after catalytic reactions.

2.3.1.3 Influence of the amount of HPW on HPW@MIL-101(Cr)

Too small amounts of HPW cannot lead to enough loading to reach good catalytic properties of HPW@MIL-101(Cr). On the contrary too large amounts of HPW can cause waste of chemicals and even affect the diffusion of reactants in the porosity of the catalyst. Samples of HPW@MIL-101(Cr) with different amounts of HPW were hence synthesized and studied in their physicochemical and catalytic properties. Here, the HPW(x)@MIL-101(Cr) (x=amount of HPW added in grams) samples were analyzed by X-ray diffraction, N_2 adsorption-desorption measurements and model catalytic reaction (esterification of n-butanol and acetic acid).

Figure 2-7 shows the XRD patterns of the as-prepared samples. The characteristic peaks of MIL-101(Cr) is present in all patterns, which confirm the formation of the MOF structure. In the patterns of the samples obtained in the presence of HPW, some extra peaks emerged between 6 ˚ and 8 ˚ 2θ, and some

redistribution of the XRD intensities took place compared with the pure MIL-101(Cr) sample. These changes were reported in previous papers and were attributed to the incorporation of HPW.[8-9]

The high crystallinity of HPW(x)@MIL-101(Cr) samples is evident from the sharp reflections in XRD patterns, which is also shown in the SEM images (Figure 2-8). The size of the crystal is in a broad range, between 50 nm and 6 μm.

The isotherms for the HPW(x)@MIL-101(Cr) samples are reported in Figure 2-9. The shapes of isotherms corresponds to type I, which indicates that the materials are microporous. The BET surface area and the total pore volume decreases with the increasing amount of HPW in HPW(x)@MIL-101(Cr) samples, which indicates the filling of pores with HPW. W content was determined for HPW(x)@MIL-101(Cr) by ICP analysis, which gives another evidence of HPW encapsulation. (Table 2-7). The W loading of the HPW(x)@MIL-101(Cr) series samples varies from 24.3 to 36.8 wt% for x=1 to 3.

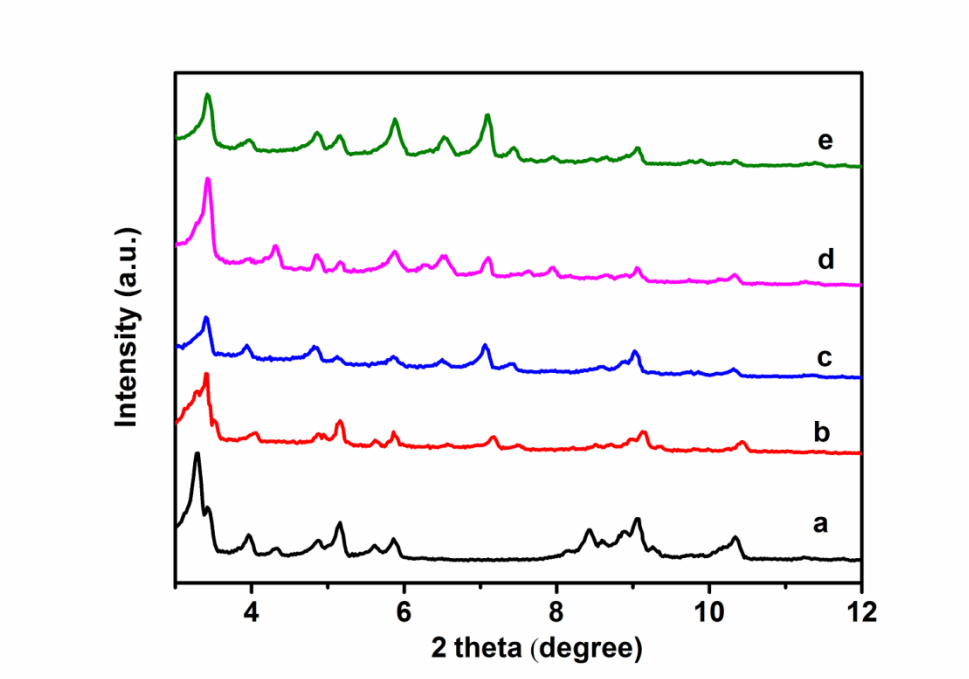

Figure 2-7 XRD patterns of (a) MIL-101(Cr), (b) HPW(0.5)@MIL-101(Cr), (c) HPW(1)@MIL-101(Cr), (d) HPW(2)@MIL-101(Cr) and (e) HPW(3)@MIL-101(Cr).

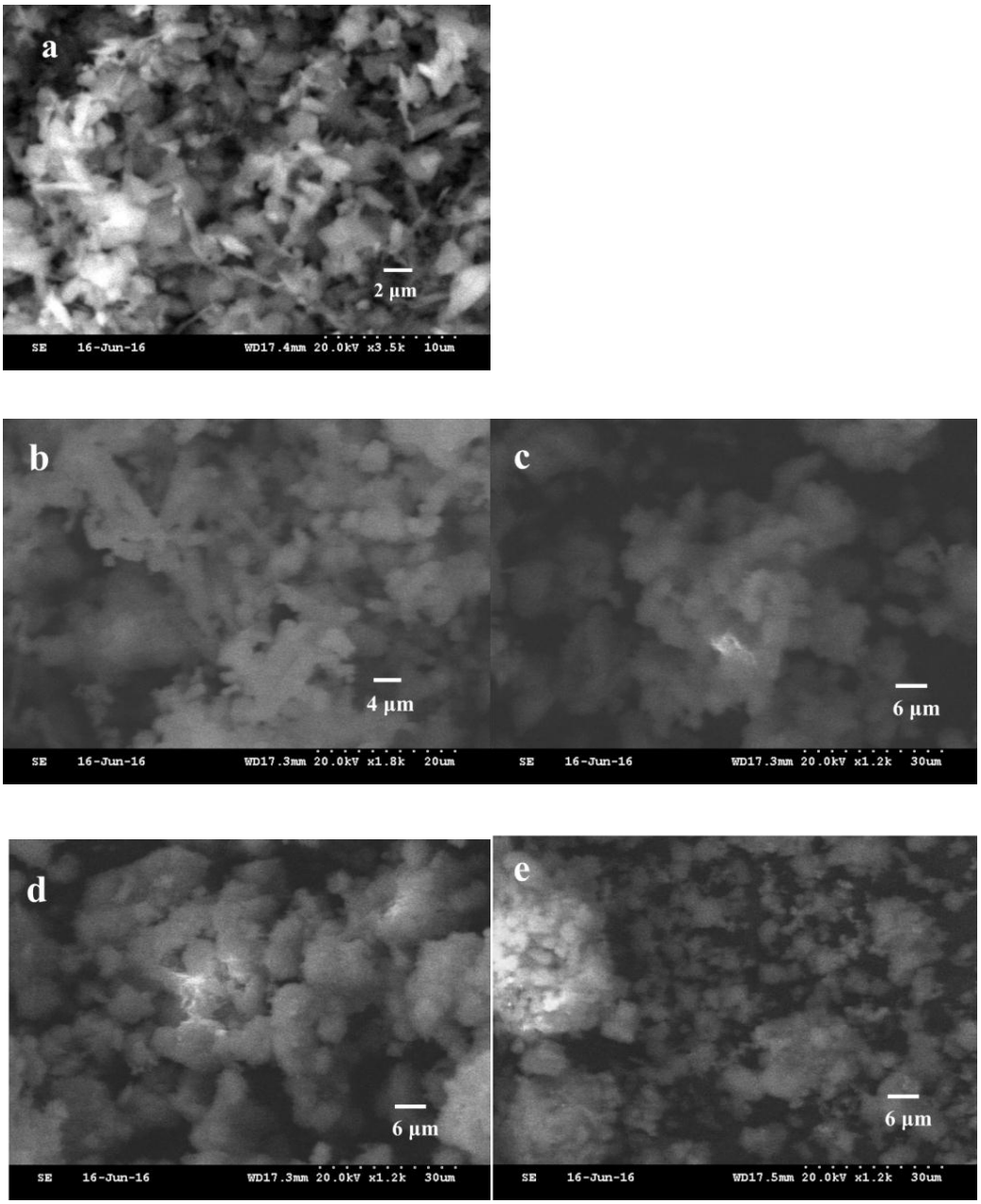

Figure 2-8 SEM images of (a) MIL-101(Cr), (b) HPW(0.5)@MIL-101(Cr), (c) HPW(1)@MIL-101(Cr), (d) HPW(2)@MIL-101(Cr) and (e) HPW(3)@MIL-101(Cr).

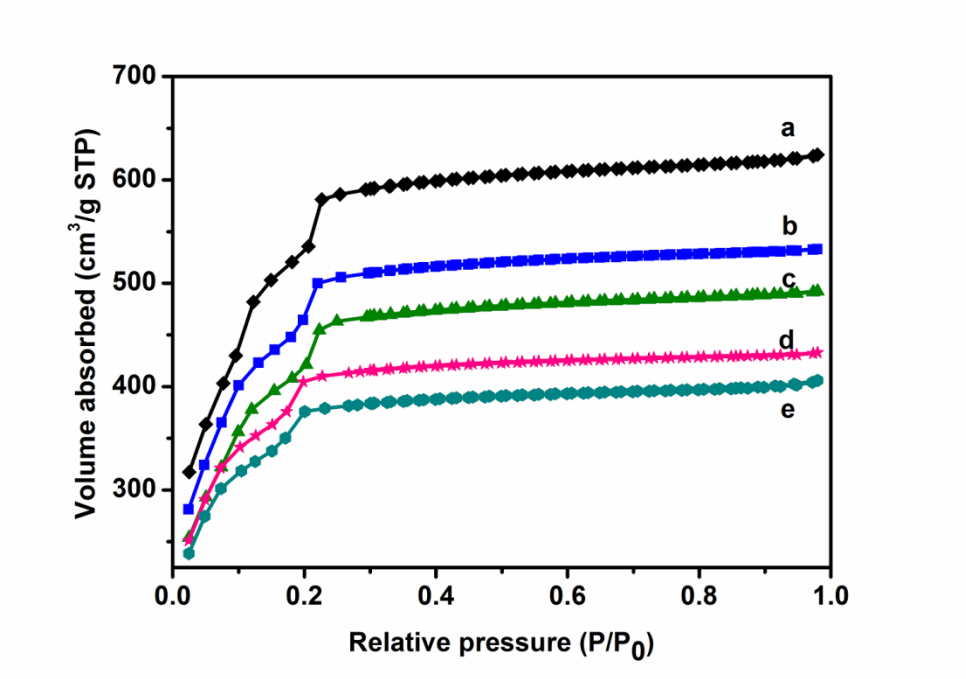

Figure 2-9 N_2 adsorption-desorption isotherms of (a) MIL-101(Cr), (b) HPW(0.5)@MIL-101(Cr), (c) HPW(1)@MIL-101(Cr), (d) HPW(2)@MIL-101(Cr) and (e) HPW(3)@MIL-101(Cr).

Table 2-7 ICP analysis results of HPW@MIL-101(Cr) materials

Samples	Cr (wt%)	W (wt%)	HPW (wt%)
HPW(1)@MIL-101(Cr)	11.5	24.3	31.8
HPW(2)@MIL-101(Cr)	8.4	34.2	44.6
HPW(3)@MIL-101(Cr)	7.7	36.8	48.0

Table 2-8 Physicochemical properties of HPW(x)@MIL-101(Cr) samples

Samples	BET surface area (m^2/g)	Langmuir surface area (m^2/g)	Pore volume (cm^3/g)
MIL-101(Cr)	1949	2800	0.96
HPW(0.5)@MIL-101(Cr)	1630	2390	0.82
HPW(1)@MIL-101(Cr)	1527	2211	0.75
HPW(2)@MIL-101(Cr)	1320	1923	0.67
HPW(3)@MIL-101(Cr)	1023	1484	0.52

The esterification of n-butanol and acetic acid was employed to investigate the catalytic performance of the HPW(x)@MIL-101(Cr) series of samples as we did before for other experimental factors. The results are reported in Table 2-9. The MIL-101(Cr) support showed similar activity as the blank test. The influence of the encapsulation of HPW in MIL-101(Cr) is obvious. The more HPW initially introduced the more active is the catalyst. Interestingly, despite similar loadings are observed in HPW(2)@MIL-101(Cr) and HPW(3)@MIL-101(Cr) according to the ICP analysis, the latter had a better activity. From the SEM images (Figure 2-8), one can see the average size of crystal of HPW(2)@MIL-101(Cr) is much larger than for HPW(2)@MIL-101(Cr), which may cause some diffusion limitations in the reaction.

Table 2-9 Catalytic properties of the HPW(x)@MIL-101(Cr) series of samples in the esterification of n-butanol and acetic acid.

Samples	Acetic acid conversion (%)	N-butanol conversion (%)	Butyl acetate yield (%)	Butyl acetate selectivity (%)
Blank	38	38	31	82
MIL-101(Cr)	39	39	30	77
HPW(1)@MIL-101(Cr)	43	44	35	81
HPW(2)@MIL-101(Cr)	45	43	36	80
HPW(3)@MIL-101(Cr)	54	54	42	78

Reaction conditions: Catalyst (0.15 g), n-butanol (0.05 mol), acetic acid (0.05 mol), T=353 K, t=4 h.

According to the catalytic performance and physicochemical properties of HPW(x)@MIL-101(Cr) materials, the amount of HPW was established to 3 g for further studies. In the following, HPW(3)@MIL-101(Cr) will be shorted as HPW@MIL-101(Cr) unless other statements.

In summary, based on the above discussions about the influence of the addition of HF, pH adjustment and amount of HPAs in the synthesis of HPAs@MIL-101(Cr), we showed that the best synthesis conditions for HPAs@MIL-101(Cr) were 3 g HPA without pH adjustment in presence of HF. Therefore, in the following,

HPW@MIL-101(Cr) and HPMo@MIL-101(Cr) samples obtained in these conditions were characterized in more depth and investigated in liquid phase reactions.

2.3.2 General characterizations of HPAs@MIL-101(Cr)

Here, two Keggin-type heteropolyacids, namely $H_3PW_{12}O_{40}$ (HPW) and $H_3PMo_{12}O_{40}$ (HPMo), which are typical catalysts applied in acid-catalyzed reactions and oxidation reactions, respectively, were used to prepare HPAs@MIL-101(Cr) samples in the best conditions determined in the previous section. Their physicochemical properties were characterized by various techniques such as XRD, SEM, TEM, FT-IR N_2 adsorption/desorption, ICP analysis, ^{31}P NMR and so on.

The crystal structures of the HPAs@MIL-101(Cr) materials were probed via XRD, the resulting patterns are shown in Figure 2-10. Remarkable changes took place in the patterns after the incorporation of HPAs, compared with that of pure MIL-101(Cr) support. Several extra peaks appeared between 6 and 8 ° 2θ and some peaks intensities were redistributed, but it is worth noticing that the peaks - including both the "new" ones and the redistributed ones - were not in the Bragg peak positions consistent with the structure of MIL-101(Cr). This suggests that the guest HPA molecules did not affect significantly the framework of MIL-101(Cr). Interestingly, these "new" peaks were not observed or much smaller in previous reports [5, 14], or the researchers did not pay attention to these peaks although they emerged in the XRD patterns of their materials.[9] Bromberg and his co-workers[8] also observed similar "new" peaks and they further designed several models of HPAs@MIL-101(Cr) composite structures to understand the configurations of HPAs in HPAs@MIL-101(Cr) materials. They refined the different calculated patterns based on their models against the experimental data, and finally, gave a well-matched model with the experimental patterns which is based on 5 ordered HPA molecules encapsulated in the large cages and 3 ordered HPA molecules in the small cages of MIL-101(Cr), but the HPAs molecules in small cages may possess a lower degree of order. In this hypothesis, the Cr/W mass ratio in HPW@MIL-101(Cr) is about 1:4.6, which is also close to our

experimental ICP results (Table 2-7). Therefore, we think that in our HPW@MIL-101(Cr) samples HPAs Keggin units occupy both the large cages and the small ones, rather than only the large cages as claimed by Férey *et al.*[5]. However, we have another explanation for the observed "new" peaks. Actually, in our work, no matter the presence or absence of HF during the synthesis, these peaks always appeared as shown in Figure 2-2. We therefore infer that the appearance of these peaks is related to the loading of HPW rather than the presence of HF. As long as the loading of HPW is high enough, the peaks that have a null intensity in pure MIL-101(Cr) will emerge in those positions, which may result from the added electron density caused by the incorporation of HPAs.

From the XRD patterns, one can observe that MIL-101(Cr) and HPAs@MIL-101(Cr) samples have both sharp and strong peaks indicating a high degree of crystallinity, which was confirmed by their SEM images (Figure 2-11). The shapes of the particles of MIL-101(Cr) was irregular and the size was between 0.5 and 3 μm (Figure 2-11a). After the incorporation of HPAs, the morphologies of the materials were less uniform and the size of the HPMo@MIL-101(Cr) particles was up to several tens of micrometers with a complex structure comprising rectangular pyramidal crystals on the surface (Figure 2-11 b, c). The size of the HPW@MIL-101(Cr) particles were of less range compared with HPMo@MIL-101(Cr) but much larger than pure MIL-101(Cr) (Figure 2-1d).

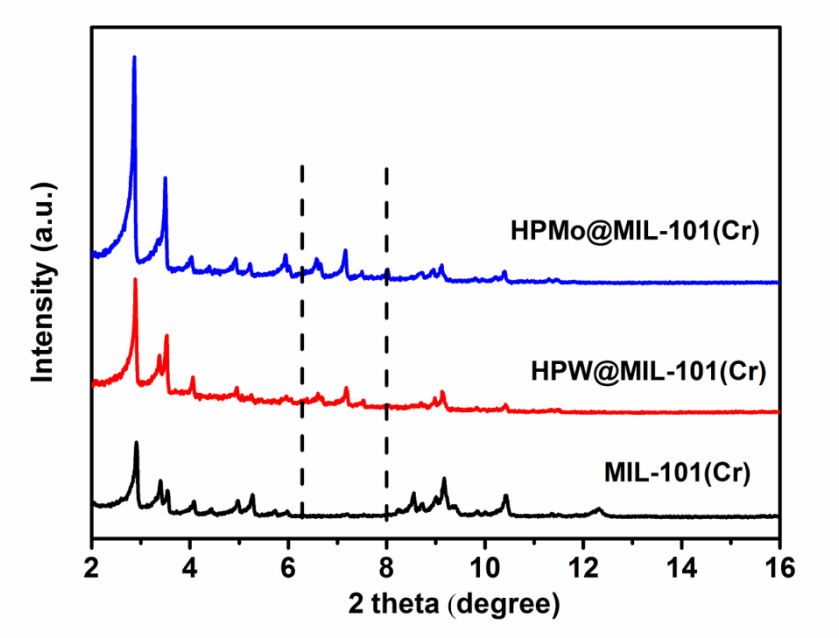

Figure 2-10 XRD patterns of MIL-101(Cr), HPW@MIL-101(Cr) and HPMo@MIL-101(Cr).

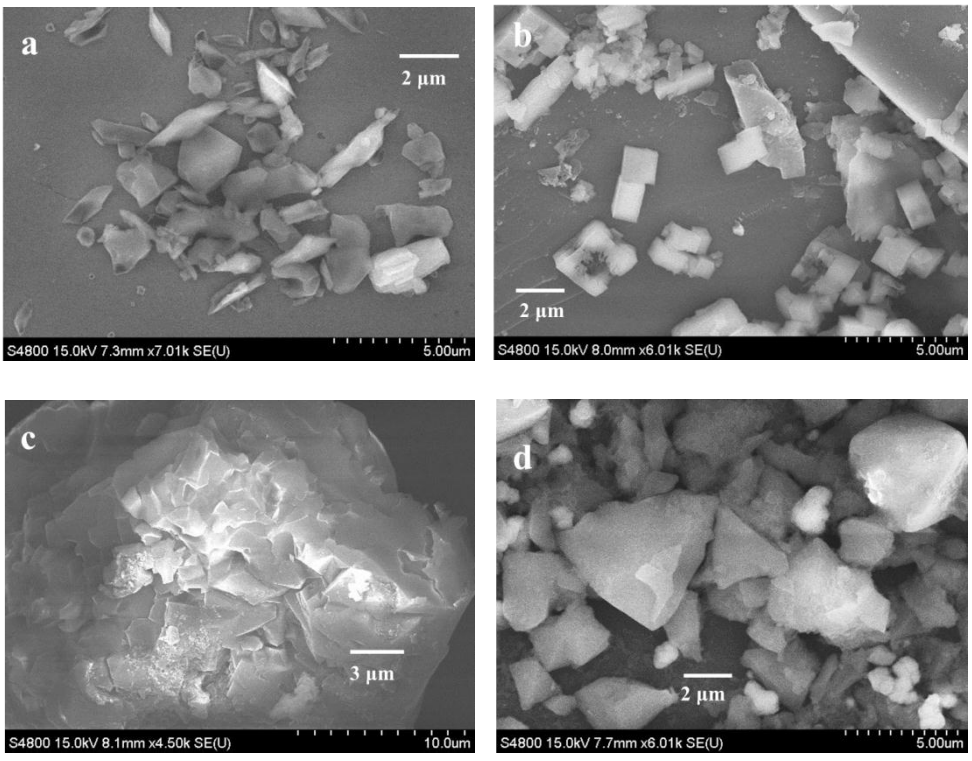

Figure 2-11 SEM images: (a) SEM image of MIL-101(Cr); (b) and (c) SEM images of

HPMo@MIL-101(Cr); (d) SEM image of HPW@MIL-101(Cr).

The IR spectra of various materials are shown in Figure 2-12. The spectra of HPAs@MIL-101(Cr) contain both corresponding Keggin-type heteropolyacids' and MOFs' characteristic bands. The characteristic bands of the framework-(O-C=O) groups around 1550 and 1430 cm^{-1} is as reported by Ferey *et al.* [5] The bands at 1017 and 748 cm^{-1} are attributed to δ(C-H) and γ(C-H) vibrations of the aromatic rings, but several characteristic bands belonging to HPAs are shifted compared with free heteropolyacids. In particular, the additional bands in the HPW@MIL-101(Cr) should be attributed to the Keggin unit of HPW at 1081 cm^{-1} (stretching frequency of P-O in the central PO_4 tetrahedron), at 978 cm^{-1} (terminal bands for W=O in the exterior WO_6 octahedron), 899 and 823 cm^{-1} (bands for the W-O_b-W and W-O_c-W bridge, respectively) and among these characteristic bands, the υ_{as}(W-O_b) and υ_{as}(W-O_c) vibration bands were remarkably shifted in comparison to free heteropolyacid (889 and 798 cm^{-1} respectively). In the spectra of HPMo@MIL-101(Cr), similar shifts of bands took place. The characteristic bands of HPMo at 870 and 788 cm^{-1} were shifted to 883 and 816 cm^{-1}. This shift is more likely due to the fact that HPAs are confined inside the cavities of MIL-101(Cr) leading to some distorsion of the structure of the Keggin units. The ^{31}P NMR spectrum of reagent-grade HPW contains a main peak at about -15.4 ppm and one other weak signal at about -13.6 ppm. The latter peak, which is also observed in Zhang's work[9], should be attributed to the impurities in the reactant. The spectra of HPW@MIL-101(Cr) and HPMo@MIL-101(Cr) present one peak at about -15.6 ppm and -3.8 ppm respectively, which are attributed to HPW and HPMo, confirming the integrity of the Keggin-type structure in the pores of MIL-101(Cr) (Figure 2-13).

The textural propreties of the HPAs@MIL-101(Cr) materials were investigated through N_2 adsorption/desorption technique (Figure 2-14). The BET surface areas and total pore volumes of HPMo@MIL-101(Cr) and HPW@MIL-101(Cr) both decreased

compared with those of MIL-101(Cr), with a 24.2 wt% loading of HPMo and a 48.0 wt% loading of HPW respectively (

Table 2-10).

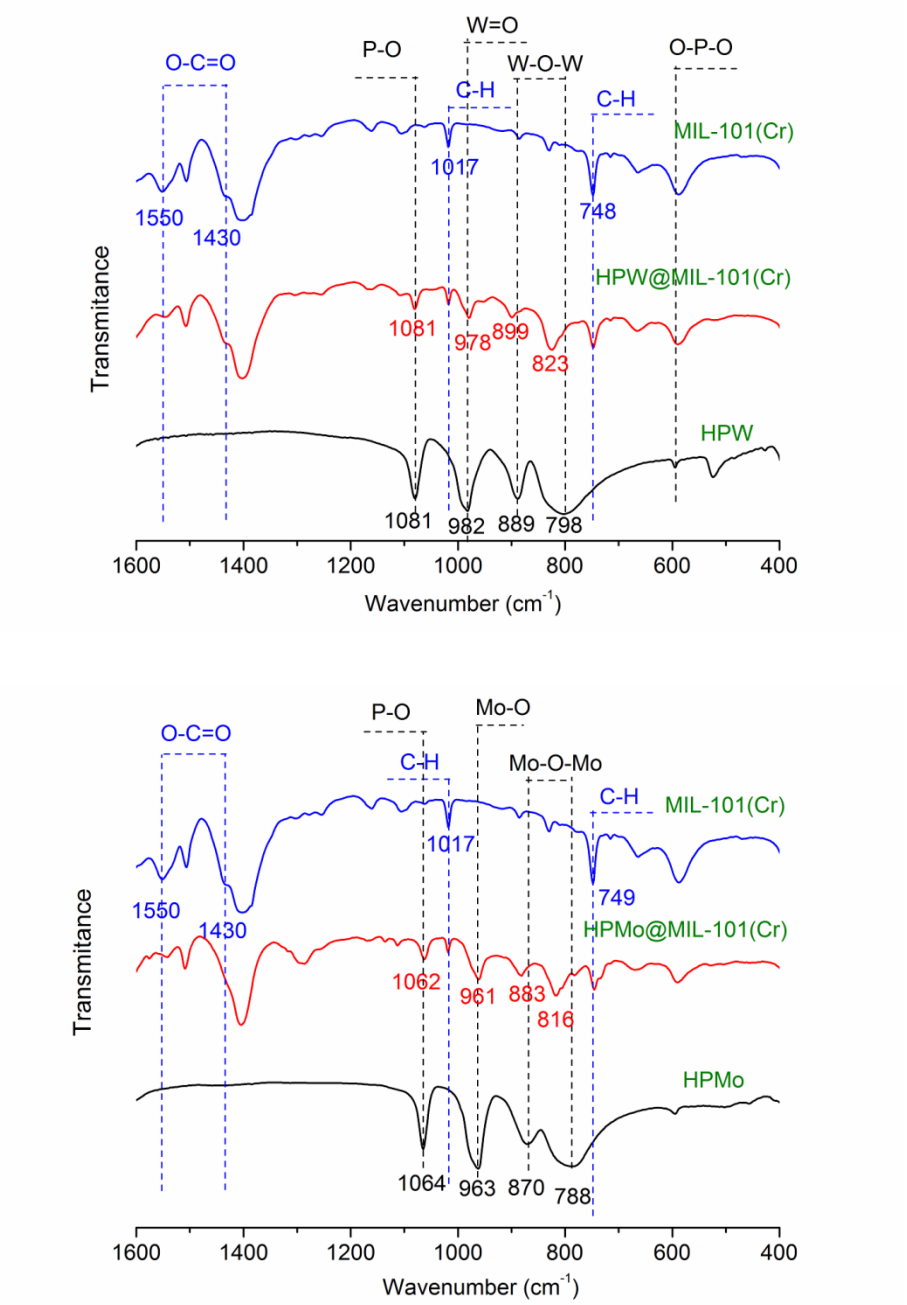

Figure 2-12 IR spectra of HPA, MIL-101(Cr) and HPA@MIL-101(Cr).

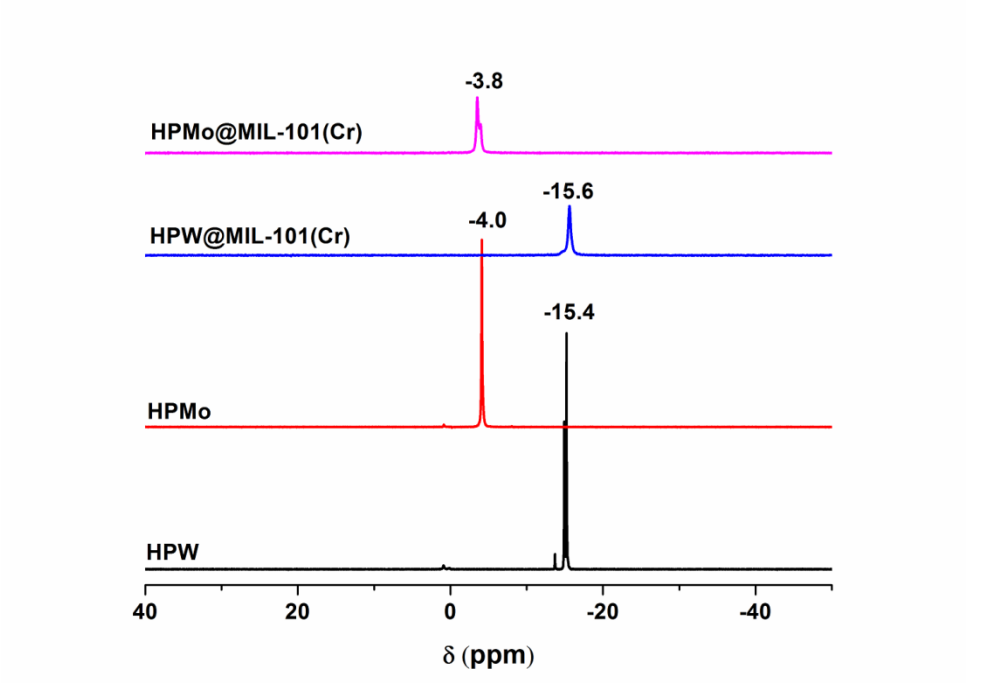

Figure 2-13 ^{31}P solid-state NMR spectra of the Keggin-type HPAs, HPW@MIL-101(Cr) and HPMo@MIL-101(Cr).

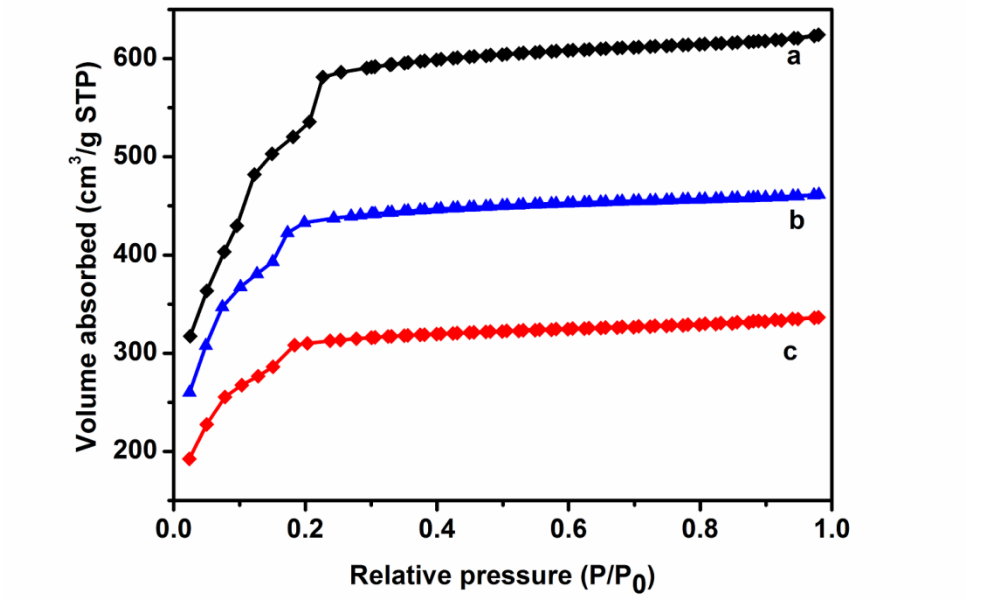

Figure 2-14 N_2 adsorption-desorption isotherms of (a) MIL-101(Cr), (b) HPMo@MIL-101(Cr) and (c) HPW@MIL-101(Cr).

Table 2-10 Textural properties of HPAs@MIL-101(Cr) materials

Samples	BET surface area [a] (m^2/g)	Pore Volume [b] (cm^3/g)	W or Mo content [c] (wt%)	HPA content (wt%) [d]
MIL-101(Cr)	1949	0.96	0	0
HPMo@MIL-101(Cr)	1400	0.71	15.3	24.2
HPW@MIL-101(Cr)	1023	0.52	36.8	48.0

[a,b] determined from nitrogen isotherms. [c,d] calculated using ICP results.

2.3.3 Catalytic performance of HPAs@MIL-101(Cr)

2.3.3.1 Esterification of n-butanol and acetic acid

The previous studies have demonstrated that HPW@MIL-101(Cr) has an interesting interesting catalytic activity in the esterification of n-butanol and acetic acid. Here, we investigated further the recycling ability of this catalyst. The results are shown in

Table 2-11. HPW@MIL-101(Cr) catalyst showed 54% conversion of acetic acid after 4 h in the first run, which is comparable to the activity obtained with bare HPW despite the yield of butyl acetate was lower (42% against 51%). However, its activity decreased gradually in the following two runs.

Table 2-11 Catalytic properties of different catalysts for esterification of n-butanol and acetic acid

Samples	Acetic acid conversion (%)	N-butanol conversion (%)	Butyl acetate yield (%)	Butyl acetate selectivity (%)
Blank	31	33	24	77
Bare HPW*	60	59	51	85
MIL-101(Cr)	39	39	30	77
HPW@MIL-101(Cr) (1^{st})	54	54	42	78
HPW@MIL-101(Cr) (2^{nd})	42	41	37	88
HPW@MIL-101(Cr) (3^{rd})	37	37	35	95

Reaction conditions: Catalyst (0.15 g), n-butanol (0.05 mol), acetic acid (0.05 mol), T=353 K, t=4 h.

* The amount of bare HPW equalled the HPW weight content in HPW@MIL-101(Cr).

In order to explore the reason of this activity loss, several characterizations were made on the samples before and after the reaction. The first obvious reason is that the leaching of HPW occurred during the reaction due to the change or damage of the MIL-101(Cr) structure or the change of the particle morphology in the liquid phase. Therefore, the confirmation of the structure and morphology of MIL-101(Cr) and the determination of HPW content after reaction were done firstly. The SEM images of HPW@MIL-101(Cr) after the third run of the catalytic reaction was not significantly changed both in size and in shapes, compared with the samples as synthesized (Figure 2-15). From Figure 2-16, one can observe that the XRD patterns

of HPW@MIL-101(Cr) after the third run was almost the same as that of the fresh sample, which indicates that the structure of MIL-101(Cr) framework kept its integrity. The ICP results showed that only limited leaching of HPW occurred in the first run, which may be attributed to the loss of some HPAs from the outer surface of MIL-101(Cr). Afterwards, the HPW content in HPW@MIL-101(Cr) remained constant after the second and the third runs. Therefore, the characterization study ruled out the possibility that the activity decrease observed for HPW@MIL-101(Cr) was caused by the leaching of HPW.

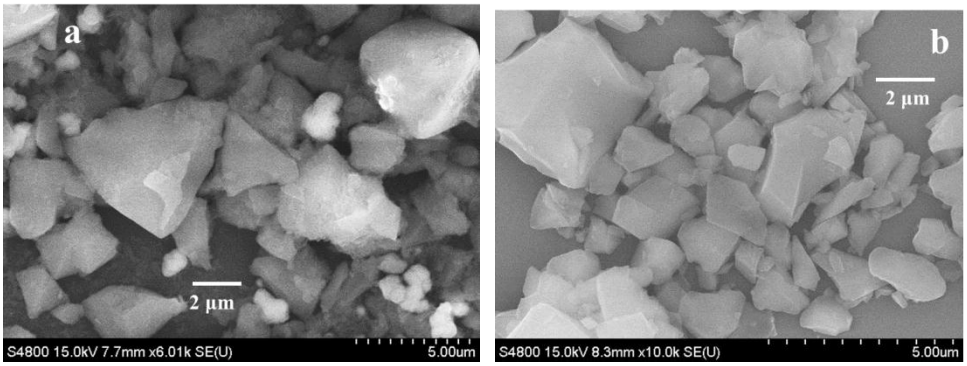

Figure 2-15 SEM images of HPW@MIL-101(Cr): fresh (a) and after the third run (b).

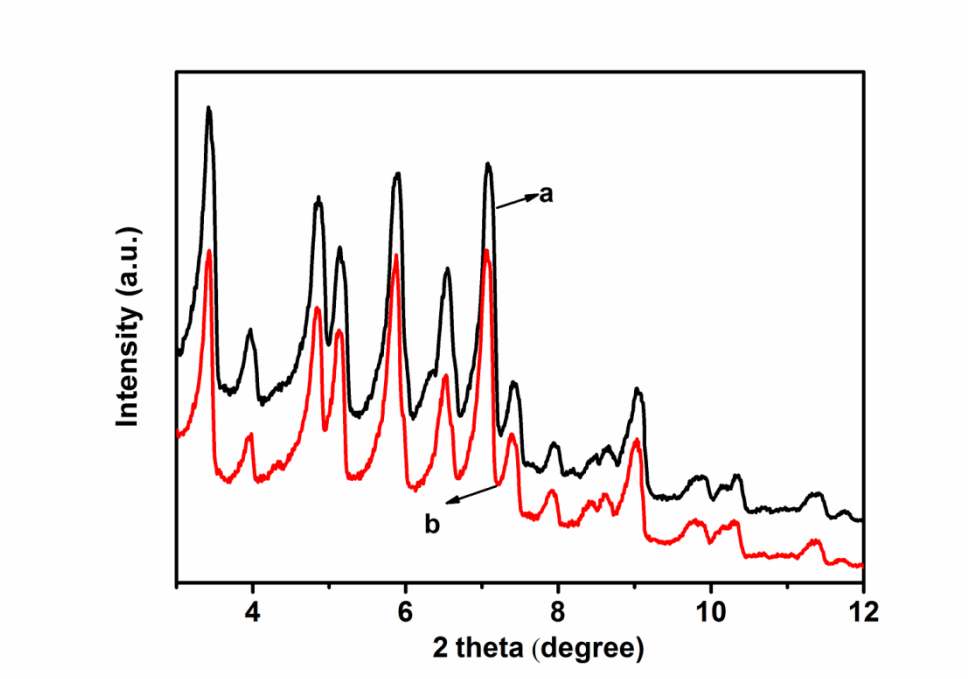

Figure 2-16 XRD patterns of HPW@MIL-101(Cr): fresh (a) and after the third run

(b).

Table 2-12 ICP analysis of HPW@MIL-101(Cr) during the recycling experiments

Samples	Cr (wt%)	W (wt%)	HPW (wt%)
Fresh HPW@MIL-101(Cr)	7.7	36.6	47.8
HPW@MIL-101(Cr) (1^{st})	7.7	33.1	43.2
HPW@MIL-101(Cr) (2^{nd})	7.5	32.6	42.5
HPW@MIL-101(Cr) (3^{rd})	7.5	33.0	43.1

Another hypothesis to explain the deactivation is that the Keggin-type structure of HPW may be destroyed during the reaction. ^{31}P NMR was employed to check if the Keggin-type structure of HPW was intact after the reaction. Figure 2-17 shows the ^{31}P NMR spectra of the materials. The spectrum of reagent-grade HPW contains a main feature at about -15.4 ppm and one other weak feature at about -13.6 ppm. The latter peak is attributed to the impurities in the reactant. There is only one peak at about -15.6 ppm in the spectra of HPW@MIL-101(Cr) sample after the third run reaction confirming the integrity of the Keggin structure in cages of MIL-101(Cr) after the recycling experiment. Therefore, we can conclude that the decreasing activity is not due to the Keggin structure's change.

In Wee's work[16], the loss of activity of their HPW@MIL-101(Cr) sample was also observed in the ring opening reaction of styrene oxide with methanol. They found that the surface area and pore volume of the recovered MIL-101(HPW) sample had a great loss in the third cycle. They believed that pore blockage by trapped reaction products caused the loss and was one of the reasons for the lower activity. Therefore, we compared the surface area of our samples before and after the reaction. However,

our HPW@MIL-101(Cr) sample did not have a significant loss in the surface area, pore volume (Table 2-13).

Coming here, the acidity decrease of the catalyst is supposed to be the probable reason. However, the common method to determine the acidity of catalysts such as NH_3-TPD and pyridine IR cannot be used since the structure of MIL-101(Cr) will be destroyed above 623 K and the carboxyl group in the framework of MIL-101(Cr) would affect the result. Therefore, we have not obtained information about the acidity of the catalysts before and after the reaction. However, Wee *et al.*[16] have reported a CO-probe IR method which could be carried out at room temperature to determine the acidity of their HPW@MIL-101(Cr). This could of high interest to apply this method to complete our work and understand if the loss of acidity is the reason of the catalysts deactivation.

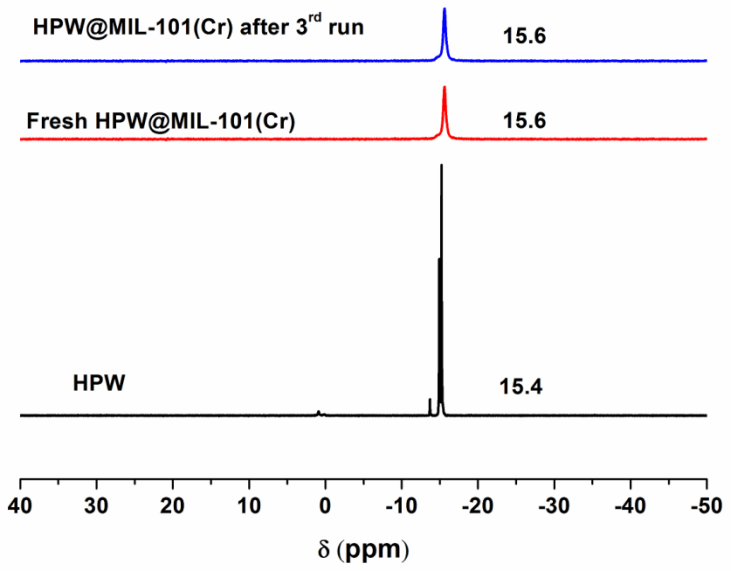

Figure 2-17 ^{31}P solid-state NMR spectra of the Keggin-type HPW (a), fresh HPW@MIL-101(Cr) (b) and HPW@MIL-101(Cr) after 3rd run (c).

Table 2-13 Comparison of the textural properties of HPW@MIL-101(Cr) before and after the catalytic reaction.

Samples	BET surface area (cm^3/g)	Pore volume (cm^3/g)	Average pore diameter (nm)
Fresh HPW@MIL-101(Cr)	1023	0.52	2.2
HPW@MIL-101(Cr) (1^{st})	1025	0.52	2.2
HPW@MIL-101(Cr) (2^{nd})	1068	0.54	2.2

2.3.3.2 Epoxidation of cyclooctene

Since HPMo is a typical oxidation catalyst, epoxidation of cyclooctene was chosen to investigate the catalytic performance of HPMo@MIL-101(Cr) catalyst. As is shown in Table 2-14, the HPMo@MIL-101(Cr) catalyst exhibited good performances for this reaction. The conversion of cyclooctene was 76% after 1 h in the first run, which is slightly higher than that of bare HPMo and the cyclooctene oxide selectivity was even better than that obtained using bare HPMo (71% against 57%). Apart from the good catalytic performances, the stability of HPMo@MIL-101(Cr) shown in the 3-run recycling experiment was also very satisfactory. Its activity only slightly decreased after the first run, which can be attributed to the leaching of HPMo molecules from the outer surface of MIL-101(Cr). Afterwards, the conversion of cyclooctene in the second and third runs stayed the same (70%).

The HPMo@MIL-101(Cr) samples after the 3-run recycling experiment were characterized by various techniques to check if the structure, morphology and elemental component changed. From the SEM images after the third run of the catalytic reaction, one can see that the material did not significantly changed both in size and in shape, compared with the samples as-synthesized (Figure 2-18). The XRD patterns of HPMo@MIL-101(Cr) after the third run was found very similar with that of the fresh sample, which indicates that the structure of MIL-101(Cr) framework kept its integrity under reaction conditions (Figure 2-19). The ^{31}P NMR spectra of HPMo@MIL-101(Cr) samples before and after the reactions both contain only one peak at -4.0 ppm or so, suggesting that the Keggin units remained intact (Figure 2-20). We calculated the HPW content in the HPMo@MIL-101(Cr) recovered after different runs using EDX data. The results showed that only limited decrease of HPMo content occurred in the first run, which may be attributed to the loss of some HPMo from the outer surface of MIL-101(Cr). Further, the HPMo content in HPMo@MIL-101(Cr) after the second and third runs can be considered as equal taking into account the instrumental error (Table 2-15). The BET surface area and pore volume of recovered HPMo @MIL-101(Cr) samples after the second run showed a minor loss compared with those of fresh sample (Table 2-16). However, this loss did not affect significantly the activity of the catalyst. The conversion of cyclooctene was 70% in the third run and was comparable to the performance of the catalyst in the second run.

Therefore, the HPMo@MIL-101(Cr) catalyst showed good catalytic activity and long-term stability in the model reaction of epoxidation of cyclooctene.

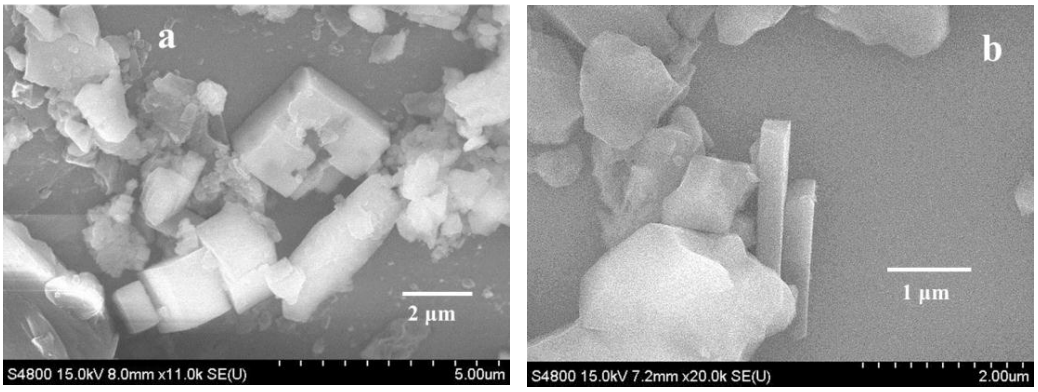

Figure 2-18 SEM images of HPMo@MIL-101(Cr): fresh (a) and after the 3rd run (b).

Table 2-14 Catalytic properties of HPMo@MIL-101(Cr) catalysts

Catalyst	Cyclooctene conversion (%)	cyclooctene oxide yield (%)	cyclooctene oxide selectivity (%)
Blank	8.5	0.44	5.2
Bare HPMo*	72	41	57
MIL-101(Cr)	29	3.7	13
HPMo@MIL-101(Cr) (1st)	76	54	71
HPMo@MIL-101(Cr) (2nd)	70	54	77
HPMo@MIL-101(Cr) (3rd)	70	50	71

Reaction Conditions: Catalyst: 0.15 g, cycloocetene (2.0 mmol), 30% hydrogen peroxide (4.0 mmol), T=348 K, t= 1 h. * The amount of bare HPMo equalled the HPMo weight content in HPMo@ MIL-101(Cr).

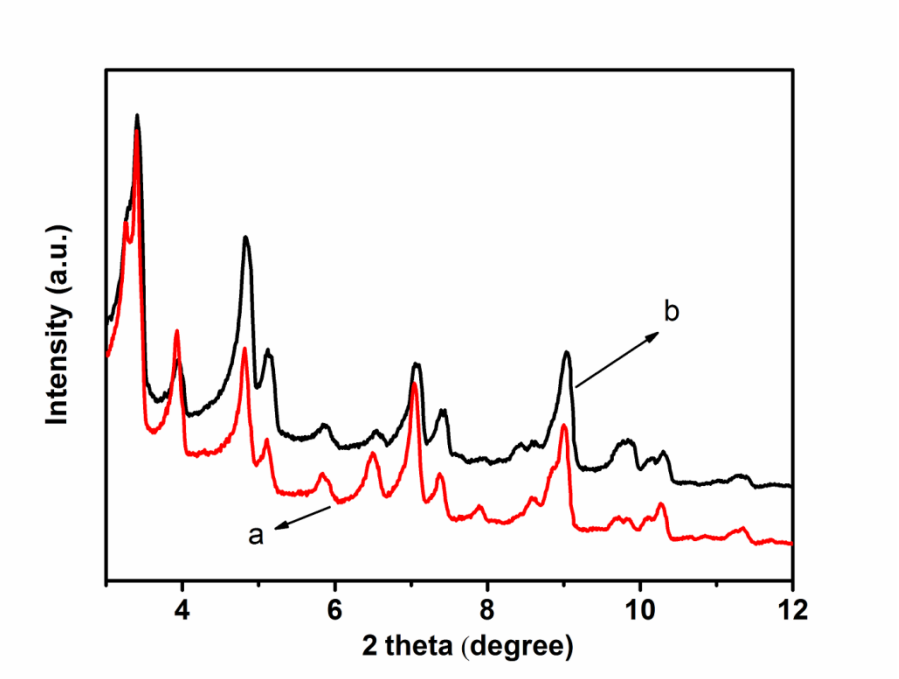

Figure 2-19 XRD patterns of HPMo@MIL-101(Cr): fresh (a) and after the third run (b).

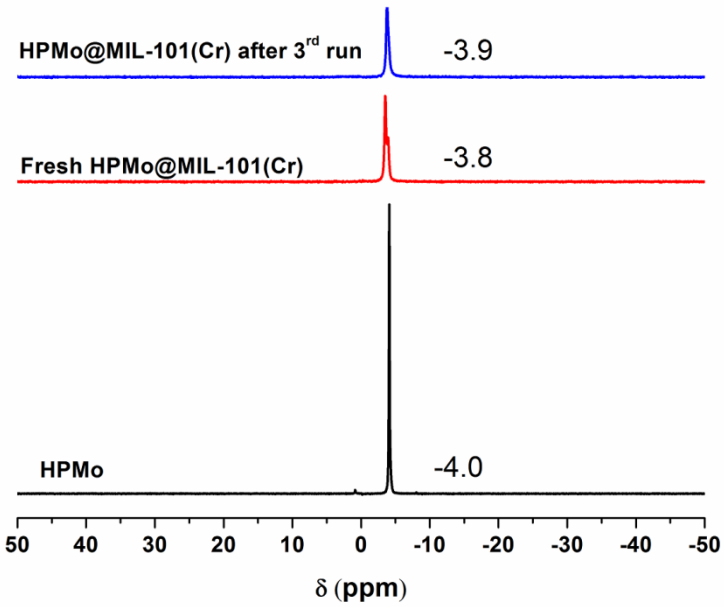

Figure 2-20 ^{31}P solid-state NMR spectra of the Keggin-type HPMo (a), fresh HPMo@MIL-101(Cr) (b) and HPMo@MIL-101(Cr) after 3rd run (c).

Table 2-15 HPMo weight content of HPMo@MIL-101(Cr) during the recycling experiments

Samples	Cr (atom%)[a]	Mo(atom%)[b]	HPMo (wt%)[c]
Fresh HPMo@MIL-101(Cr)	11.75	14.69	57.6
HPMo@MIL-101(Cr) (1^{st})	14.75	17.06	53.4
HPMo@MIL-101(Cr) (2^{nd})	16.83	18.29	50.1
HPMo@MIL-101(Cr) (3^{rd})	15.22	17.39	52.7

[a,b] determined by Energy-Dispersive X-ray spectroscopy (EDX); [c] The formula of MIL-101(Cr) and HPMo are respectively considered as $Cr_3F(H_2O)_2O[(C_6H_4)\text{-}(CO_2)_2]_3.15H_2O$ and $H_3PMo_{12}O_{40}$ during the calculation.

Table 2-16 Comparison of textural properties of HPMo@MIL-101(Cr) before and after the catalytic reaction

Samples	BET surface area (m^2/g)	Pore volume (cm^3/g)
Fresh HPMo@MIL-101(Cr)	1400	0.71
HPMo@MIL-101(Cr) after 1^{st} run	1392	0.71
HPMo@MIL-101(Cr) after 2^{nd} run	1266	0.65

2.3.4 HPAs@MIL-100(Fe)

As aforementioned, MIL-100(Fe) has attracted more and more attention due to its lower toxicity and more suitable window sizes of its cages, compared with MIL-101(Cr). We therefore also synthesized HPW@MIL-100(Fe) and HPMo@MIL-100(Fe) samples using similar hydrothermal treatments. The materials were characterized by XRD, SEM, IR, N_2 absorption/desorption, ^{31}P NMR, etc. Their catalytic performances in model reactions were also investigated.

2.3.4.1 Characterizations of HPAs@MIL-100(Fe)

The XRD patterns of HPAs@MIL-100(Fe) materials illustrated in Figure 2-21 shows that the positions of Bragg peaks of HPAs@MIL-100(Fe) are similar to those of MIL-100(Fe), but a strong change in relative intensities, especially at low angles (2θ from 3 to 8 °) is observed. This could be attributed to the change in the electronic density within the pores of MIL-100(Fe) after the incorporation of HPAs. This change was also observed in HPAs@MIL-101(Cr) samples as shown hereinbefore.

From the SEM images (Figure 2-22), one can see that all samples are of good crystallinity, which is in agreement with the XRD patterns. All samples have irregular morphologies and their sizes range from several hundred nanometers to several micrometers. The HPAs@MIL-100(Fe) show larger degree of faceting than MIL-100(Fe) and no agglomerates can be seen in SEM images of HPAs@MIL-100(Fe), which indicates that HPAs are well-dispersed in MIL-100(Fe).

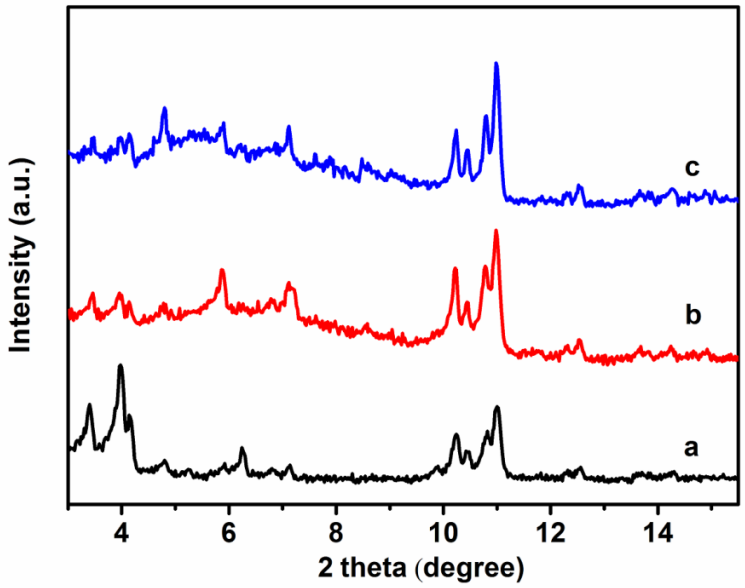

Figure 2-21 XRD patterns of (a) MIL-100(Fe), (b) HPMo@MIL-100(Fe) and HPW@MIL-100(Fe).

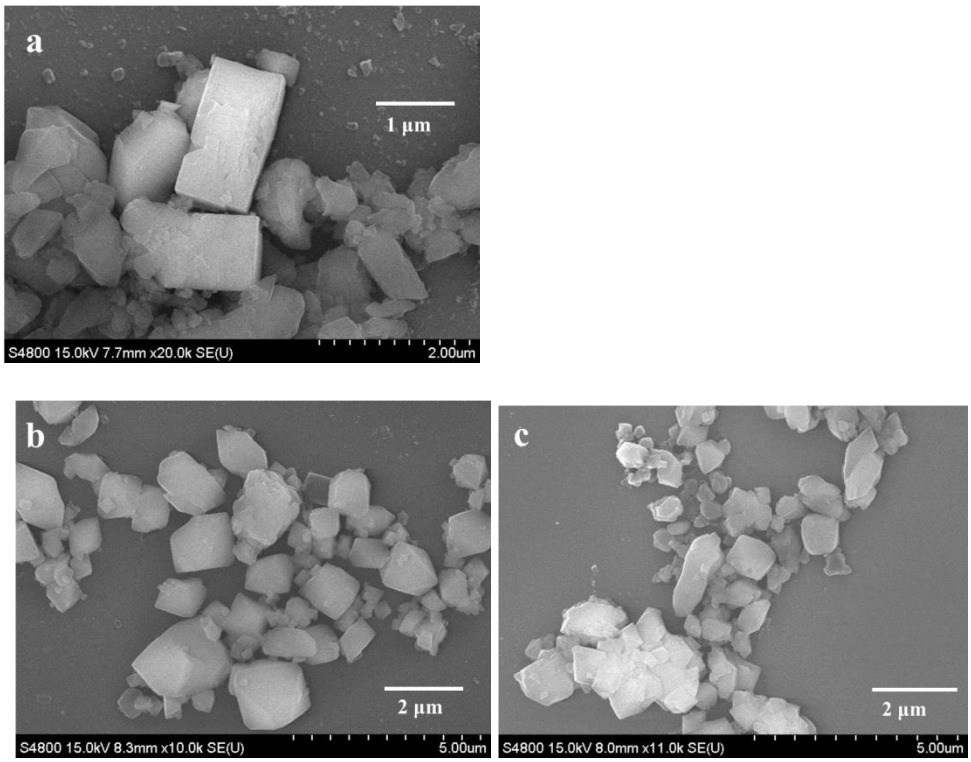

Figure 2-22 SEM images of (a) MIL-100(Fe), (b) HPW@MIL-100(Fe) and (c) HPMo@MIL-100(Fe).

The IR spectra of HPAs@MIL-100(Fe) contain both corresponding characteristic bands of Keggin-type HPAs and MIL-100(Fe) (Figure 2-23). The characteristic band at 1717 cm^{-1} is attributed to the C=O group from carboxylic acid and the bands at 1630, 1580, 1450, 748 cm^{-1} confirm the existence of the aromatic rings issued from the structure of MIL-100(Fe). However, several characteristic bands belonging to HPAs are shifted compared with free heteropolyacids. In particular, the bands in the HPW@MIL-100(Fe) at 1067 cm^{-1} (stretching frequency of P-O in the central PO_4 tetrahedron), at 964 cm^{-1} (terminal bands for W=O in the exterior WO_6 octahedron), 890 and 819 cm^{-1} (bands for the W-O_b-W and W-O_c-W bridge, respectively) should be attributed to the Keggin unit of HPMo and among these characteristic bands, the υ_{as}(P-O) and υ_{as}(W=O) vibration bands were remarkably shifted in comparison to free heteropolyacid (1081 and 982 cm^{-1} respectively). In the spectra of HPMo@MIL-100(Fe), similar shifts of bands took place. The characteristic bands of HPMo at 1067 and 802 cm^{-1} were shifted to 1058 and 814 cm^{-1}. This shift reveals the confinement effect of HPAs inside the cages of MIL-100(Fe).

The solid-state ^{31}P NMR spectrum of HPAs@MIL-100(Fe) is similar to those of HPAs (as mentioned above, in the spectrum of HPW, there is the weak peak of impurity in reagent grade HPW at -13.6 ppm), which indicates that the integrity of the Keggin unit is kept in cavities of MIL-100(Fe) (Figure 2-24).

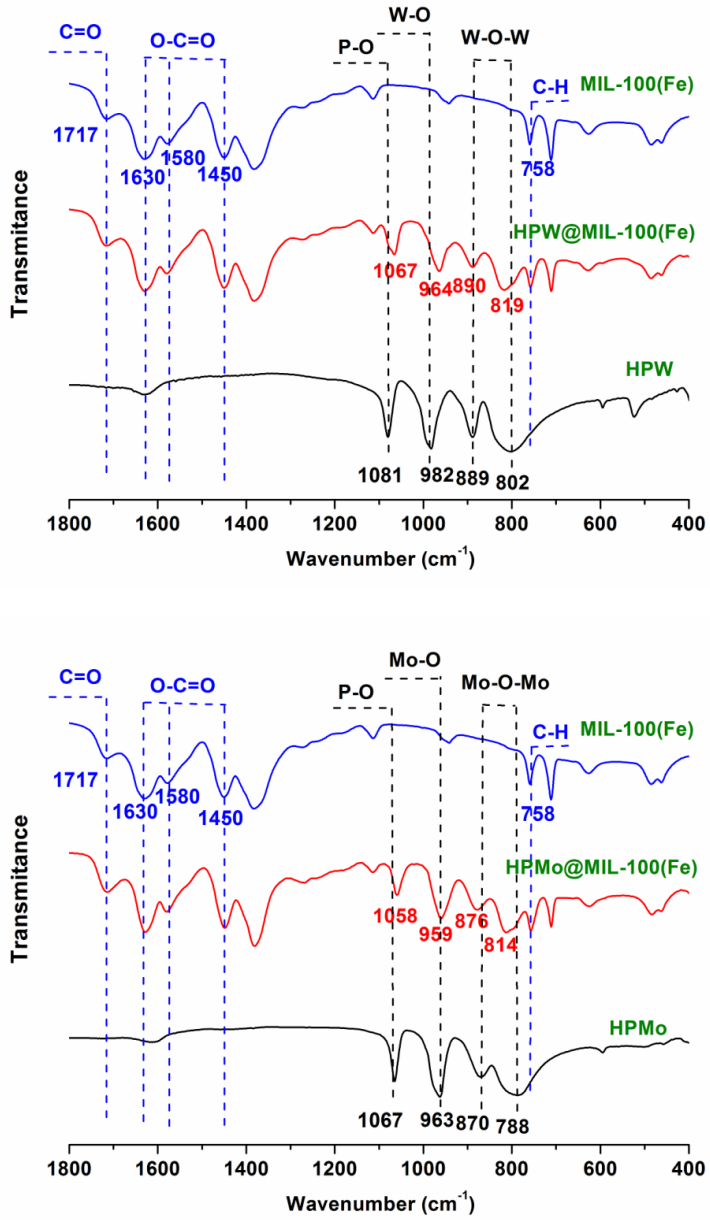

Figure 2-23 IR spectra of HPA, MIL-100(Fe) and HPA@MIL-100(Fe).

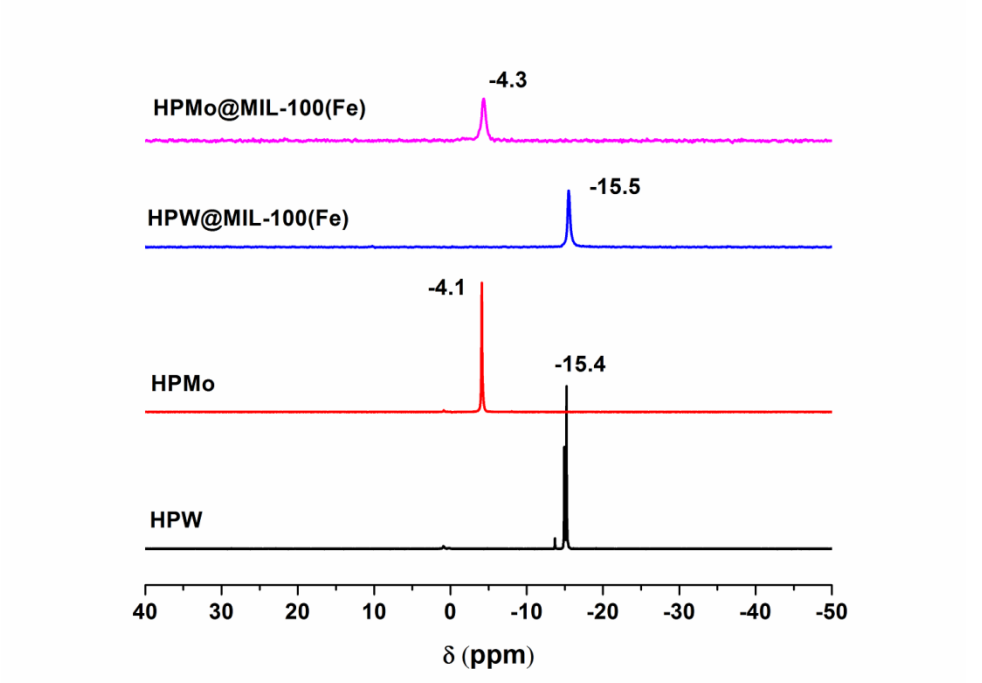

Figure 2-24 ^{31}P solid-state NMR spectra of the Keggin-type HPW, HPMo, HPW@MIL-100(Fe) and HPMo@MIL-100(Fe).

The isotherms of N_2 adsoprtion/desorption for the HPAs@MIL-100(Fe) are illustrated in Figure 2-25. The shapes of isotherms corresponds to type I, which indicates the materials are microporous. The BET surface areas of HPMo@MIL-100(Fe) and HPW@MIL-100(Fe) were 232 and 317 m^2/g respectively which are both remarkably low compared with that of MIL-100(Fe) (1192 m^2/g). The total pore volumes had the same tendency, in particular, that of HPMo@MIL-100(Fe) was 0.32 m^3/g and HPMo@MIL-100(Fe) was 0.48 m^3/g against 0.62 m^3/g for MIL-100(Fe). This is in agreement with the presence of HPAs in the porosity of the MOF (Table 2-17). The ICP analysis further confirm the presence of HPA (Table 2-18). In HPW@MIL-100(Fe) and HPMo@MIL-100(Fe) samples, the contents of HPW and HPMo are 37.8% and 21.4% respectively.

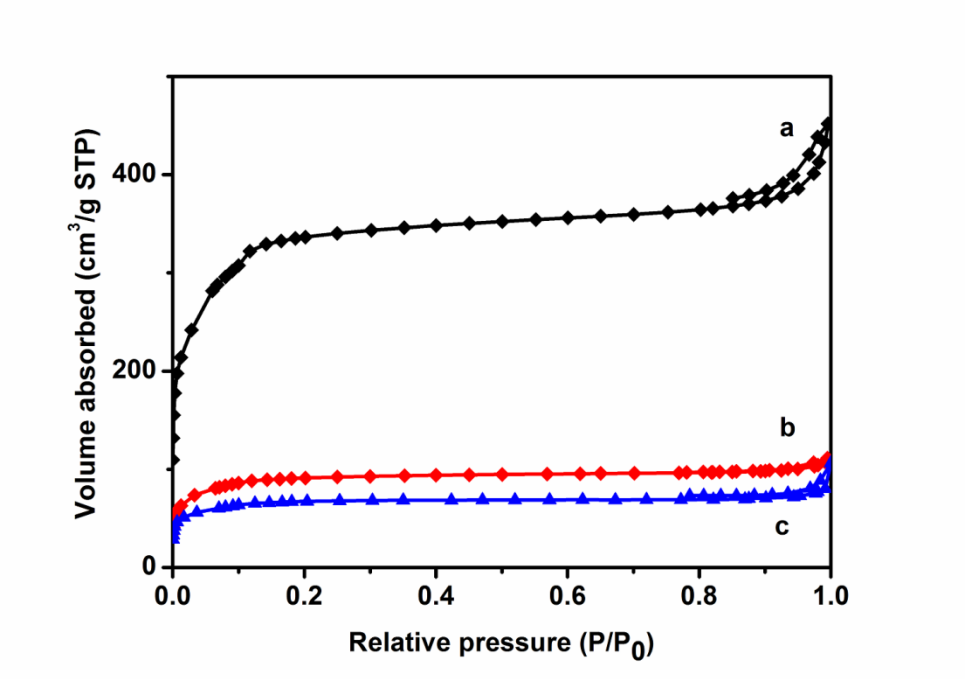

Figure 2-25 N_2 adsorption-desorption isotherms of MIL-100(Fe) (a), HPW@ MIL-100(Fe) (b) and HPMo@MIL-100(Fe) (c).

Table 2-17 Textural properties of HPAs@MIL-100(Fe) samples

Samples	BET surface area (m^2/g)	Lagmuir surface area (m^2/g)	Pore volume[b] (cm^3/g)
MIL-100(Fe)	1192	1614	0.62
HPMo@MIL-100(Fe)	232	313	0.32
HPW@MIL-100(Fe)	317	424	0.48

Table 2-18 ICP analysis results of HPAs@MIL-100(Fe) materials

Samples	Fe (wt%)	W or Mo (wt%)	HPW or HPMo (wt%)
MIL-100(Fe)	17.1	0	0
HPW@MIL-100(Fe))	11.0	28.9	37.8
HPMo@MIL-100(Fe)	12.5	25.8	21.4

2.3.4.2 Epoxidation of cyclooctene

Epoxidation of cyclooctene was employed to determine the catalytic activity of HPMo@MIL-100(Fe). The results obtained at 348 K after 1 h are displayed in Table 2-19. In the first cycle, HPMo@MIL-100(Fe) shows 46% cyclooctene conversion, which is much higher than the 6.4% obtained for MIL-100(Fe). However, the activity of HPMo@MIL-100(Fe) decreased remarkably in the second run. The conversion of cyclooctene was then 25%. The decreased activity leads to the hypothesis of leaching of HPMo and the yellow color of filtrates of the reaction mixture in the two runs further deepen this hypothesis because cyclooctene and cyclooctene oxide are both transparent (Figure 2-26). Fe^{3+} and phosphomolybdic acid ion both can bring the yellow color, we thus chosen to add hydrazine as a reducer into the filtrate to figure out which ion cause the change of color. After adding hydrazine, the filtrate became deep blue immediately, which reveals that it is phosphomolybdic acid that leached to liquid phase. Actually, phosphomolybdic acid can be reduced to molybdenum blue. Fe^{3+} would have been reduced to light green Fe^{2+} (Figure 2-27). Moreover, when HPMo@MIL-100(Fe) was removed from the solution by filtration after 0.5 h of reaction, cyclooctene oxide continued to be produced, which is another evidence of leaching of HPMo. We assume that H_2O_2 partly damaged the MIL-100(Fe) framework, which caused the leaching of HPMo, therefore some reactions using

oxidants with less oxidative power than H_2O_2 should be considered in the following.

Table 2-19 Catalytic performance of HPMo@MIL-100(Fe) in epoxidation of cyclooctene

Catalyst	Cyclooctene conversion (%)	Cyclooctene oxide yield (%)	Cyclooctene oxide selectivity (%)
Blank	4.1	0.5	13
MIL-100(Fe)	6.4	4.3	68
HPMo@MIL-100(Fe) (1^{st})	46	31	68
HPMo@MIL-100(Fe) (2^{nd})	25	17	70

Reactions were run under air at 348 K for 1 h

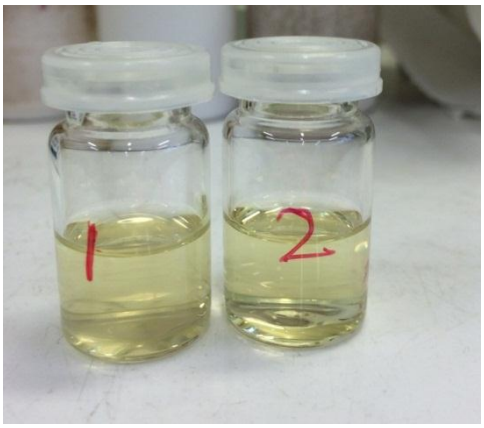

Figure 2-26 Pictures of the filtrates of reaction mixtures in epoxidation of cyclooctene catalyzed by HPMo@MIL-100(Fe) (Bottle 1 was from the first run, Bottle 2 was from the second run).

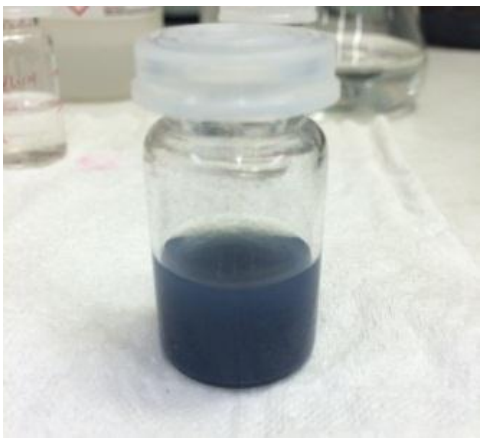

Figure 2-27 Picture of the filtrates of reaction mixtures in epoxidation of cyclooctene catalyzed by HPMo@MIL-100(Fe) after adding hydrazine.

2.4 Conclusion

The development of HPAs@MOFs using the concept of "building a bottle around the ship" has been successfully demonstrated. HPAs@MIL-101(Cr) are remarkably stable with no leaching during liquid phase reactions such as esterification of n-butanol and acetic acid and epoxidation of cyclooctene according to the ICP results. HPMo@MIL-101(Cr) exhibits very good oxidative activity and reusability in epoxidation of cyclooctene, which is very promising. HPW@MIL-101(Cr) also shows some activity in esterification of n-butanol and acetic acid, however, its activity decreased in recycling experiment. Several possible reasons of this deactivation such as the leaching of HPAs, the damage of the structure of HPAs and the blockage of the pores of HPW@ MIL-101(Cr) have been ruled out according to the characterization done on the samples before and after reaction. A probable reason, which still needs to be to be studied more in depth, is the change of acidity of HPW@MIL-101(Cr) under reaction conditions. Finally, it has been found that HPMo@MIL-100(Fe) is not stable in presence of H_2O_2.

2.5 Reference

[1] J. Gascon, A. Corma, F. Kapteijn, F. X. Llabrés i Xamena, Metal Organic Framework Catalysis: Quo vadis? *ACS Catal.* **2014,** *4* (2), 361-378.

[2] I. V. Kozhevnikov, Catalysis by heteropoly acids and multicomponent polyoxometalates in liquid-phase reactions. *Chem. Rev.* **1998,** *98* (1), 171-198.

[3] S.-S. Wang, G.-Y. Yang, Recent Advances in Polyoxometalate-Catalyzed Reactions. *Chem. Rev.* **2015,** *115* (11), 4893-4962.

[4] Y. Izumi, R. Hasebe, K. Urabe, Catalysis by heterogeneous supported heteropoly acid. *J. Catal.* **1983,** *84* (2), 402-409.

[5] G. Férey, C. Mellot-Draznieks, C. Serre, F. Millange, J. Dutour, S. Surblé, I. Margiolaki, A chromium terephthalate-based solid with unusually large pore volumes and surface area. *Science* **2005,** *309* (5743), 2040-2042.

[6] L. Bromberg, T. A. Hatton, Aldehyde-Alcohol Reactions Catalyzed under Mild Conditions by Chromium (III) Terephthalate Metal Organic Framework (MIL-101) and Phosphotungstic Acid Composites. *ACS Appl. Mater. Interfaces* **2011,** *3* (12), 4756-4764.

[7] S. Ribeiro, C. M. Granadeiro, P. Silva, F. A. Almeida Paz, F. F. de Biani, L. Cunha-Silva, S. S. Balula, An efficient oxidative desulfurization process using terbium-polyoxometalate@MIL-101(Cr). *Catalysis Science & Technology* **2013,** *3* (9), 2404-2414.

[8] L. Bromberg, Y. Diao, H. Wu, S. A. Speakman, T. A. Hatton, Chromium (III) Terephthalate Metal Organic Framework (MIL-101): HF-Free Synthesis, Structure, Polyoxometalate Composites, and Catalytic Properties. *Chem. Mater.* **2012,** *24* (9), 1664-1675.

[9] Y. Zhang, V. Degirmenci, C. Li, E. J. Hensen, Phosphotungstic Acid Encapsulated in Metal–Organic Framework as Catalysts for Carbohydrate Dehydration to 5‐Hydroxymethylfurfural. *ChemSusChem* **2011,** *4* (1), 59-64.

[10]W. Salomon, F.-J. Yazigi, C. Roch-Marchal, P. Mialane, P. Horcajada, C. Serre, M. Haouas, F. Taulelle, A. Dolbecq, Immobilization of Co-containing polyoxometalates in MIL-101(Cr): structural integrity versus chemical transformation. *Dalton Trans.* **2014,** *43* (33), 12698-12705.

[11] N. V. Maksimchuk, K. A. Kovalenko, S. S. Arzumanov, Y. A. Chesalov, M. S. Melgunov, A. G. Stepanov, V. P. Fedin, O. A. Kholdeeva, Hybrid Polyoxotungstate/MIL-101 Materials: Synthesis, Characterization, and Catalysis of H2O2-Based Alkene Epoxidation. *Inorg. Chem.* **2010,** *49* (6), 2920-2930.

[12] X. Hu, Y. Lu, F. Dai, C. Liu, Y. Liu, Host–guest synthesis and encapsulation of phosphotungstic acid in MIL-101 via " bottle around ship": an effective catalyst for oxidative desulfurization. *Micropor. Mesopor. Mater.* **2013,** *170*, 36-44.

[13] R. Canioni, C. Roch-Marchal, F. Sécheresse, P. Horcajada, C. Serre, M. Hardi-Dan, G. Férey, J.-M. Grenèche, F. Lefebvre, J.-S. Chang, Stable polyoxometalate insertion within the mesoporous metal organic framework MIL-100 (Fe). *J. Mater. Chem.* **2011,** *21* (4), 1226-1233.

[14] J. Juan-Alcañiz, E. V. Ramos-Fernandez, U. Lafont, J. Gascon, F. Kapteijn, Building MOF bottles around phosphotungstic acid ships: One-pot synthesis of bi-functional polyoxometalate-MIL-101 catalysts. *J. Catal.* **2010,** *269* (1), 229-241.

[15] A. Rezaeifard, R. Haddad, M. Jafarpour, M. Hakimi, {Mo_{132}} Nanoball as an Efficient and

Cost-Effective Catalyst for Sustainable Oxidation of Sulfides and Olefins with Hydrogen Peroxide. *ACS Sustainable Chemistry & Engineering* **2014,** *2* (4), 942-950.
[16] L. H. Wee, F. Bonino, C. Lamberti, S. Bordiga, J. A. Martens, Cr-MIL-101 encapsulated Keggin phosphotungstic acid as active nanomaterial for catalysing the alcoholysis of styrene oxide. *Green Chem.* **2014,** *16*, 1351-1357.

3 Study of the immobilization of Keplerate-type polyoxometalate {Mo_{132}} into MCM-48 silica

3.1 Introduction

Keplerate-type polyoxometalates (POMs) have attracted much attention since Müller and his co-workers first reported the highly symmetrical fullerene-like molecular clusters $\{Mo_{132}\}$ in 1998.[1] As expected by Müller's group, a number of new Keplerate-type POMs based on the structure of $\{Mo_{132}\}$ has been discovered. The acetate ligands can be exchanged for several other carboxylates, such as oxalate[2], butyrate[3], propionate[4], isobutyrate and pivalate[5]. The 30 Mo_2^{V} units can also be fully replaced by other trivalent $M^{III}(H_2O)$ (M=Fe, V and Cr), retaining a Keplerate-type structure to form another type of Keplerate $\{Mo_{72}M_{30}\}$ clusters.[6-7] Keplerate-type tungsten oxide-based clusters such as $\{W_{72}Mo_{60}\}$, $\{W_{72}Fe_{30}\}$, etc. have been discovered by Müller's group later.[8] Besides, many studies related to the tuning of the structure[9-11], the structure-forming processes[12] and their physicochemical properties such as the thermal stability[13], the stability in aqueous solutions[6, 14] and electronic properties[15] have been reported.

However, only a limited number of applications of these materials in adsorptive separation, photoelectronic devices and catalysis have been investigated.[4, 8, 16-17] Among them, catalytic oxidations are the most studied. To our knowledge, the first report in the catalytic oxidation activity of Keplerate-type POMs is the work about the catalytic properties of the $\{Mo_{72}M_{30}\}$ cluster in the selective oxidation of sulfides.[18] After that, the epoxidation of olefins using molecular oxygen and hydrogen peroxide and pyridine oxidation to N-oxides catalyzed by Keplerate POMs were reported.[19-21] In all these reactions, the Keplerate POMs have the same drawback as Keggin-type POMs: all Keplerate POMs are soluble in polar media, which brings the difficulty for the recovery of the catalysts. Therefore, in this work, we make some attempts in heterogenization of $\{Mo_{132}\}$ through encapsulating it into MCM-48 porous silica applying the concept of "building a ship in the bottle" and through immobilization of the Keplerate in the MCM-48 porosity by chemical bonds. Although the expected results were not totally reached, these explorations could be useful to further studies on the development of heterogeneous Keplerate POMs. The catalytic performance of

{Mo_{132}} in epoxidation of cylcooctene was also studied.

3.2 Experimental

3.2.1 Chemicals

Hydrazine sulfate ($N_2H_4 \cdot H_2SO_4$; ACS reagent, ⩾99%), ammonium acetate (CH_3COONH_4; 98%), ammonium molybdate tetrahydrate ($(NH_4)_6Mo_7O_{24} \cdot 4H_2O$; ACS reagent, ⩾ 99%), acetic acid (CH_3COOH; ACS reagent, ⩾ 99.7%), cis-cyclooctene (C_8H_{14}, contains 100-200 ppm Irganox 1076 FD as antioxidant, 95%), tetraethyl orthosilicate ($Si(OC_2H_5)_4$, ⩾99.0%, GC), sodium hydroxide (NaOH, ACS reagent, ⩾97.0%), cetyltrimethylammonium bromide ($CH_3(CH_2)_{15}N(Br)(CH_3)_3$, for molecular biology, ⩾99.0%), ammonium nitrate (NH_4NO_3, ACS reagent, ⩾98%), toluene ($C_6H_5CH_3$, for HPLC, ⩾ 99.9%), aminopropyltriethoxysilane ($H_2N(CH_2)_3Si(OC_2H_5)_3$, 98%) and hydrogen peroxide solution (H_2O_2, ⩾30%, for trace analysis), were purchased from Sigma－Aldrich and used without further purification.

3.2.2 Catalyst preparations

3.2.2.1 MCM-48

MCM-48 sample was prepared using a method that was developed by Xu and his co-workers.[22] The initial molar proportion of the reactants was SiO_2/ NaOH/CTAB/H_2O=1:0.46:0.55:112. In a typical preparation, 9.446 g of cetyltrimethylammonium bromide (CTAB) and 0.867 g of NaOH were dissolved in 350 mL and 50 mL of distilled water, after a sufficient stirring, 41.335 g of tetraethyl orthosilicate (TEOS) was added to the aqueous solution. After stirring for about 0.5 h, the resulting homogeneous mixture was crystallized under hydrothermal conditions at 373 K in a Teflon autoclave for 72 h. The product was filtered, thoroughly washed with deionized water and air-dried overnight. The as-synthesized samples were

calcined at 823 K in air for 6 h (1 ℃/min) to remove the CTAB.

3.2.2.2 {Mo_{132}}@MCM-48

{Mo_{132}}@MCM-48 sample was synthesized according to the concept of "building a ship in the bottle", namely, {Mo_{132}} molecules were expected to assemble in the pores of MCM-48. The molar proportions of reactants used for {Mo_{132}} cluster formation correspond to the description of Müller's group.[1] Typically, 2 g of MCM-48 was added into a three-neck Pyrex flask and evacuated by a membrane pump. Subsequently, a solution of 1.12 g of $(NH_4)_6Mo_7O_{24}.4H_2O$ and 2.5 g of NH_4OOCCH_3 dissolved in 40 mL of water was added dropwise to the flask. Afterwards, the suspension was kept stirring for 24 h, a solution of 0.16 g of $N_2H_4.H_2SO_4$ dissolved in 10 mL of water was added into the flask dropwise. The mixture was kept stirring for 1 h before 16.6 mL of 50% CH_3COOH was subsequently added. The reaction mixture, currently green, was kept at room temperature without further stirring for four days (in the fume hood). The resulting reddish-brown product was filtered and washed with NaAc-HAc buffer solution (pH=3.77), and then with 90% ethanol and diethyl ether. The product became white from reddish-brown after washing. The resulting product was dried in air at 313 K overnight and was denoted as {Mo_{132}}@MCM-48.

3.2.2.3 {Mo_{132}}

The {Mo_{132}} reference was prepared following a method from Müller and his co-workers.[1] In a typical synthesis, a solution of 0.4 g $N_2H_4.H_2SO_4$ in 25 mL of water was dropwise added into a solution of 2.8 g of $(NH_4)_6Mo_7O_{24}.4H_2O$ and 6.25 g of NH_4OOCCH_3 dissolved in 100 mL of water. 41.5 ml of 50% (v/v) CH_3COOH was subsequently added dropwise, afterwards the reaction mixture was stirred for 20 min. The resulting deep green reaction mixture was then kept at room temperature without further stirring (in the fume hood). After four days, the reddish-brown crystalline residue was filtered through a glass frit (pore size G3) and washed with 90 % ethanol

and diethyl ether, and finally dried in air at 313 K overnight.

3.2.2.4 {Mo_{132}}@ NH_2-MCM-48

The surface modification of MCM-48 by amine functional groups was carried out utilizing a method inspired from literature.[23] In a typical preparation, 1.7 g of MCM-48 was treated with the aqueous solution of ammonium nitrate to remove the sodium cations remaining after the synthesis. The resulting material was filtered off and calcined again at 673 K under nitrogen. The calcined MCM–48 sample was contacted with a refluxing toluene solution containing 1% aminopropyltriethoxysilane (APTS) for 5 h. Afterwards, the solid was filtered off, washed with toluene and then dried under vacuum, firstly at room temperature and then at 413 K overnight. The modified MCM-48 was denoted as NH_2-MCM-48. The NH_2-MCM-48 material was then suspended in a solution of 120 mg {Mo_{132}} dissolved in 20 mL of water. The slurry was kept under stirring at room temperature for 24 h. A brown solid was obtained after washing with water, 90% ethanol and diethyl ether and dried at room temperature. The sample was denoted as {Mo_{132}}@NH_2-MCM-48.

3.2.3 Catalyst characterizations

The as-prepared materials were characterized using X-Ray diffraction, nitrogen adsorption/desorption and Fourier-Transformed Infrared Spectroscopy. These techniques are explained in the following paragraphs.

3.2.3.1 X-Ray Diffraction

The crystal structures of MCM-48, {Mo_{132}}, NH_2-MCM-48 and {Mo_{132}}@ NH_2-MCM-48 were recorded by X-Ray Diffraction (XRD) using the same method ad described in 2.2.3.1.

The structure of the decomposition of {Mo_{132}} was determined by single crystal X-ray diffraction. The X-ray intensity data were collected on a Bruker DUO-APEX2

CCD area-detector diffractometer using Mo-Kα radiation (λ = 0.71073 Å) with an optical fiber as collimator.

3.2.3.2 Nitrogen adsorption/desorption

The textural properties of materials including the specific surface area, pore size distribution and pore volume were determined by N_2 adsorption/desorption experiments at liquid nitrogen temperature. The experimental parameters were the same as those described in 2.2.3.2.

3.2.3.3 Fourier Transformed Infrared Spectroscopy

Fourier-Transformed Infrared (FT-IR) Spectra were recorded on a Nicolet 380 FT-IR spectrometer equipped with a MCT detector at 4 cm^{-1} optical resolution from 400 to 4000 cm^{-1}. Prior to the measurements, the samples were pressed with KBr in the discs.

3.2.4 Catalytic reactions

Epoxidation of cyclooctene was performed according to a similar procedure described by Rezaeifard *et al*[19]: 57.2 mg of $\{Mo_{132}\}$ were added into a mixture of cyclooctene (2 mmol, 0.26 mL) and hydrogen peroxide (⩾30%, 4 mmol, 0.40 mL) in 4.0 mL of ethanol, then the mixture was stirred at 348 K for 1 h. After completion of the reaction, the filtrate of the reaction mixture was determined by gas chromatography equipped with FID detector and an Alltech® EC-1000 capillary column (30 m × 0.53 mm × 1.2 μm). The injected volume of the filtrate was 0.5 μL each time.

The conversion of cyclooctene, the yield of cyclooctene oxide and the selectivity of cyclooctene oxide were calculated as follows:

Conversion (mole%)

$$X = \frac{n_0 - n}{n_0} \times 100\%$$

Where n_0 is the initial number of mole of cyclooctene and n is the final number of mole of cyclooctene remaining in the reactor after reaction.

Yield of cyclooctene oxide (mole%)

$$Y = \frac{n_a}{n_0} \times 100\%$$

Where n_a is the number of mole of cyclooctene oxide and n_0 is the initial number of mole of cyclooctene.

Selectivity (%)

$$S = \frac{n_a}{n_0 - n} \times 100\%$$

Where n_a is the number of mole of cyclooctene oxide, n_0 the initial number of mole of cyclooctene and n the final number of mole of cyclooctene remaining in the reactor after reaction.

3.3 Results and Discussion

3.3.1 Encapsulating {Mo_{132}} into MCM-48

The first step of encapsulating {Mo_{132}} into MCM-48 is the synthesis of the MCM-48 host according to the concept of "building a ship in the bottle". The MCM-48 sample synthesized via a hydrothermal treatment was characterized by XRD and N_2 absorption/desorption to confirm the structure of MCM-48.

As shown in Figure 3-1, the reflection peaks 211 to 420 are resolved in the XRD pattern of the as-prepared MCM-48 sample, which illustrates that the MCM-48 sample has a cubic structure belonging to the *Ia*3*d* space group, in agreement with literature.[22, 24-25]

The N_2 adsorption/desorption isotherm of the MCM-48 sample is shown in

Figure 3-2. A type IV isotherm as defined by IUPAC clearly indicates the typical mesoporous materials.[26] A sharp inflection between 0.2 and 0.33 of the relative pressure P/P_0 corresponds to capillary condensation within uniform mesopores. No well-defined hysteresis loop is observed in the adsorption and desorption branch upon the pore condensation, which may be attributed to the small size of the particles. The inserted graph of Figure 3-2 shows the pore size distribution of MCM-48 calculated by the BJH method. As one can see, the distribution is extremely narrow with a maximum at ca. 2.8 nm. The BET surface area and the total pore volume of MCM-48 are 1136 cm^2/g and 0.79 cm^3/g, respectively.

The well-defined XRD peaks and the narrow pore size distribution give a clear evidence of the high-quality of the MCM-48 material. Furthermore, the large total pore volume and the average pore size (3.1 nm) provide the feasibility of encapsulation of $\{Mo_{132}\}$, which molecule diameter is about 2.9 nm.

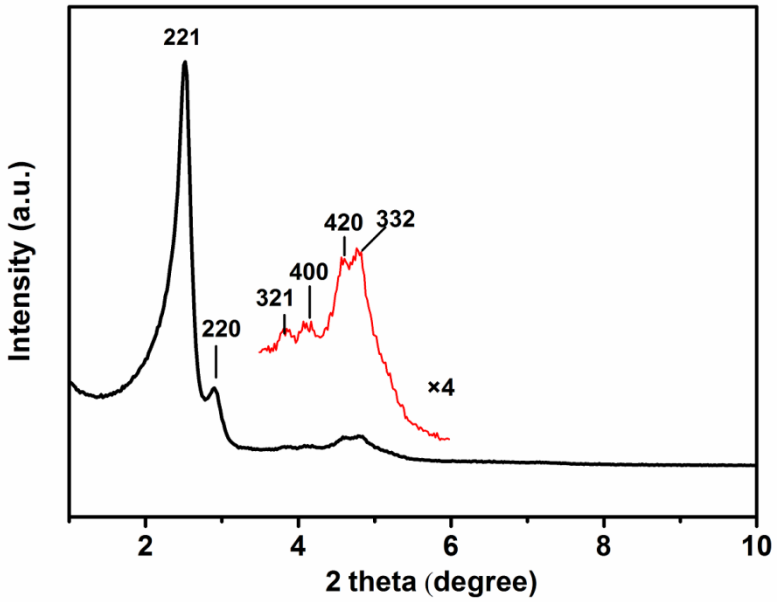

Figure 3-1 XRD patterns of as-prepared MCM-48.

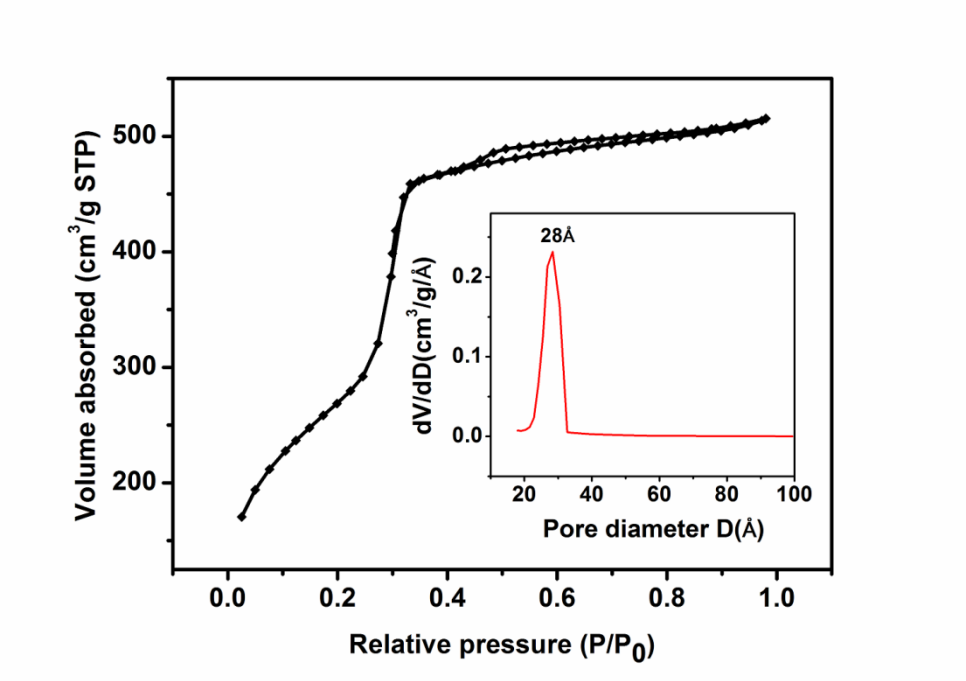

Figure 3-2 N_2 adsorption-desorption isotherms of as-prepared MCM-48.

After confirming the achievement of "the bottle", the building of the ship started. Taking into account the significant diffusion limitations in the pores of MCM-48, low-pressure conditions were used before addition of the solution of reactants for {Mo_{132}} synthesis. After the dropping of the solution of $(NH_4)_6Mo_7O_{24}.4H_2O$ and NH_4OOCCH_3, the particles of MCM-48 were completely immersed in the solution, which indicates that the solution successfully entered the pores of MCM-48. However, the final reddish-brown particle became white after the washing with water, which indicates that no or few {Mo_{132}} molecules were assembled inside the pores of MCM-48.

In order to explore this assumption, IR spectroscopy was employed to check the presence of {Mo_{132}} in {Mo_{132}}@MCM-48. From the spectrum of the MCM-48 sample (Figure 3-3), the characteristic bands of Si-OH (υ_s, 966 cm^{-1}), Si-O-Si (υ_{as}, 799 cm^{-1}, υ_s, 1087 cm^{-1}) (where υ_s, υ_{as} represents symmetric stretching and asymmetric stretching respectively) are present, in accordance with the previous reports of

MCM-48.[27-28] The strong bands of OH (3452 cm^{-1}) and H_2O (1637 cm^{-1}) can be attributed to the –OH groups and H_2O existing on the surface of MCM-48. However, in the spectrum of {Mo_{132}}@MCM-48, no additional bands were observed, which confirms the hypothesis that no {Mo_{132}} molecules were formed in pores of MCM-48.

There are two possible reasons for the failure of encapsulating {Mo_{132}} into the pores of MCM-48. One is that the pore size is not large enough to allow the {Mo_{132}} molecules to be assembled inside. One has to keep in mind that the average pore size of MCM-48 was 3.1 nm, which is very close to the diameter of {Mo_{132}}, whereby the maximum of the pore size distribution was centred around 2.8 nm, which is even smaller than the size of {Mo_{132}}. The second possibility is that the {Mo_{132}} molecules were formed inside the pores of MCM-48 but were washed out during the washing step although MCM-48 possesses a unique gyroid structure.[29-30] In order to exclude the 2nd hypothesis, we decided to modify the MCM-48 using aminopropyltriethoxysilane to introduce $–NH_2$ to try to immobilize {Mo_{132}} molecules in MCM-48 by chemical bonding.

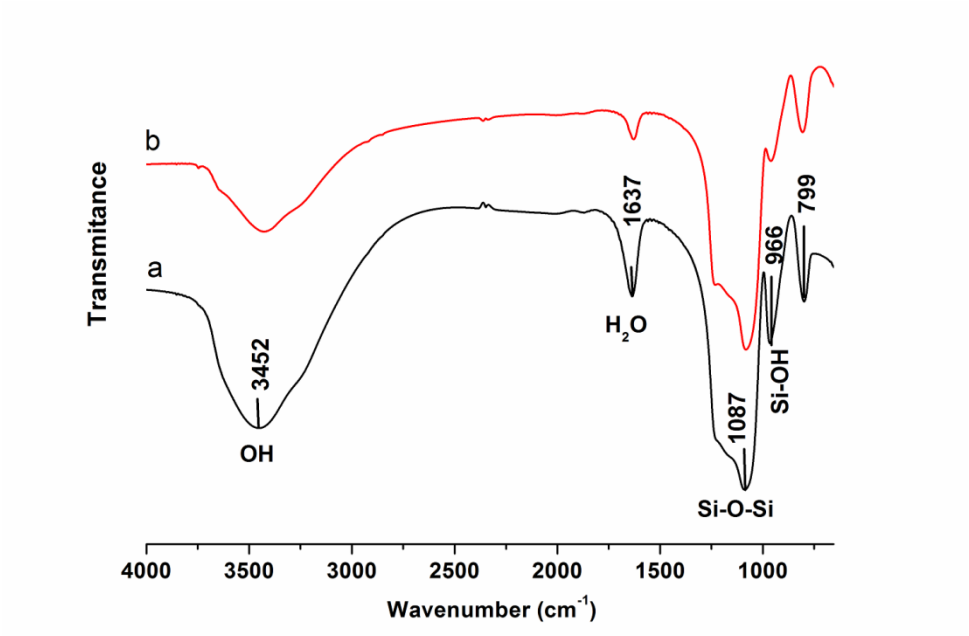

Figure 3-3 IR spectra of (a) MCM-48 and (b) {Mo_{132}}@MCM-48.

3.3.2 {Mo_{132}}@NH_2-MCM-48

In this strategy, the immobilization of {Mo_{132}} in MCM-48 was carried out by establishing a chemical bond between amino-modified MCM-48 and {Mo_{132}} as reported in the literature.[23, 31-32] The mechanism of the immobilization proposed by Vansant and coworkers[32-33] is that the aminopropyltriethoxysilane molecules which are initially connected to the silica surface via the amine groups turn to display an amine upward position as a result of the so-called "flip mechanism" so that the exposed amine groups might react with the –OOC groups of {Mo_{132}} to form the salt ≡Si$(CH_3)_3NH_2$ ·{Mo_{132}} by which the {Mo_{132}} will be immobilized into the surface of MCM-48.

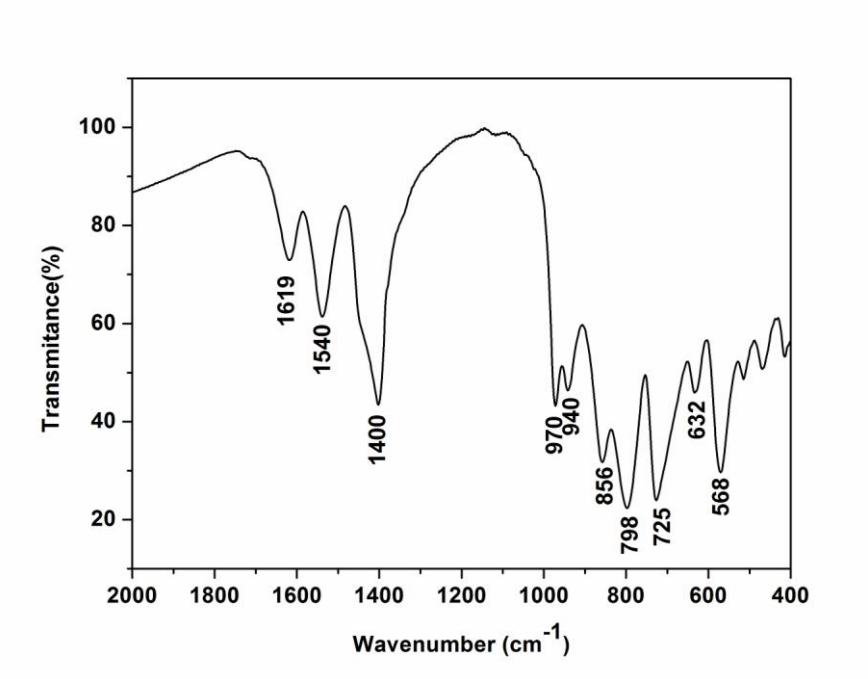

Figure 3-4 IR spectrum of {Mo_{132}}.

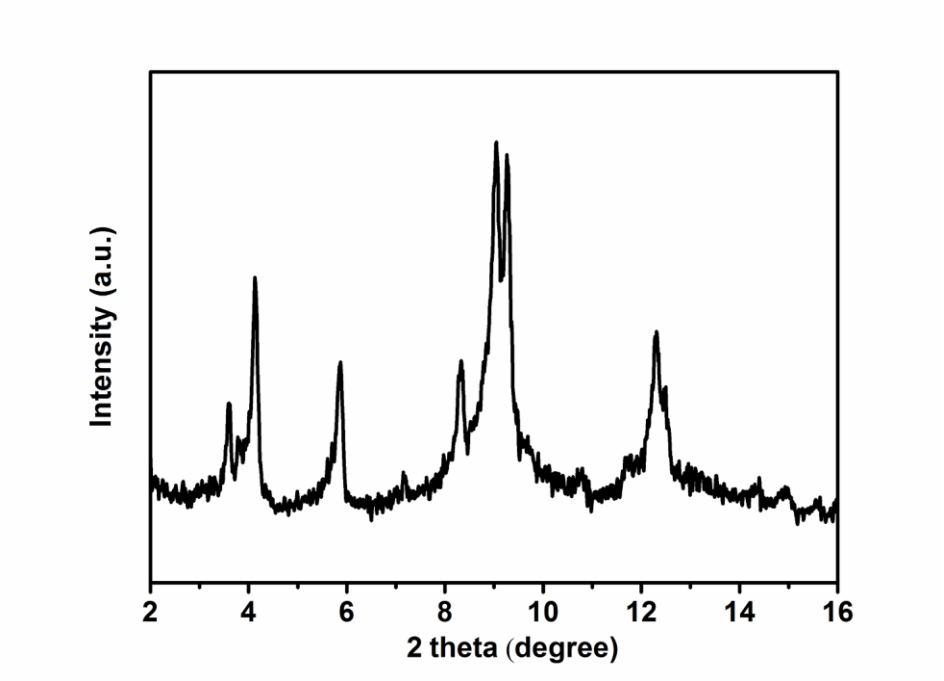

Figure 3-5 XRD patterns of {Mo_{132}}.

In this case, {Mo_{132}} and MCM-48 were synthesized separately and the surface of MCM-48 was then modified by post-synthesis and the modified MCM-48 was finally impregnated with {Mo_{132}}. The {Mo_{132}} sample synthesized using the method of Müller's group was characterized by XRD and FT-IR technologies. Figure 3-4 displays the IR spectrum of {Mo_{132}}. The characteristic bands at 1619 cm^{-1} ($\delta(H_2O)$), 1540 cm^{-1} ($\upsilon_{as}(COO)$), 1400 cm^{-1} ($\delta_{as}(NH_4^+)$), 970 and 940 cm^{-1} ($\upsilon(Mo=O)$), 856 and 798 cm^{-1} ($\upsilon_{as}(Mo\text{-}O)$), 725 cm^{-1}, 632 cm^{-1} and 568 cm^{-1} are attributed to the framework of {Mo_{132}}, matching with the literature reference.[1] The XRD pattern further confirmed the successful achievement of {Mo_{132}} cluster (Figure 3-5).

The textural properties of the samples were studied by N_2 physisorption analysis. The results are presented in Table 3-1. From the BET results one can see that the specific surface steadily decreased by the functionalization of the aminosilane group and the impregnation by {Mo_{132}}. The functionalization notably reduced the mesopore volume of MCM-48 from 0.83 cm^3/g to 0.34 cm^3/g after the surface modification, which gives the first evidence that the surface of MCM-48 was

successfully modified. The following addition of {Mo_{132}} further decreased the mesopore volume to 0.15 cm^3/g, which strongly suggests that some {Mo_{132}} molecules were immobilized onto MCM-48. Regarding the structure, although the XRD patterns of NH_2-MCM-48 and {Mo_{132}}@NH_2-MCM-48 suggested that the structure of MCM-48 collapsed after the functionalization (Figure 3-6), the N_2 isotherm showed that the hysteresis at p/p_0 from 0.5 to 0.9 remained intact (Figure 3-7), which manifested that the mesoporous structure of MCM-48 was not affected, neither by functionalization nor impregnation.

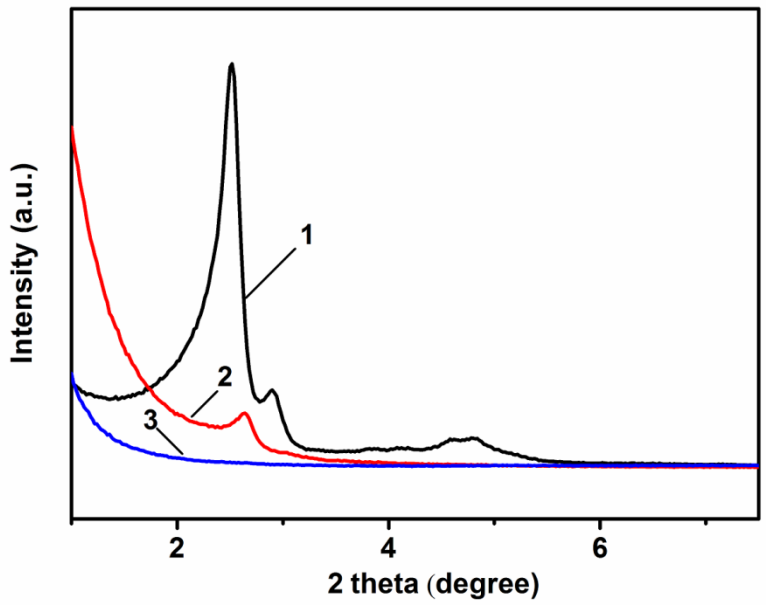

Figure 3-6 XRD patterns of (1) MCM-48, (2) NH_2-MCM-48 and (3) {Mo_{132}}@NH_2-MCM-48.

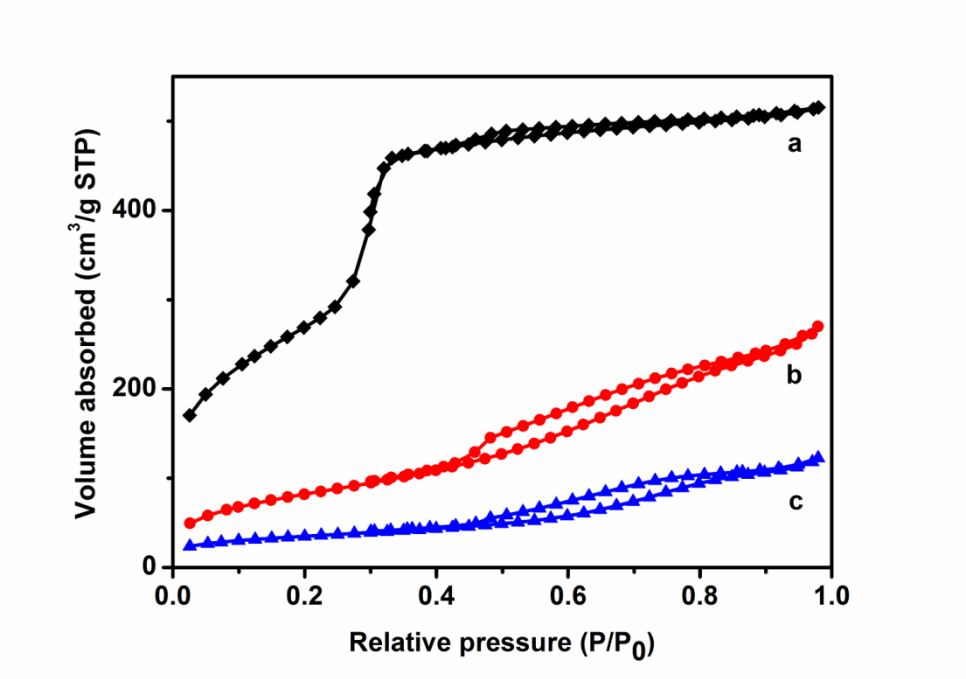

Figure 3-7 N_2 adsorption-desorption isotherms of (a) MCM-48, (b) NH_2-MCM-48, (c) $\{Mo_{132}\}$@NH_2-MCM-48.

Table 3-1 Textural properties of as-prepared samples

Samples	BET surface area (m^2/g)	Total pore volume (cm^3/g)	Mesopore volume (cm^3/g)
MCM-48	1136	0.79	0.83
NH_2-MCM-48	300	0.39	0.34
$\{Mo_{132}\}$-NH_2-MCM-48	123	0.17	0.15

Figure 3-8 displays the IR spectra of MCM-48, NH_2-MCM-48, $\{Mo_{132}\}$@NH_2-MCM-48 and $\{Mo_{132}\}$. From the figure, one can see that the characteristic bands at 2934 and 1554 cm^{-1} belonging to the NH_2 group exist in the spectrum of NH_2-MCM-48, which reveals the successful functionalization of MCM-48.

After the impregnation with {Mo_{132}}, several peaks appeared in the spectrum compared with that of NH_2-MCM-48. Peaks at 1629 ($\delta(H_2O)$), 1548 ($\upsilon_{as}(COO)$), 1416 ($\delta_{as}(NH_4^+)$) cm^{-1} could be ascribed to the framework of {Mo_{132}}, while compared with the typical {Mo_{132}} bands, all these bands were blue-shifted, which could be attributed to the overlap with the bands belonging to NH_2-MCM-48 at 1636,1554 cm^{-1} and the substitution with electron-accepting groups. The FT-IR results suggest that some {Mo_{132}} molecules anchored on the surface of MCM-48, in agreement with the results of N_2 absorption/desorption. The color of the solid of {Mo_{132}}@NH_2-MCM-48 remained brown after the washing of water (the filtrated water was transparent in the last time), which could be another evidence of the successful immobilization of {Mo_{132}} (Figure 3-9).

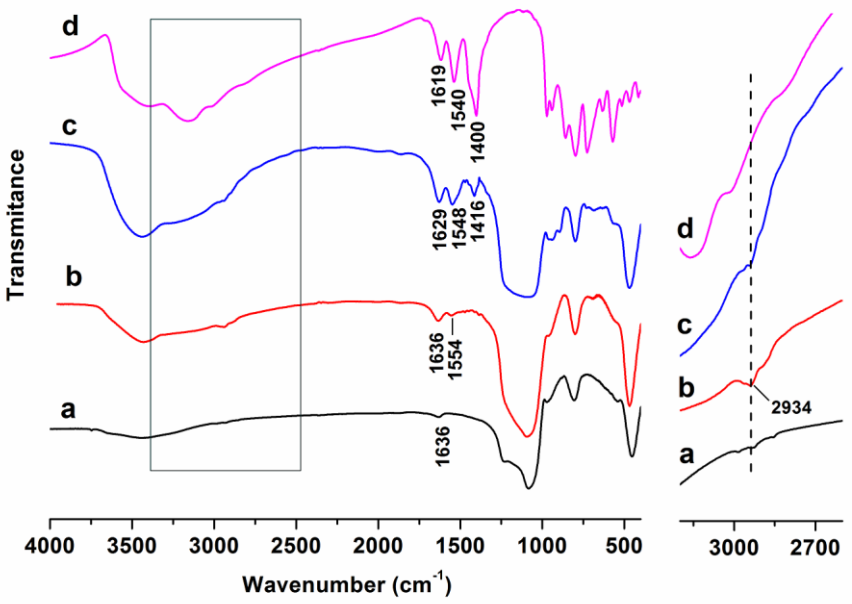

Figure 3-8 IR spectra of (a) MCM-48, (b) NH_2-MCM-48, (c) {Mo_{132}}@NH_2-MCM-48 and (d) {Mo_{132}}.

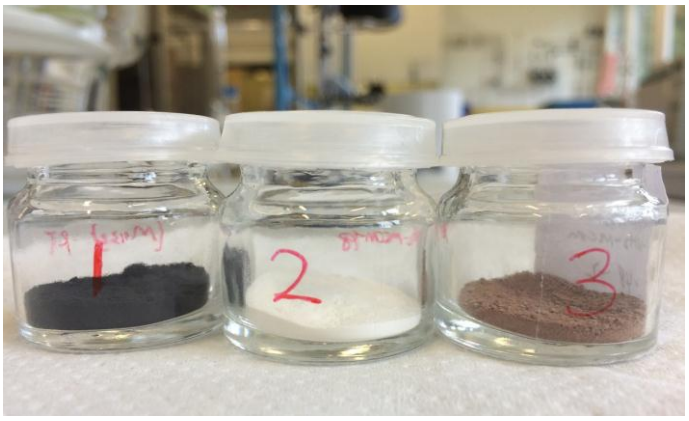

Figure 3-9 Pictures of as-prepared samples: (1) {Mo_{132}}, (2) NH_2-MCM-48 and (3) {Mo_{132}}@NH_2-MCM-48.

In summary, the strategy of encapsulating {Mo_{132}} into MCM-48 via the method of building a ship in the bottle did not allow the heterogenization of Keplerate {Mo_{132}}, but the strategy of the chemical immobilization by the introduction of aminosilane groups in the surface of MCM-48 successfully obtained the heterogeneous {Mo_{132}} catalyst. Further study about the {Mo_{132}}@NH_2-MCM-48 will be done in the future.

3.3.3 Epoxidation of cyclooctene

As mentioned above, some applications of {Mo_{132}} in liquid phase reactions were reported recently. Among these reactions, the aerobic epoxidation of olefins in water at ambient temperature and pressure in the absence of reducing agent attracted our first attention because the reaction has the advantages that no byproducts are generated and the cost of O_2 is low, which is consistent with the principle of "Green Chemistry". We thus utilized the epoxidation of cyclooctene to test the oxidation capacity of {Mo_{132}} according to the description of Rezaeifard *et al.*[20] However, no cyclooctene was oxidized even if the flow of O_2 was increased. Therefore, H_2O_2, which has a stronger oxidative power than O_2 was chosen to oxidize cyclooctene. The reaction was made following the procedure in literature.[19] It is surprising that the reddish brown suspension turned to a yellow solution after the adding of H_2O_2 (Figure 3-10), which indicates that the {Mo_{132}} cluster decomposed. Since the structure of

POMs is pH dependent and it is reported that the Keplerate-type polyoxomatalates are less stable and even break with the increase of pH value of solvents[6, 20, 34], we adjusted the pH value of the initial suspension of {Mo_{132}} in ethanol to 2 and 10 before adding H_2O_2. As shown in (Figure 3-11), the color of the suspension of {Mo_{132}} became white from reddish after the pH had been adjusted to 10 and remain the same at pH=2. This suggests that the structure of {Mo_{132}} changed under alkaline conditions but was maintained under acidic conditions. However, the reddish suspension at pH=2 became yellow as after adding of H_2O_2, which reveals that the decomposition of {Mo_{132}} cluster should rather be related to the addition of H_2O_2 than to the pH. In order to confirm the effect of H_2O_2 for the decomposition of {Mo_{132}}, 0.4 mL of 30% H_2O_2 solution was added directly on 57.2 mg of {Mo_{132}}. As a result, the {Mo_{132}} solid was digested immediately after a gently shaking (Figure 3-12), which confirms that the addition of H_2O_2 caused the decomposition of {Mo_{132}} in our case.

Figure 3-10 Pictures of (left) the reddish suspension of {Mo_{132}} with cyclooctene in ethanol and (right) the yellow solution from the suspension after adding H_2O_2.

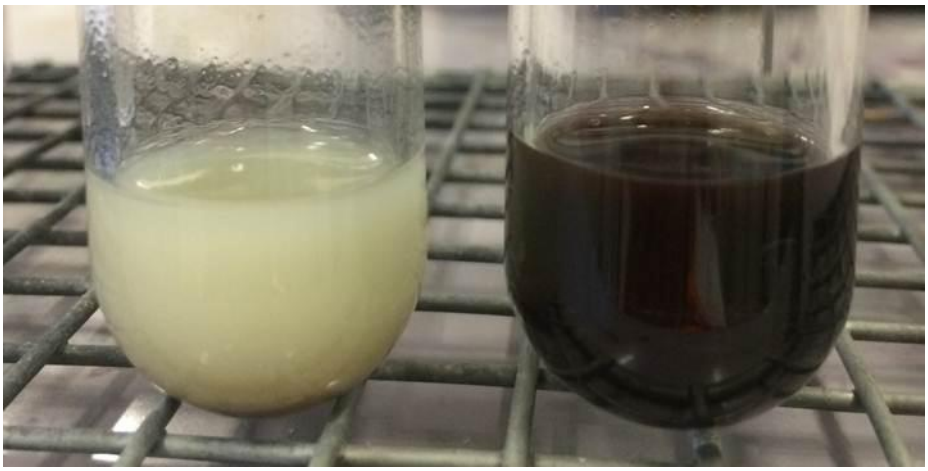

Figure 3-11 Pictures of the suspension of {Mo_{132}} with cyclooctene and ethanol at pH=10 (left) and pH=2 (right) before adding H_2O_2.

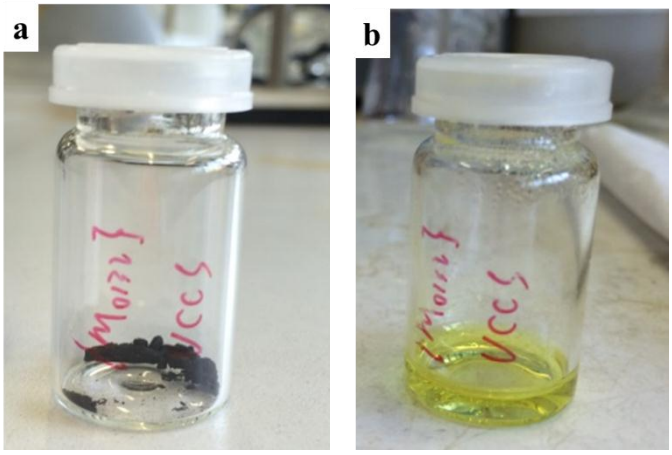

Figure 3-12 Pictures of (a) the as-prepared {Mo_{132}} sample and (b) the solution of {Mo_{132}} sample after adding H_2O_2.

Although the decomposition of {Mo_{132}} happened after the addition of H_2O_2, we still heated the yellow solution at 348 K for 1 h and analyzed the organic phase by GC. The reaction results are displayed in Table 3-2. As one can see, cyclooctene had no conversion in absence of H_2O_2. On the other hand, the oxidation proceeded when the 30% H_2O_2 solution was added. The conversions of cyclooctene were 69% and 85% when the amounts of H_2O_2 solution were 0.2 and 0.4 mL, respectively. It is obvious

that one or more of the decomposition products of {Mo_{132}} can catalyze the epoxidation of cyclooctene. Therefore, the yellow solution containing products of decomposition of {Mo_{132}}, ethanol, cyclooctene and 30% H_2O_2 solution was left in the hood at room temperature to evaporate the liquid slowly. Yellow plate-like crystals (Figure 3-13a) were obtained and analysed by single crystal X-ray structure analysis. It was found that the crystal data of the decomposition products of {Mo_{132}} are well-matched with the previous report of $(NH_4)_4Mo^{VI}_8(O_2)_2O_{24}(H_2O)\bullet 4H_2O$ (denoted as {Mo_8}, space group: $P2_1/n$, a = 10.427(3) Å, b = 7.915(5) Å, c = 18.103(3) Å, β = 96.10(2) °, V = 1485.58 $Å^3$)[35]. Its crystal structure is shown in Figure 3-13b.

The solution obtained from {Mo_{132}} after directly adding H_2O_2 was also evaporated in the hood slowly. The resulting solid, {Mo_{132}} and {Mo_8} were analyzed by FT-IR in order to further verify that the decomposition of {Mo_{132}} is caused by H_2O_2. Their spectra are presented in Figure 3-14. It is obvious that the spectrum of the solid resulting from {Mo_{132}} treated with H_2O_2 was the same as that of {Mo_8} but different from the spectrum of {Mo_{132}}, further indicating that {Mo_{132}} decomposes into the {Mo_8} cluster after the addition of H_2O_2.

On the basis of above results, we infer that {Mo_8} cluster, which has only one more molybdenum atom than $(NH_4)_6Mo_7O_{24}\cdot 4H_2O$-the reagent used for synthesizing {Mo_{132}}, is the actual catalyst in the epoxidation of cyclooctene. To explore the assumption, {Mo_8} obtained from the solution containing {Mo_{132}} and H_2O_2 was used to catalyze the epoxidation of cyclooctene in the same experimental conditions as the experiment of {Mo_{132}}. As expected, {Mo_8} exhibits a catalytic activity in this reaction, which confirms our hypothesis. {Mo_8} indeed has been reported as dehydrogenation and desulphurisation catalysts.[36] It should be mentioned that the decomposition of {Mo_{132}} in the reaction was unexpected and it contradicts the work of Rezaeifard *et al.*[19]. However, Yang and coworkers[21] also observed a similar decomposition in the pyridine oxidation to N-oxides with H_2O_2 using {Mo_{132}}.

Table 3-2 Epoxidation of cyclooctene in ethanol using H_2O_2 catalysed by $\{Mo_{132}\}$

Catalyst	Amount			Cyclooctene conversion (%)	Cyclooctene oxide yield (%)	Cyclooctene oxide selectivity (%)
	Cyclooctene (mL)	30% H_2O_2 (mL)	Ethanol (mL)			
Blank	0.26	0.4	4	0	0	0
$\{Mo_{132}\}$	0.26	0	4	0	0	0
$\{Mo_{132}\}$	0.26	0.2	4	69	55	79
$\{Mo_{132}\}$	0.26	0.4	4	85	62	72

Reactions were run under air at 75 ℃ for 1 h.

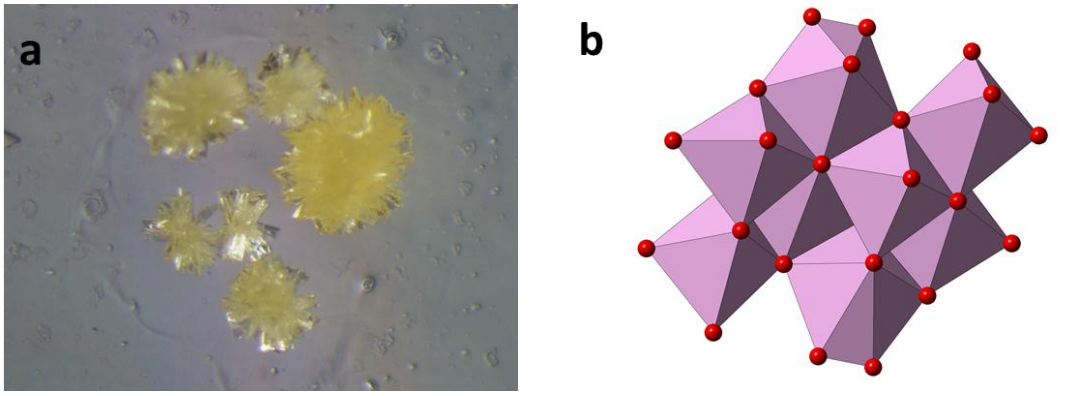

Figure 3-13 (a) solid obtained from the solution containing products of decomposition of $\{Mo_{132}\}$, ethanol, cyclooctene and 30% H_2O_2 solution; (b) Structure of $\{Mo_8\}$ (The red small balls represent oxygen atoms).

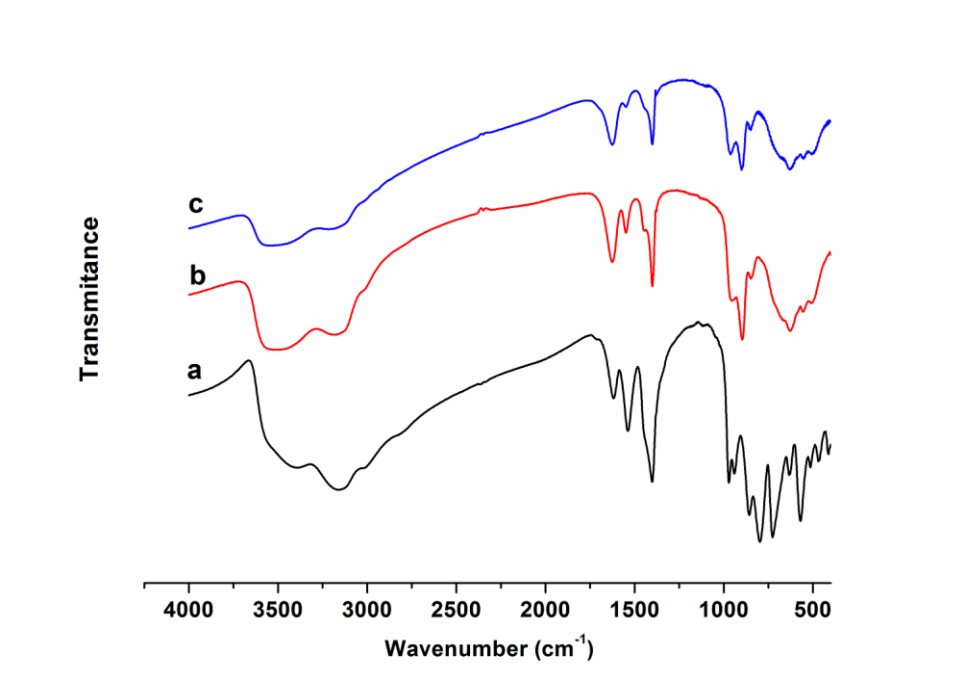

Figure 3-14 IR spectra of (a) {Mo_{132}}, (b) {Mo_8} and (c) the solid obtained from {Mo_{132}} treated with H_2O_2.

3.4 Conclusion

In this chapter, we used two strategies, the encapsulation according to the concept of "building a ship in the bottle" and the chemical immobilization by a chemical bonding between amino-modified MCM-48 and {Mo_{132}}, to prepare heterogeneous MCM-48 supported {Mo_{132}} catalyst. Although the encapsulation method did not work well, but the chemical immobilization successfully carried out the heterogenization of {Mo_{132}}. The study of epoxidation of cyclooctene with H_2O_2 using {Mo_{132}} gives the evidence that {Mo_{132}} cluster is not stable in presence of H_2O_2 and decomposes to the {Mo_8} cluster, which is active in the epoxidation of cyclcooctene. Even though the results about the application of {Mo_{132}} in the epoxidation of cyclcooctene are not satisfactory, these provides more specific information for the change of the structure of {Mo_{132}} in liquid phase, which is of significance for the applications of {Mo_{132}} in liquid-phase catalysis in the future.

3.5 Reference

[1] A. Müller, E. Krickemeyer, H. Bögge, M. Schmidtmann, F. Peters, Organizational Forms of Matter: An Inorganic Super Fullerene and Keplerate Based on Molybdenum Oxide. *Angew. Chem. Int. Ed.* **1998,** *37* (24), 3359-3363.

[2] A. Muller, L. Toma, H. Bogge, M. Henry, E. T. K. Haupt, A. Mix, F. L. Sousa, Reactions inside a porous nanocapsule/artificial cell: encapsulates' structuring directed by internal surface deprotonations. *Chem. Commun.* **2006,** (32), 3396-3398.

[3] C. Schäffer, H. Bögge, A. Merca, I. A. Weinstock, D. Rehder, E. T. K. Haupt, A. Müller, A Spherical 24 Butyrate Aggregate with a Hydrophobic Cavity in a Capsule with Flexible Pores: Confinement Effects and Uptake–Release Equilibria at Elevated Temperatures. *Angew. Chem. Int. Ed.* **2009,** *48* (43), 8051-8056.

[4] C. Schäffer, A. M. Todea, H. Bögge, O. A. Petina, D. Rehder, E. T. K. Haupt, A. Müller, Hydrophobic Interactions and Clustering in a Porous Capsule: Option to Remove Hydrophobic Materials from Water. *Chemistry – A European Journal* **2011,** *17* (35), 9634-9639.

[5] A. Ziv, A. Grego, S. Kopilevich, L. Zeiri, P. Miro, C. Bo, A. Müller, I. A. Weinstock, Flexible Pores of a Metal Oxide-Based Capsule Permit Entry of Comparatively Larger Organic Guests. *J. Am. Chem. Soc.* **2009,** *131* (18), 6380-6382.

[6] R. Mekala, S. Supriya, S. K. Das, Fate of a Giant {Mo72Fe30}-Type Polyoxometalate Cluster in an Aqueous Solution at Higher Temperature: Understanding Related Keplerate Chemistry, from Molecule to Material. *Inorg. Chem.* **2013,** *52* (17), 9708-9710.

[7] F. Jalilian, B. Yadollahi, M. R. Farsani, S. Tangestaninejad, H. A. Rudbari, R. Habibi, New perspective to Keplerate polyoxomolybdates: Green oxidation of sulfides with hydrogen peroxide in water. *Catal. Commun.* **2015,** *66*, 107-110.

[8] A. Muller, P. Gouzerh, From linking of metal-oxide building blocks in a dynamic library to giant clusters with unique properties and towards adaptive chemistry. *Chem. Soc. Rev.* **2012,** *41* (22), 7431-7463.

[9] A. Müller, S. Sarkar, S. Q. N. Shah, H. Bögge, M. Schmidtmann, S. Sarkar, P. Kögerler, B. Hauptfleisch, A. X. Trautwein, V. Schünemann, Archimedean Synthesis and Magic Numbers:“Sizing” Giant Molybdenum‐Oxide‐Based Molecular Spheres of the Keplerate Type. *Angew. Chem. Int. Ed.* **1999,** *38* (21), 3238-3241.

[10] J. Yan, J. Gao, D.-L. Long, H. N. Miras, L. Cronin, Self-Assembly of a Nanosized, Saddle-Shaped, Solution-Stable Polyoxometalate Anion Built from Pentagonal Building Blocks: [H34W119Se8Fe2O420]54−. *J. Am. Chem. Soc.* **2010,** *132* (33), 11410-11411.

[11] T. L. Lai, M. Awada, S. Floquet, C. Roch‐Marchal, N. Watfa, J. Marrot, M. Haouas, F. Taulelle, E. Cadot, Tunable Keplerate Type‐Cluster “Mo132” Cavity with Dicarboxylate Anions. *Chemistry–A European Journal* **2015,** *21* (38), 13311-13320.

[12] S. Biswas, D. Melgar, A. Srimany, A. Rodríguez-Fortea, T. Pradeep, C. Bo, J. M. Poblet, S. Roy, Direct Observation of the Formation Pathway of [Mo132] Keplerates. *Inorg. Chem.* **2016,** *55* (17), 8285-8291.

[13] A. A. Ostroushko, M. O. Tonkushina, A. P. Safronov, S. Y. Men’shikov, V. Y. Korotaev, Thermal behavior of polyoxometalate Mo132. *Russ. J. Inorg. Chem.* **2009,** *54* (2), 172-179.

[14] A. A. Ostroushko, M. O. Tonkushina, Destruction of porous spherical Mo132 nanocluster polyoxometallate of keplerate type in aqueous solutions. *Russ. J. Phys. Chem. A* **2016,** *90* (2),

436-442.
[15] B. Botar, A. Ellern, R. Hermann, P. Kögerler, Electronic Control of Spin Coupling in Keplerate-Type Polyoxomolybdates. *Angew. Chem. Int. Ed.* **2009,** *48* (48), 9080-9083.
[16] L. Zhang, Z. Shi, L. Zhang, Y. Zhou, S. u. Hassan, Fabrication and optical nonlinearities of ultrathin composite films incorporating a Keplerate type polyoxometalate. *Mater. Lett.* **2012,** *86*, 62-64.
[17] S. Xu, Y. Wang, Y. Zhao, W. Chen, J. Wang, L. He, Z. Su, E. Wang, Z. Kang, Keplerate-type polyoxometalate/semiconductor composite electrodes with light-enhanced conductivity towards highly efficient photoelectronic devices. *Journal of Materials Chemistry A* **2016,** *4* (36), 14025-14032.
[18] N. Izarova, O. Kholdeeva, M. Sokolov, V. Fedin, Catalytic properties of the macromolecular polyoxomolybdate cluster in selective oxidation of sulfides. *Russ. Chem. Bull.* **2009,** *58* (1), 134-137.
[19] A. Rezaeifard, R. Haddad, M. Jafarpour, M. Hakimi, {Mo_{132}} Nanoball as an Efficient and Cost-Effective Catalyst for Sustainable Oxidation of Sulfides and Olefins with Hydrogen Peroxide. *ACS Sustainable Chemistry & Engineering* **2014,** *2* (4), 942-950.
[20] A. Rezaeifard, R. Haddad, M. Jafarpour, M. Hakimi, Catalytic epoxidation activity of keplerate polyoxomolybdate nanoball toward aqueous suspension of olefins under mild aerobic conditions. *J. Am. Chem. Soc.* **2013,** *135* (27), 10036-10039.
[21] C. Yang, W. Zhao, Z. Cheng, B. Luo, D. Bi, Catalytic system for pyridine oxidation to N-oxides under mild conditions based on polyoxomolybdate. *RSC Advances* **2015,** *5* (46), 36809-36812.
[22] J. Xu, Z. Luan, H. He, W. Zhou, L. Kevan, A reliable synthesis of cubic mesoporous MCM-48 molecular sieve. *Chem. Mater.* **1998,** *10* (11), 3690-3698.
[23] W. Kaleta, K. Nowinska, Immobilisation of heteropoly anions in Si-MCM-41 channels by means of chemical bonding to aminosilane groups. *Chem. Commun.* **2001,** (6), 535-536.
[24] A. Sayari, Novel synthesis of high-quality MCM-48 silica. *J. Am. Chem. Soc.* **2000,** *122* (27), 6504-6505.
[25] K. Schumacher, M. Grün, K. K. Unger, Novel synthesis of spherical MCM-48. *Micropor. Mesopor. Mater.* **1999,** *27* (2–3), 201-206.
[26] S. Brunauer, L. S. Deming, W. E. Deming, E. Teller, On a Theory of the van der Waals Adsorption of Gases. *J. Am. Chem. Soc.* **1940,** *62* (7), 1723-1732.
[27] P. Yang, P. Yang, X. Teng, J. Lin, L. Huang, A novel luminescent mesoporous silica/apatite composite for controlled drug release. *J. Mater. Chem.* **2011,** *21* (14), 5505-5510.
[28] S. Gai, P. Yang, D. Wang, C. Li, N. Niu, F. He, M. Zhang, J. Lin, Luminescence functionalization of MCM-48 by YVO 4: Eu 3+ for controlled drug delivery. *RSC Advances* **2012,** *2* (8), 3281-3287.
[29] V. Alfredsson, M. W. Anderson, Structure of MCM-48 Revealed by Transmission Electron Microscopy. *Chem. Mater.* **1996,** *8* (5), 1141-1146.
[30] K. Schumacher, P. I. Ravikovitch, A. Du Chesne, A. V. Neimark, K. K. Unger, Characterization of MCM-48 Materials. *Langmuir* **2000,** *16* (10), 4648-4654.
[31] K. C. Vrancken, P. Van Der Voort, K. Possemiers, E. F. Vansant, Surface and Structural Properties of Silica Gel in the Modification with γ-Aminopropyltriethoxysilane. *J. Colloid*

Interface Sci. **1995,** *174* (1), 86-91.
[32] P. Van Der Voort, E. Vansant, Modification of the silica surface with aminosilanes. *Pol. J. Chem.* **1997,** *71* (5), 550-567.
[33] P. V. Der Voort, E. Vansant, Silylation of the silica surface a review. *J. Liq. Chromatogr. Relat. Technol.* **1996,** *19* (17-18), 2723-2752.
[34] T. Liu, B. Imber, E. Diemann, G. Liu, K. Cokleski, H. Li, Z. Chen, A. Müller, Deprotonations and Charges of Well-Defined {Mo72Fe30} Nanoacids Simply Stepwise Tuned by pH Allow Control/Variation of Related Self-Assembly Processes. *J. Am. Chem. Soc.* **2006,** *128* (49), 15914-15920.
[35] A. J. Ward, G. J. Arrow, T. Maschmeyer, A. F. Masters, P. Turner, J. K. Clegg, Tetraammonium diaquadiperoxidooctamolybdate (VI) tetrahydrate. *Acta Cryst. E* **2009,** *65* (7), i53-i54.
[36] http://www.lookchem.com/Ammonium-molybdate-tetrahydrate/.

4 General conclusions and perspectives

4.1 General conclusions

In the previous chapters we have followed two strategies to prepare encapsulated heteropolyacid-based catalysts for the applications in liquid phase reactions. The first attempt used the "building a bottle around the ship" methodology, whereby the ship was a pre-formed Keggin-type heteropolyacid (HPA) and the bottle was a Metal-Organic Framework (MOF). The corresponding methodology was successfully applied to $H_3PW_{12}O_{40}$ as the ship and MIL-101(Cr) playing the role of the bottle. Hereby, the influence of several reaction parameters was studied, namely the presence of HF during synthesis, the amount of HPA loading and the pH value during the synthesis.

According to our results, the presence of HF during the synthesis showed only little impact on the physical and structural parameters, since the specific surface, porosity and also the XRD patterns (crystal size) were in the same order of magnitude, no matter if HF was employed during the synthesis or not. This result may add another brick to the discussion currently ongoing in literature. On the other hand – even though the physical and structural parameters were comparable, the catalysts prepared using HF in the synthesis method exhibited increased catalytic performance in the esterification of acetic acid with butanol. The corresponding result may be explained by the impact of HF – and notably the remaining fluorine ions after synthesis – on the acid properties.

Of course, the acid properties are a crucial factor in the esterification reaction of acetic acid and butanol, but the determination of this parameter is not straightforward in case of Metal Organic Framework encapsulated heteropolyacids. In fact, due to the low thermal stability of the MOF, the classical methods like temperature programmed desorption of ammonia or FT-IR with pyridine as a probe molecule are not applicable.

In the following, we studied the upper limit of HPA loading which could be encapsulated into MIL-101(Cr). Hereby, loadings of up to 50 wt% could be achieved when using phosphotungstic acid. From the results is also became clear that the

incorporation of HPA resulted in a significant decrease in the specific surface of the catalyst. As an example, the specific surface dropped from 1949 m^2/g (bare support) to 1630 m^2/g for the catalyst containing 32 wt% $H_3PW_{12}O_{40}$ (HPW), to 1218 m^2/g for the material with 48 wt% loading. Nevertheless, these values also demonstrate that the porosity was still accessible and the MIL-101 structure was still intact. In terms of catalytic performance, the higher loading also resulted in a higher reaction rate, which was directly expressed as a significantly higher conversion for the catalyst containing 48 wt% $H_3PW_{12}O_{40}$.

As a last parameter, the pH value during the synthesis was studied. In fact, the pH is a critical value when using heteropolyacids in solutions, since the latter can easily be decomposed when the pH increased to neutral or even basic conditions. Thus, the pH was deliberately kept constant at 2.6 during the synthesis. From the results one can see that the constant pH value decreased the amount of HPA encapsulated into the MIL-101. Even worth, the material obtained at constant pH value showed no significant catalytic activity in the esterification reaction. At the current moment, these results cannot be explained. A deeper characterization using i.e. microcalorimetry could allow obtaining further information.

In terms of the catalytic performance in the esterification of acetic acid and butanol, we also stated that the as-prepared materials were not very promising – neither in terms of yield, nor in terms of reusability. However, the unsatisfactory performance cannot be attributed to the leaching of HPAs under reaction conditions, which is the most likely to think of. In fact, only little leaching (4.6 wt% loss of HPAs) occurred after the first use, which can be explained by the desorption of HPAs in the outer surface of MIL-101(Cr). And the HPA content remained stable at 43% or so in the next two runs. Therefore, the reason for the decreased activity in recycling needs a further study.

As an alternative reaction to the esterification, the epoxidation of cyclooctene was studied. Therefore, another catalyst was prepared using $H_3PMo_{12}O_{40}$ (HPMo) this time.

Again the "building the bottle around the ship" methodology was applied whereby a loading of 24.2 wt% HPA (ICP analysis) could be encapsulated.The application of the corresponding material in the epoxidation reaction yielded up to 70% in the desired product. Furthermore, the leaching of the active phase under these conditions was also significantly suppressed. In fact, from the results one can see that similarly to $H_3PW_{12}O_{40}$@MIL-101(Cr) catalysts, only during the first reaction, some loss of phosphomolybdic acid took place. Afterwards, the amount remained stable at 53 wt%, which suggests that during the first reaction only the HPA from the outer surface of the MIL-101(Cr) host was leached out, whereas the one in the porosity remained unaffected.

MIL-100(Fe), another typical MOF material with less toxicity, was also used as the host of Keggin HPAs. HPW@MIL-100(Fe) and HPMo@MIL-100(Fe) were synthesized using the "building a bottle around the ship" method. The encapsulation of HPAs remarkably decreased the porosity of MIL-100(Fe), the specific surface dropped from 1192 m^2/g (bare support) to 232 m^2/g for HPMo@MIL-100(Fe) with the 21.4 wt% loading of HPMo and to 317 m^2/g for HPW@MIL-100(Fe) containing 37.8 wt% HPW. Nevertheless, MIL-100(Fe) still possesses certain porosity after the incorporation of HPAs, indicating their potential application in catalysis.

The catalytic performance of HPMo@MIL-100(Fe) was thus explored by the epoxidation of cyclooctene. Although HPMo@MIL-100(Fe) exhibited some activity the catalyst is not reusable due to the leaching of HPMo during the reaction. Considering that leaching might be caused by the destruction of some MIL-100(Fe) framework after the addition of H_2O_2, the oxidation of benzyl alcohol using O_2 was employed to determine the catalytic properties of HPMo@MIL-100(Fe). However, the framework is not stable at a temperature above 80 ˚C.

In the second part of the thesis, the application of the "building the ship in the bottle" methodology was evaluated. Therefore, a Keplerate type POM – $\{Mo_{132}\}$ – was chosen. The latter has a kinetic diameter of about 2.9 nm. With respect to this size, a mesoporous silica – namely MCM-48 – was chosen as host material. The pore-size of

the latter can be tuned via the synthesis conditions, allowing to obtain a material with a pore diameter in the range of 2-10 nm.

From the characterization results one could see that the corresponding methodology did not work out to obtain the desired encapsulated Keplerate. Several hypotheses were evoked. The first is related the significant sterical constraints to build the Keplerate inside the porous network of the MCM-48 host material. In fact, either the small pore diameter caused problems for the diffusion of the reactants, or the surrounding silica framework inhibited the formation of the Keplerate.

As a second possibility, the loss of the Keplerate during the final washing step was evoked. This seems possible since the pore diameter of the silica host is still slightly larger than the Keplerate structure (3.1 nm vs. 2.9 nm).

In order to avoid the leaching of the Keplerate by washing, the functionalization of the silica support using propylamino groups was studied. The latter allow the immobilization of the Keplerate via an ionic linkage, whereby the amino groups are protonated and act as a positive charged ammonium cation.

From the characterization results it could be concluded that the methodology carried out for the heterogenization of $\{Mo_{132}\}$ was nevertheless a success: the textural parameters suggested the successful functionalization and linkage of $\{Mo_{132}\}$ which is further supported by FT-IR, showing clearly the presence of the Keplerate in $\{Mo_{132}\}@NH_2$-MCM-48.

Finally, the application of the as-prepared materials in the epoxidation of cyclooctene was studied. Unfortunately, the presence of hydrogen peroxide immediately caused the decomposition of the $\{Mo_{132}\}$ Keplerate, resulting in the digestion of the catalyst. Nevertheless, high conversion was observed, which was ascribed to the decomposition products of the Keplerate, acting as a homogeneous catalysts, whereby notably the $\{Mo_8\}$ clusters were identified. Even though these results are very disappointing, one has to mention that they contradict some results

reported in literature.[1]

4.2 Perspectives

At the end of this thesis, some problems remain unsolved for the two types of encapsulated catalysts studied. However, some suggestions can be made to go further in the understanding of the use of these materials as catalysts for biomass valorization. In the following, we will describe respectively the further study we would suggest for the Keggin-type HPAs and Keplerate-type POMs encapsulated catalysts.

In the study of Keggin-type HPAs encapsulated catalysts, the reason for the decreased activity of HPW@MIL-101(Cr) in esterification of n-butanol and acetic acid has not been clearly established. Based on the current results, we infer that the acidity of this catalyst play an important impact on its performance. Therefore, the determination of the acidity of HPW@MIL-101(Cr) should be completed first. Since the common methods are not suitable for this catalyst, a CO_2-probe IR method based on the report of Wee *et al.*[2] would be of very high interest. HPMo@MIL-101(Cr) catalyst showed a very interesting performance for the epoxidation of cyclooctene. The conditions of the reaction could be optimized and other subtsrtaes could be explored. Concerning the HPAs@MIL-100(Fe), their behavior in liquid phase should be carefully studied in order to improve their hydrothermal stability.

The exploration of encapsulating Keplerate-type $\{Mo_{132}\}$ into MCM-48 gives information for further development of "building a ship in the bottle" methodology and the heterogenization of Keplerate-type POMs. The method of "building a ship in the bottle" is much more difficult to realize than that of "building a bottle around the ship" because the porous structures of "the bottle" is hard to keep during the synthesis of "the ship" and the steric hindrance from the pores and the properties of the support's surface both can influence the formation of active phases. Therefore, in our case, porous materials with an excellent hydrothermal stability would be better choices such as zeolites, carbon and porous metallic oxides. Rational surface modifications could also also beneficial. On the other hand, the heterogenization of

Keplerate-type POMs might be done more easily through a chemical immobilization method because that method can be done at room temperature, which is more convenient for the fragile structure of Keplerates. However, methods of chemical immobilization still need further study in order to minimize the influence of strong interactions between the active phase and the supports on the activity of the obtained catalysts. Finally it would be of high interest to study in details the process of decomposition of $\{Mo_{132}\}$ in the presence of H_2O_2.

4.3 Reference

[1] A. Rezaeifard, R. Haddad, M. Jafarpour, M. Hakimi, {Mo_{132}} Nanoball as an Efficient and Cost-Effective Catalyst for Sustainable Oxidation of Sulfides and Olefins with Hydrogen Peroxide. *ACS Sustainable Chemistry & Engineering* **2014,** *2* (4), 942-950.

[2] L. H. Wee, F. Bonino, C. Lamberti, S. Bordiga, J. A. Martens, Cr-MIL-101 encapsulated Keggin phosphotungstic acid as active nanomaterial for catalysing the alcoholysis of styrene oxide. *Green Chem.* **2014,** *16*, 1351-1357.